Reviews of Modern Plasma Physics (2022) 6:36
https://doi.org/10.1007/s41614-022-00084-2

PLASMA INNOVATION LECTURE

Radical-controlled plasma processes

Masaru Hori[1]

Received: 12 April 2022 / Accepted: 22 July 2022 / Published online: 10 November 2022
© The Author(s) 2022

Abstract

In plasmas, a variety of radicals which are defined as electrically neutral radicals in this article are efficiently produced by collisions between electrons and gas molecules. These radicals can subsequently undergo gas phase reactions with solids, liquids and living organisms that result in non-equilibrium surface/interface physicochemical processes. The specific phenomena produced by these reactions remain largely unknown, even though these plasma-based processes could lead to disruptive technological innovations. As an example, in the case of semiconductor microfabrication processes, the density, energy and lifetime of individual radicals, as well as the reaction time constants of these species with various materials should be ascertained. This would allow the identification and control of the effective radical species during processes, such as the high-precision etching and deposition of functional thin films. In addition, the type of reactions occurring between radicals generated in plasmas with liquids or living organisms is still an unexplored area. Establishing a theoretical system for these radical reactions and controlling the associated mechanisms could lead to innovations in the fields of functional devices and materials as well as in the areas of environmental protection, medicine and agriculture/fisheries. Focusing on the non-equilibrium surface/interface physicochemical reactions between radicals and solids occurring in semiconductor plasma processing, this paper describes the formation of nanostructured thin films by top-down mechanisms based on controlled radical production and bottom-up processes involving radical-induced self-organization. As well, this review examines next-generation medical and agricultural applications, such as the selective killing of cancer cells and plant growth promotion and functionalization. These systems result from the interactions of radicals generated in atmospheric-pressure, low-temperature plasmas with liquids, or the interactions of gas or liquid phase radicals with biological species. Finally, the importance of academic research into radical-controlled plasma processes and potential future technologies based on this interdisciplinary field are examined.

Keywords Low-temperature plasma science · Radical · Plasma material science · Plasma medicine · Plasma agriculture

Extended author information available on the last page of the article

Abbreviations

a-Si	Amorphous silicon
AI	Artificial intelligence
ALD	Atomic layer deposition
ALE	Atomic layer etching
CDE	Chemical dry etching
COD	Calcium oxalate dihydrate
CRDS	Cavity ring down spectroscopy
DFT	Density functional theory
DX	Digital transformation
ECR	Electron cyclotron resonance
EEDF	Electron energy distribution function
EELS	Electron energy loss spectroscopy
ESR	Electron spin resonance
FBS	Fetal bovine serum
FePc	Iron phthalocyanine
FTIR	Fourier transform infrared
Gly1-Gly2-Gly3-Gly4-Gly5	Pentaglycine
GX	Green transformation
HA	Hyaluronan (HA)
HAR	High-aspect-ratio
IC	Integrated circuit
ICP	Inductively coupled plasma
IRLAS	Infrared diode laser absorption spectroscopy
L-Ala1-D-iso-Gln2-L-L-Lys3-D-Ala4	L-alanine-D-iso-glutamine-L-lysine-D-alanine
IAMS	Ion attachment mass spectrometry
LIF	Laser-induced fluorescence
LMP	Lysosomal membrane permeabilization
μc-Si	Microcrystalline silicon
MD	Molecular dynamics
MHCL	Micro hollow-discharge cathode lamp
NAC	N-Acetyl-L-cysteine
OES	Optical emission spectroscopy
1D	One-dimensional
PAL	Plasma-activated Ringer's lactate solution
PAM	Plasma-activated medium
PBS	Phosphate-buffered saline
PECVD	Plasma enhanced chemical vapor deposition
PG	Peptidoglycan
PS	Polystyrene
P/S	Penicillin streptomycin
QMS	Quadrupole mass spectrometry
RF	Radio frequency

RNS	Reactive nitrogen species
RONS	Reactive oxygen and nitrogen species
ROS	Reactive oxygen species
RIPECVD	Radical injection plasma enhanced chemical vapor deposition
SEM	Scanning electron microscope
3D	Three-dimensional
2D	Two-dimensional
TEM	Transmission electron microscope
ULSIs	Ultra-large scale integrated circuits
$\mathbf{V_{dc}}$	Self-bias voltage
VHF	Very high frequency
VUVAS	Vacuum ultraviolet absorption spectroscopy
VUVLAS	Vacuum ultraviolet laser absorption spectroscopy
XPS	X-ray photoelectron spectroscopy

1 Introduction

Beginning in the 1970s, basic research regarding the use of plasma in semiconductor manufacturing emerged and, with the development of large-scale integrated circuits, the field of advanced semiconductor plasma processing has become important. Today, plasmas are used in 80% of semiconductor manufacturing processes and contribute to the manufacture of many items used in daily life. Approximately 55 years have passed, since Moore's law was first proposed as both a summary of and a prediction for the growing semiconductor industry (Moore 1965). This law states that the number of transistors on an integrated circuit (IC) chip doubles every 18 months, and highlights the importance of miniaturization in the semiconductor industry. As a result of the ongoing miniaturization of ICs based on technological innovations aimed at increasing the number of components per chip, this law has continued to hold true. The increasing integration of semiconductor chips has been closely associated with the development of plasma processes such that, at present, plasma processing is the key technology driving semiconductor microfabrication. Currently, semiconductor devices are primarily fabricated using core plasma processes, including plasma etching, deposition and surface modification techniques. As these technologies are refined, revolutionary innovations are expected to occur that will create the society of the future.

Figure 1 depicts the innovations resulting from improvements in plasma science and technology, which has undergone a major evolution in association with the development of semiconductor plasma processing. This technology comprises plasma diagnostics, generation and control, along with modeling and simulation. Research into plasma technology incorporates disciplines within both science and engineering, including mathematics, informatics, chemistry, physics, agriculture, medicine, pharmacy and so on, making this a truly interdisciplinary endeavor.

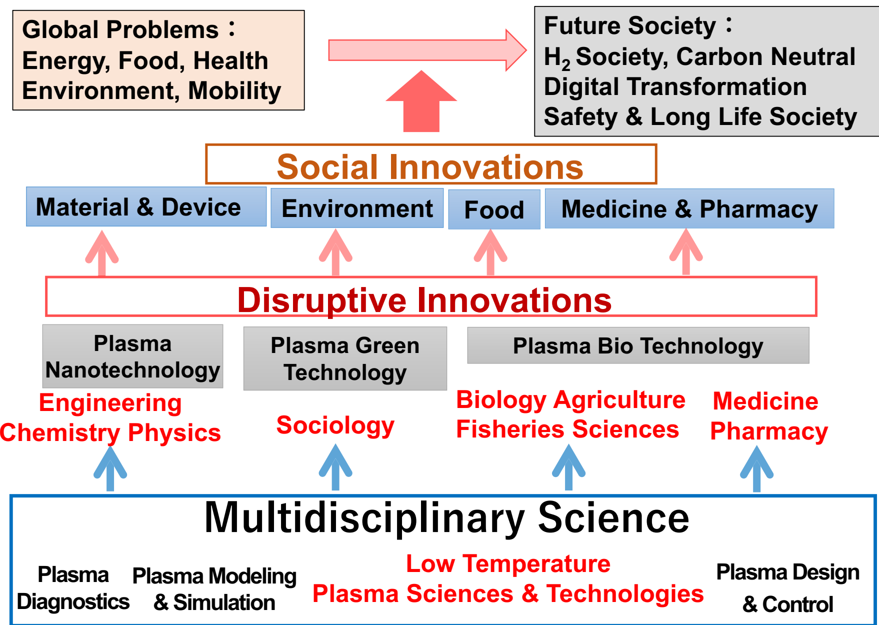

Fig. 1 The innovations resulting from improvement in plasma science and technology

Plasma-based materials and processes have resulted in the appearance of new academic fields, such as plasma electronics and plasma chemistry, and have made significant contributions to industry. However, many of the non-equilibrium physical and chemical reactions resulting from the interactions among electrons, ions, radicals, radiation and solids in plasmas have not yet been fully elucidated. More recently, atmospheric-pressure non-equilibrium plasmas and in-liquid plasmas have been developed and have attracted significant attention based on their potential applications in industry as well as in medicine, agriculture and fisheries. In particular, new research concerning the interactions between plasmas and liquids has become a global trend. The microscopic structures of plasmas and their physicochemical reactions at the plasma-liquid interface is an unexplored scientific field. In addition, research and development of plasma processes, which is a cutting-edge core science and technology, has become extremely significant as a field that creates basic science while leading industry.

The non-equilibrium physical and chemical reaction fields caused by plasmas have also produced a variety of phenomena that have led to disruptive innovations. Plasmas have been incorporated into the microfabrication technology used to manufacture semiconductors because of the discovery of phenomena that cannot be realized by existing physical chemistry occurring in thermal equilibrium, opening up new fields of application. Thus, plasma science and technology is an interdisciplinary field that is expected to bring about various innovations in fields, such as nanotechnology, green technology, agriculture and fisheries, and medicine. This progress could enable the creation of future devices and materials while providing solutions

to environmental problems, increased agricultural production and novel medical breakthroughs. Plasma-based technologies are also thought to have the potential to bring about social innovations such as the creation of devices and materials for digital transformation and to allow the mitigation of environmental problems, such as by ensuring carbon neutrality.

Despite the potential of plasma-based technology, 50 years of continuous research and development in this field has not kept pace with technological progress in general. One reason for this lack of progress is that available techniques for assessing the active species in plasmas have not been used sufficiently. Of course, plasma diagnostics and measurement techniques have been developed over the past five decades (Hori and Goto 2002; Bruggeman et al. 2016) and have revealed previously unknown phenomena and greatly advanced the development of plasma processes. In particular, methods to measure the densities and energies of electrons, ions, radicals, and radiation in plasmas have been devised and are relatively well established, with the exception of the measurement of some special active species. However, these techniques for the analysis of plasmas are not presently widely applied to plasma-based manufacturing and high-precision control processes to collect and systematize practical and reliable information.

It is evident that plasmas involve complex reaction systems and, as such, many researchers continue to use a trial-and-error research approach based on experience and intuition. Consequently, there is a need to develop more systematic processes that use scientific data. To this end, it is especially necessary to systematize the various phenomena produced by plasmas and to evaluate plasma processes and non-equilibrium plasmas. Figure 2 illustrates a potential approach to the systematic

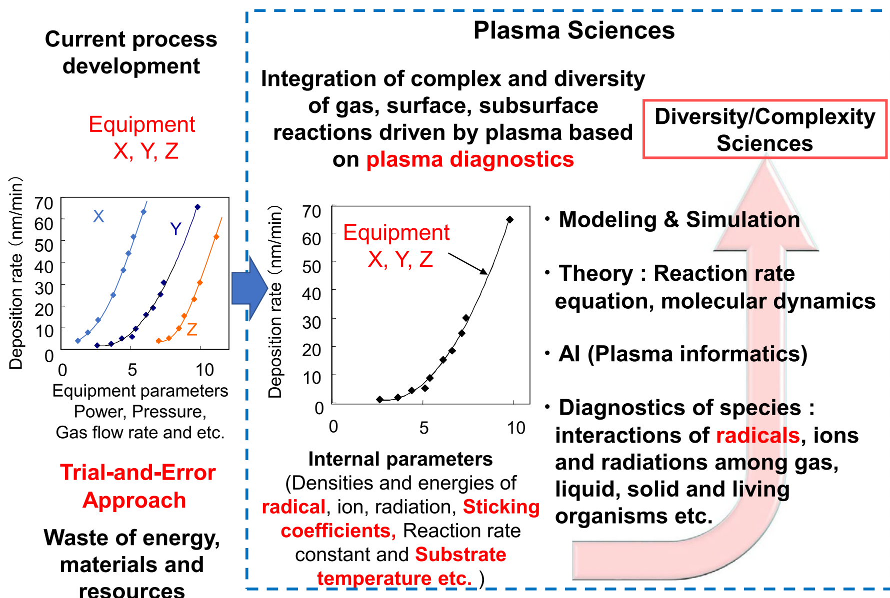

Fig. 2 A potential approach to the systematic development of plasma science

development of plasma science. As an example, in the case of the plasma processing of semiconductors, factors such as the deposition rate are related to the plasma power, pressure and gas flow rate. These external parameters are, in turn, strongly dependent on the type and geometry of plasma equipment, such that the deposition rate characteristics vary from equipment to equipment. As such, these etching characteristics are not purely scientific data. Because a plasma comprises electrons, ions, radicals and radiation, ascertaining the density and energy of these components and describing the deposition characteristics in terms of particle-based parameters (that is, internal parameters) provides equipment-independent scientific data. Monitoring the internal parameters of the plasma, especially the particle properties, can assist in describing various plasma-induced phenomena such that a reliable scientific understanding can be achieved.

During the plasma processing of semiconductors, particles in the plasma interact with solid surfaces and induce phenomena, such as etching and deposition. In particular, the interactions of charged ions and neutral radicals are thought to play a major role in non-equilibrium physicochemical reactions occurring on solid surfaces and/or subsurfaces. Thus, it is important to determine the types of ions and radicals on a solid surface, along with the absolute densities and energies of these species, and to evaluate the reaction rate constants and the loss probabilities of these particles. Such data can be correlated with quantitative etching and deposition characteristics so as to better understand non-equilibrium physicochemical reaction fields.

The reactions in plasmas are diverse and complex as a result of the many reactive species that can be present. The densities and energies of electrons, ions and radiation can be measured using relatively simple methods, while the absolute densities and energies of radicals are very difficult to ascertain, because these species are electrically neutral. As noted, developing a plasma processing science will require an understanding of the behavior of particles in plasmas and of correlations between particles and processing characteristics. The difficulty associated with measuring the densities of radicals is a major challenge in realizing this approach and so the system illustrated in Fig. 2 has not yet been achieved. Furthermore, because plasma treatments are carried out in various environments and there are numerous methods of generating plasmas, data regarding the in situ spatio-temporal distributions of particles, while reactions are taking place are required to understand these processes.

When evaluating the densities of ions and radicals in plasma processes, the densities of the latter will be more than an order of magnitude higher than those of the former. Consequently, radicals play an important role in these systems and should be systematically defined. The standard definition of a free radical is a species having an unpaired electron that is extremely reactive even at room temperature. However, in plasma processes, any electrically neutral reactive particle having a relatively short lifetime that participates in chemical reactions can be referred to as a radical. In a plasma, gas molecules are typically dissociated by collisions with electrons to generate reactive particles, after which these particles collide with other species in the gas phase and eventually reach the surface of the solid or liquid. These reaction processes are very complex. In particular, as the pressure increases, the frequency of collisions between particles in the gas phase increases and the radicals produced by electron impact are transformed into more diverse types by particle collisions.

Therefore, it becomes necessary to measure the spatio-temporal distributions of radicals to fully understand the plasma process and to control the behavior of these species.

Recently, non-equilibrium atmospheric-pressure plasmas have been developed and so the behavior of radicals at ambient pressure has attracted much attention. The mean free path of particles at atmospheric pressure is on the micrometer level and the reactions due to particle collisions in the gas phase are very complex, with many radical species being generated as a result of such collisions. Furthermore, these radical species react with solid surfaces based on their surface loss probabilities. The loss probability for radicals at the surface (equal to the surface reaction probability) is, in turn, determined by the type of radical and its energy, and this probability varies greatly depending on the interactions of the radical with ions. In general, the reactivity of radicals can be increased by irradiation with high-energy ions. The reactions of such radicals with solid surfaces can lead to etching, deposition and surface modification, and some radicals can also form structures with unpaired electrons in solids. Recently, with the development of non-equilibrium atmospheric-pressure plasmas (that is, low-temperature atmospheric-pressure plasmas), the interactions of radicals with liquids have also become of interest as gas phase radicals will react with liquids to produce new radical species in the liquid.

The reactions of radicals in liquids are more complex than those on solid surfaces, and these species are typically transformed into chemically stable particles within a short time frame. Reactions between radicals in liquids and living organisms can also have bioactive effects, such as stimulating an organism to generate radicals and inactivating molecules in the organism by inducing various signal transductions (that is, forming in vivo radicals). The various bioactive substances that can be induced in living organisms in this manner can potentially result in the selective destruction of cancer cells as well as wound healing, gene transfer, regeneration of living tissues, promotion of plant growth, inactivation of viruses and killing of pathogens. The potential for chains of radical reactions from the gas phase to the interiors of living organisms has led to the emergence of new fields, namely, plasma medicine and plasma agriculture.

Figure 3 provides an overview of potential future innovations that could be brought about by the systematization and control of radical reactions in plasma processes. These processes have the potential to realize nano-information devices and environmental innovations that will create an advanced future society. To accomplish these goals, several developments are required. These include devising means of assessing the spatio-temporal distributions of radicals, quantification of the fundamental physical properties of radicals (such as surface reaction probabilities) and the effects of these properties, modeling and simulation of radical reactions, development of approaches to controlling radicals, and research into new technologies to control radicals. As shown in Fig. 3, innovations in silicon-based ultra-large scale integrated circuits (ULSIs), quantum devices, cell phones, artificial intelligence (AI) and nano-information devices may allow the realization of an advanced society. These innovations will require ultra-precise control of the behavior of radicals and ions in ultra-high density plasmas. In particular, the development of large-area, high-throughput, ultra-high density plasma devices and autonomous plasma

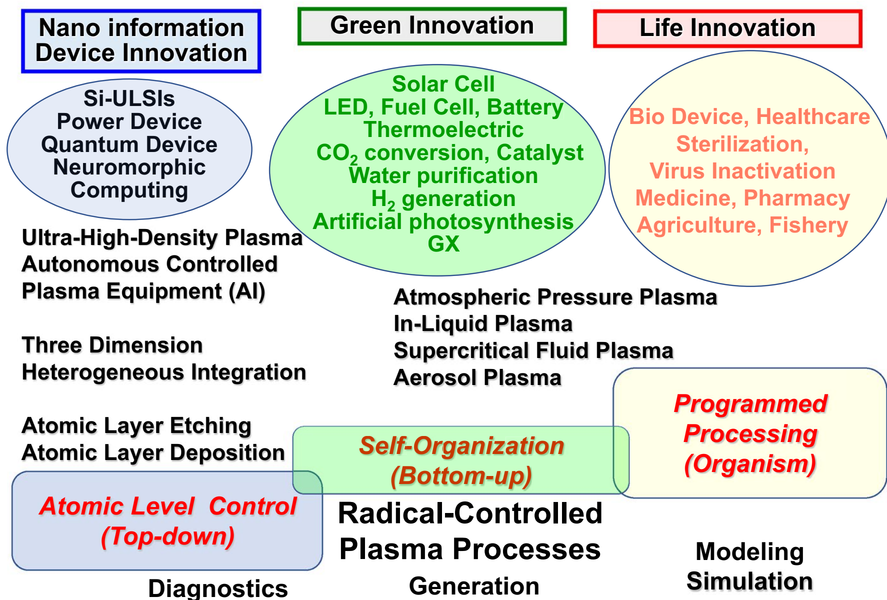

Fig. 3 An overview of potential future innovations that could be brought about by systematization and control of radical reactions in plasma processes

generation systems capable of fine spatio-temporal control of particle fluctuations will be necessary (Hori et al. 2011). It will also be a requirement to incorporate self-organized reactions to allow the fabrication of ULSIs in conjunction with ultra-fine processing on the 1 or 2 nm scale. Currently, technologies to process materials in atomic layer units (atomic layer etching) (Kanarik et al. 2015; Oehrlein et al. 2015) and to deposit thin films in atomic layer units while processing solid surfaces (ALE: atomic layer deposition) are being developed (George 2010; Puurunen 2014; Johnson et al. 2014). Therefore, it is necessary to control the spatio-temporal fluctuations of the densities and energies of radicals in the plasma and to be able to observe and precisely control the solid surface reactions induced by radicals at the atomic level.

The plasma processes on which etching is based are able to produce three-dimensional (3D) heterogenous integrated microstructures by controlling the particles in the plasma, meaning that this is a so-called top-down process. As shown in Fig. 3, the use of self-organization phenomena induced by plasmas has attracted attention as a mean of realizing environmentally friendly innovations related to fuel cells, batteries, light-emitting diodes, solar cells, power devices, thermal electronic devices, carbon dioxide conversion and catalysis. The tuning of radical reactions could also allow the synthesis of nanomaterials with one-dimensional (1D), two-dimensional (2D) or 3D structures through self-assembly, equivalent to a bottom-up process. Thus, radical-controlled plasmas are expected to result in the creation of functional materials with ultrafine structures and new properties via the integration of top-down and bottom-up processes.

The last part of Fig. 3 shows the development of non-equilibrium atmospheric-pressure plasmas and non-equilibrium liquid plasmas, which has been actively pursued since approximately 2000. Studies have led to industrial applications, such as ultrafast material surface modification, bonding processes and the high-speed synthesis of nanoparticles. The development of room-temperature and room-pressure plasmas have also made it possible to irradiate pathogens, cells and biological tissues with plasmas. Starting with the use of plasmas for sterilization and disinfection, plasmas were later applied in the fields of medicine, pharmacy, agriculture and fisheries. As an example, it is now evident that plasma-based radicals can interact with various biological tissues to induce controlled and regulated cell suicide in vivo, meaning programmed cell death, such as apoptosis.

In this review, the principles of radical-controlled plasma processes are explained in Sect. 2, followed by examinations of techniques for assessing gas phase radicals during plasma processing in Sect. 3, approaches to radical-controlled plasma processes in Sect. 4, and radical-controlled plasma etching, thin-film deposition and growth processes in Sect. 5. Autonomously controlled radical processes are described in Sect. 6, radical control in atmospheric-pressure plasma processing in Sect. 7, the effects of direct irradiation with radicals on living organisms in Sect. 8, the development of plasma-activated media in Sect. 9, radical-induced material processing in liquids and/or interfaces in Sect. 10, and future prospects in Sect. 11. Section 12 provides a summary of radical-controlled plasma processes.

2 Principles of radical-controlled plasma processes

2.1 Generation of radicals

Figure 4 summarizes a plasma-based process. In such systems, active species such as ions, radicals and photons are generated on the basis of the ionization, attachment, dissociation and excitation of gaseous species by collisions with electrons. Reactive plasmas produce non-equilibrium physico-chemical reaction fields due to the inclusion of chemically active species, and these can be distinguished from the physical fields associated with noble gas plasmas. It is important to note that the formation of radicals in a plasma is completely different from the dissociation of molecules resulting from thermal excitation or other means. During the dissociation of a molecule in response to heat, the position and velocity of the molecule change and the distance between the nuclei along the dissociation potential curve varies. This causes the potential energy of the system to increase above the bond dissociation energy such that the molecule dissociates. In contrast, in the case of a plasma, collisions with electrons excite molecules without changing their position or velocity, leading to ionization and/or dissociation according to the Frank–Condon principle. Thus, when electrons having energies of several eV collide with gas phase molecules, high-energy active species (ions, radicals and photons) are produced. The generation of these products via thermal energy requires temperatures of several thousand degrees, whereas these can be obtained at relatively low temperatures in a plasma.

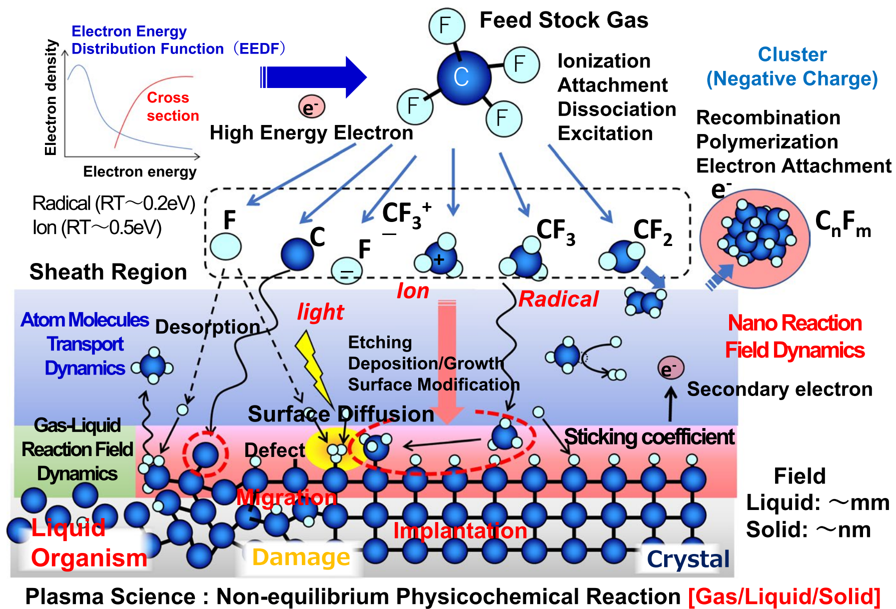

Fig. 4 The scheme of the plasma-based process

The frequency at which a given feedstock gas undergoes electron impacts can be expressed as kn_e, where k and n_e denote the rate constant for the collision process and the electron density, respectively. Therefore, the rate of generation of active species by ionization, dissociation or excitation per second per unit volume can be written as

$$G = k\, n_e n_g, \tag{2.1}$$

where n_g is the feedstock gas density. The value of k can be calculated as

$$k = \int \sigma(E) \cdot v \cdot f(E)\, \mathrm{d}E = < \sigma v >, \tag{2.2}$$

where E is the energy of electrons in the plasma, $\sigma(E)$ is the cross-sectional area of the collision process between electrons and the source gas (that is, the probability that the molecules will be ionized or dissociated in a given collision), and v is the velocity of an electron during a collision, that is $(2E/m)^{1/2}$ and $f(E)$ are the electron energy distribution function ($EEDF$). The value of $f(E)$ can be obtained based on Maxwell's energy distribution equation, written as

$$f(E) = \left(\frac{4E}{\pi}\right)^{\frac{1}{2}} \left(\frac{1}{k_B T_e}\right)^{\frac{3}{2}} exp\left(-\frac{1}{k_B T_e}\right) \tag{2.3}$$

where T_e and k_B are the electron temperature and Boltzmann constant, respectively. The number of reactive particles produced is determined by the collision cross section for each process relative to the energy distribution of the electrons.

During the formation of radicals, the dissociation cross section for the gas is determined by the type of gas molecules that are present. Therefore, the *EEDF* in the plasma and the choice of feedstock gas are important aspects of reactive particle formation. In reactive plasma processes, a wide variety of active species are produced simultaneously. Some of these are important to the processing performance, while others are detrimental to the process. If the density of active species required for high processing performance can be increased (in particular that of radicals) and an optimal plasma composition can be obtained, then very high precision can be achieved. This is the essence of radical-controlled plasma processing, which is the primary subject of the present paper. As indicated by Eq. (2.1), it is important to select the optimum gaseous reactant so as to achieve the desired radical composition and density, and to control the ionization and dissociation of the raw material to provide the optimum *EEDF* and electron density for radical generation.

The residence time of gas molecules in the plasma, τ, can be expressed as

$$\tau = pV/S, \tag{2.4}$$

where p is the pressure, V is the volume of the plasma, and S is the flow rate of the gas. The density, n, of radicals produced by collisions between electrons and the reaction gas in the plasma is

$$n = \tau n_e < \sigma v > n_g \tag{2.5}$$

Equation (2.5) demonstrates that, because the *EEDF* is a function of electron temperature, the radical generation process in the plasma can be tuned by controlling the reaction gas type, electron temperature, electron density and gas residence time.

Finally, the density of the radicals (based on the balance between radical generation and loss) can be expressed by Eq. (2.6). Here, k_e and k_e' are the rate constants for electron impact dissociation (in the case that the electron temperature varies spatially), while n_e is the electron density, n_g is the density of the feedstock gas, n is the density of the active species (that is, neutral radicals), N_1 is the density of particles, k_1 is the rate constant for reactions between particles and radicals, for example, N_2 is the density of other particles, and k_2 is the rate constant for reactions between these particles and radicals. The radical production rate resulting from electron impact is $k_e n_e n_g$, while that resulting from reactions is $k_1 n N_1$. The losses stemming from electron impact, gas phase reactions, reactions at surfaces or walls and diffusion or pumping are $k_e' n_e n$, $k_2 n N_2$, n/τ_s and n/τ, respectively. Here, τ_s and τ are the lifetimes of the particles before they are depleted by surface reactions or by diffusion/pumping, respectively.

For these particles, the conservation rate in the steady state (meaning that production and loss are in equilibrium) can be expressed as

$$\frac{dn}{dt} = k_e n_e n_g + k_1 \, \mathrm{n} N_1 - k_e^{'} n_e \mathrm{n} \; - k_2 \mathrm{n} N_2 - \; \mathrm{n}/\tau_s - \; \mathrm{n}/\tau, \tag{2.6}$$

The diffusion lifetime, τ_s, can be calculated as (Chantry 1987)

$$\tau_s = \frac{p\Lambda}{D} + \frac{2l_0}{v\beta}(2 - \beta) \tag{2.7}$$

where Λ_0 and l_0 are the geometric diffusion length and the volume-to-area ratio of the chamber, D is the diffusion coefficient and β is the loss probability for radicals.

2.2 Extinction terms for radicals

As shown in Fig. 4, the radicals produced in the plasma are injected into a material (either a solid or liquid) via collisions in the gas phase which depend on the mean free path. The velocities of the neutral particles (that is, the radicals) produced by the plasma have a Maxwellian distribution at thermodynamic equilibrium. Therefore, the average velocity, $< v >$, of these particles when incident on a surface will equal the sum of the velocities of all the molecules divided by the total number of molecules. Consequently, the velocity (or flux) of the particles at a given solid surface can be expressed as

$$\begin{aligned}
\Gamma_x &= \int_0^\infty v_x dn\left(v_x\right) \\
&= n\left(\frac{m}{2\pi k_B T}\right)^{\frac{1}{2}} \int_0^\infty v_x \exp\left(-\frac{m v_x^2}{2k_B T}\right) \\
&= n\left(\frac{k_B T}{2\pi m}\right)^{\frac{1}{2}} \\
&= \frac{1}{4} n\langle v \rangle
\end{aligned} \tag{2.8}$$

where

$$\langle v \rangle = \sqrt{\frac{8k_B T}{\pi m}} \tag{2.9}$$

Here, m and T are the mass and temperature of the radicals. Radicals that contact the surface of a solid or liquid will react with that surface to cause etching, deposition or surface modification, upon which the radical disappears.

Figure 5 presents a diagram of the surface reactions of such radicals and indicates that some of the incident radicals do not contribute to the surface reaction and are reflected directly, based on the reflection probability. Others diffuse across the

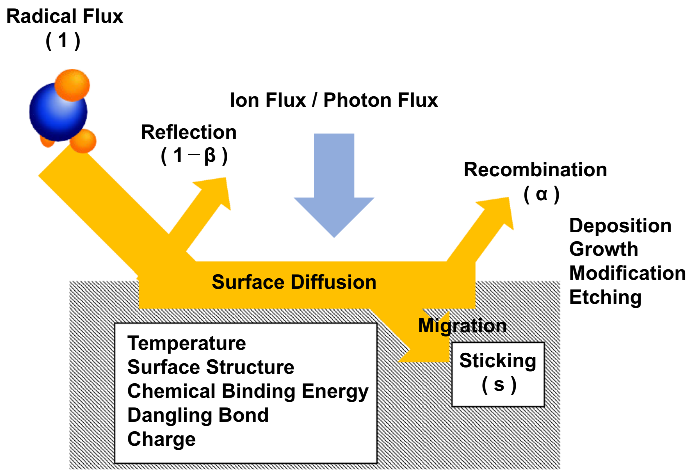

Fig. 5 The schematic diagram of the surface reaction of radicals

surface, recombine to form other molecules and disappear, based on the recombination probability (γ). Those that remain will adhere to the surface and result in reactions, according to the sticking probability (s). Therefore, the total loss probability (β) is $\gamma + s$ and the reflection probability is 1-β. It is important to understand this loss probability to control the radicals (Perrin et al. 1998). The relationships between processing characteristics (such as etching, deposition and surface modification) and the value of β or s can be summarized as

$$\Gamma_{\text{radical}} = n\sqrt{\frac{8kT}{\pi m}} \tag{2.10}$$

and

$$\Gamma_{radical} = \frac{1}{4}\frac{s}{1-\beta}n'\sqrt{\frac{8kT}{\pi m}}, \tag{2.11}$$

where n' is the density of radicals at the surface of the substrate. It should be noted that the spatial distribution of radicals is required to estimate their contribution to the reaction using Eq. (2.11). The radical loss probability can vary greatly depending on several factors. These factors include the chemical binding energy, the presence of dangling bonds and defects, the surface structure and the surface morphology, all of which can affect the chemical composition and energy states of the material with which the radicals react. Other important parameters are the temperature of the material, the surface charge, and the densities and energies of charged and neutral particles. It is known that these factors can greatly affect the etching and deposition rates, especially as the interactions between the incident ions and radicals with the substrate are modified. In the case that the incident ion energy is low, the ions can

interact with radicals to promote thin-film formation (Shiratani et al. 1998) and surface modification on the substrate and/or reactor walls. In contrast, if the ion bombardment energy exceeds the material bond threshold, the substrate will be etched by reactive sputtering and the etching rate will increase along with the incident ion energy. Therefore, the loss term at the surface will vary greatly as the density and energy of the incident ions are changed.

On this basis, it is evident that tuning the radical surface loss probability is a very important aspect of radical-controlled plasma processing. This tuning requires that the correlations between processing characteristics (such as etching rate, deposition rate and surface modification), and the surface loss probability under various conditions, are known. In contrast, when atmospheric-pressure non-equilibrium plasmas interact with liquids, the surface loss probability for radicals entering from the gas phase is expected to be almost unity, although data to this effect have not yet been reported and so this represents a new research area in this field. A variety of radical species, such as reactive oxygen species (ROS) and reactive nitrogen species (RNS), are generated in liquids irradiated with plasma. Since the densities and lifetimes of these radicals are greatly affected not only by the type of liquid but also by temperature and pH, there is a need to establish technology to control radicals in liquids. Of particular interest are the various radical scavengers that have been developed to inactivate radicals in solution. The resulting concentration of radicals can be determined by the balance between the generation and annihilation rates as in Eq. (2.6) and adjusting these terms allows the density of radicals in the liquid to be tuned.

Figure 6 summarizes the possible radical generation and extinction processes that are available for radical control. Radical-controlled plasma processes can be realized

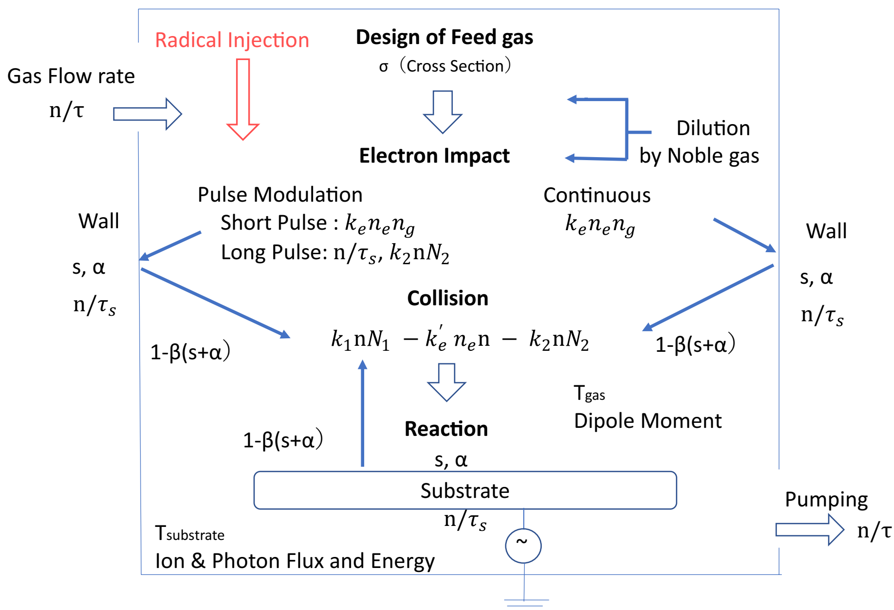

Fig. 6 The scheme of the possible radical generation and extinction processes for radical control

by adjusting the factors in Eq. (2.6). In addition, Hiramatsu et al. (2004) have developed a new radical control method, which was named radical injection by Hori in which the desired radicals are pre-generated externally and injected into the plasma processing space, as described in Sect. 5.10.1. Using this method, it is possible to control radicals beyond the framework of the gas generation term based on electron impact and reaction factors.

3 Measuring gas phase radicals during plasma processing

A number of methods have been developed to ascertain the composition, density and dynamics of radicals in plasma processes and to understand the behavior of these radicals, which play important roles in the process. Figure 7 presents the typical techniques used to monitor radicals and trends in the various radical types with respect to the particle parameters that determine the radical generation term in Eq. (2.5). Further information regarding techniques for measuring radicals in plasmas is available in the literature (Hori et al. 2002; Bruggeman et al. 2016).

A variety of gases are used in plasma processes and numerous radical species can appear in plasmas. As an example, when fluorocarbons, hydrocarbons or silicon hydride are introduced as the feedstock gas, radicals are generated according to Eq. (2.5). The density and energy distribution function for electrons in the plasma, which are important factors in the generation of these radicals, can be measured

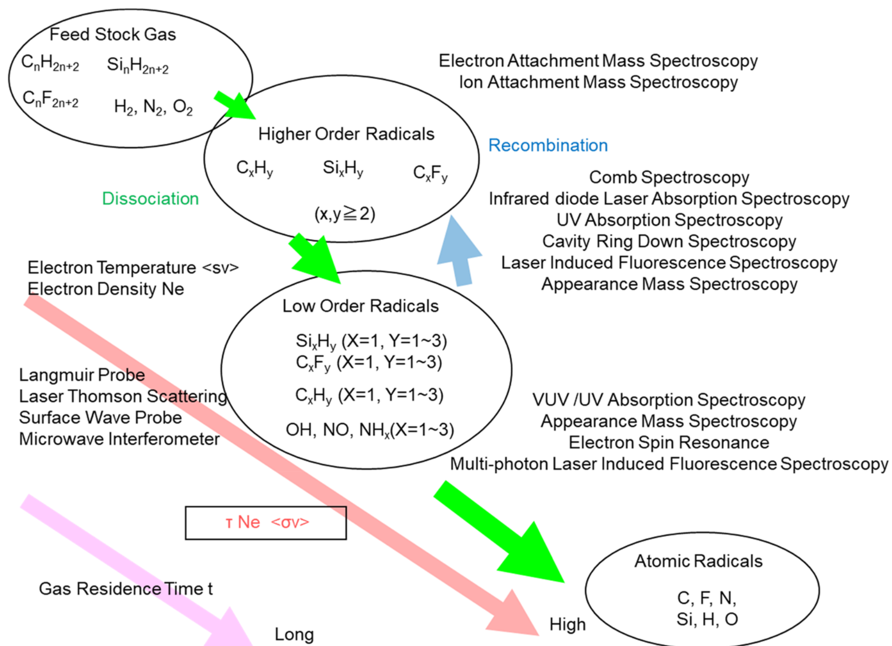

Fig. 7 The typical techniques used to monitor radicals and trends in the various radical types with respect to the particle parameters that determine the radical generation term in Eq. (2.5)

using a Langmuir probe, absorption probe, laser Thomson scattering spectroscopy or microwave interferometry. Radicals produced by electron impact dissociation of the feedstock gas molecules can be classified into higher order, lower order or atomic radicals. The higher order radicals can be monitored using electron or ion attachment mass spectrometry, while lower order radicals can be measured by mid-infrared time-resolved frequency comb, infrared diode laser absorption, ultraviolet absorption, ring-dye laser absorption, cavity ring-down, laser-induced fluorescence (LIF), laser resonance ionization or appearance mass spectroscopic techniques. Atomic radicals can be examined using vacuum ultraviolet absorption spectroscopy (VUVAS), multiphoton LIF, appearance mass spectrometry or electron spin resonance (ESR). Comb spectroscopy in particular has recently received much attention and dual comb techniques can generate a wide range of wavelengths in the mid-to-near-infrared region, allowing OH radicals to be monitored.

In radical-controlled plasma processing, it is also necessary to determine the spatio-temporal distribution of various radicals in the gas phase with respect to parameters, such as the absolute density and energy of the radicals (meaning the oscillation, rotation and translation temperatures). In the case of the pulsed plasmas described below, high-precision plasma processing can be obtained using pulses to control the dynamics of radical formation and annihilation based on the fundamental properties of radicals, such as their reaction and diffusion constants and extinction and attachment probabilities. In particular, the lifetimes of radicals during the off time between pulses is an important factor when designing the process.

4 Approaches to radical-controlled plasma processes

Abe et al. (2008) proposed an approach to developing a plasma-based etching process in which the reaction products are removed by an exhaust stream. For this method to be viable, it is necessary to determine the reaction products in the plasma while assuming that the products will eventually become volatile such that they can be removed using a pump. As an illustration of this process, the chemical binding energies and volatilities/vapor pressures and boiling points of the reaction products that may be produced by the interaction of radicals and ions in the plasma during ULSIs fabrication are summarized in Table 1. Based on these data, we can estimate the possible reactions that can occur in the plasma, the volatile reaction products and the required processing temperatures and energies. In particular, from the vapor pressure values, it is possible to define the gas pressure and plasma source needed to drive the desired etching reaction, shape (isotropic or anisotropic) and rate. The raw material gas that is required and the radicals that will be produced from that gas are determined based on Eq. (2.5). Here, the important parameter is the electron temperature, which is responsible for the majority of the gas-dependent plasma characteristics and in turn is affected by the gas pressure, gas flow rate, applied field strength and frequency, reactor structure and wall material, in addition to the processing conditions. The accumulation of the self-bias voltage (V_{dc}) that appears on the surface of a substrate on a radio frequency (RF) biased electrode is also an important process parameter that can control the energy of the incoming ions and

Table 1 Properties of typical gases and materials used in plasma etching processes

Material	Substance	Mask	Gas	Bond dissociation Energy (eV)	Boiling point (℃)	
Semiconductor	Si GaN	Organic SiO_2	F_2 SF_6 NF_3 Cl_2 HBr	Si-Si:3.21, Si-H:3.04 Si-F:5.97, Si-Cl:4.32, Si-Br:3.71 Ga-Ga:<1.10 Ga-H:2.76, Ga-O:3.88, Ga-N:2.4 Ga-F:6.05, Ga-Cl:4.80, Ga-Br:4.17 N-N:9.76, N-H:<3.51, N-O:6.55 N-F:<3.62, N-Cl:3.46, N-Br:2.91	SiH_4:-112 SiF_4:-86 $SiCl_4$:59 $SiBr_4$:154 Ga_2H_6:139 GaF_3:1000 $GaCl_3$:201 $GaBr_3$:279	Cl_2:-34 F_2:-188 HBr:-67 NF_3:-129 NCl_3:71 CCl_4:-77
	Graphene		H_2 O_2	C-C:6.41 C-H:3.51, C-O:11.16, C-N:7.77 C-F:5.33, C-Cl:4.09, C-Br:3.30	CO:-192 CO_2:-78	
Metal	W	Organic	SF_6 NF_3 Cl_2	W-W:6.90 W-O:7.46 W-F:5.64, W-Cl:4.34	WF_6:17 WCl_6:337 $WOCl_4$:232	
	Al	Organic	Cl_2 HBr	Al-Al:2.74, Al-H:2.98, Al-O:5.20, Al-N:3.81 Al-F: 7.00, Al-Cl:5.20, Al-Br:4.45	$AlCl_3$:180 AlF_3:1276	
Dielectric	SiO_2 $SiOCH_3$ Si_3N_4	Organic Carbon	CF_4 C_2F_6 C_4F_8 CHF_3	Si-O:8.29, Si-N:4.53, Si-C: 4.63	CH_4:-161.5 CHF_3:-82 CH_2F_3:-52 CH_3F:-78	CF_4:-128 C_2F_6:-78 C_4F_8:-6.0
	Organic	SiO_2 Carbon	H_2 N_2 O_2	CH_3-C(O)OH: 4.0 $CH_3C(O)$-OCH_3:4.4 CH_3COOC-H_3:4.2	C_2N_2:-21	

their distribution. When selecting the feedstock gas, it is also important to carefully select the global warming potential of this gas to protect the environment.

When developing plasma processes, it is vital to understand the correlation between equipment parameters (that is, external parameters), such as pressure, power and gas flow rate, and internal parameters related to electron temperature, electron density and particle densities/energies, as shown in Fig. 2. Figure 8 summarizes the particle parameters based on the radicals in the plasma as well as approaches to controlling radicals during plasma processes. As a model process, we here discuss thin-film deposition using a SiH_4 plasma as an example, in accordance with Fig. 8. Chittick et al. (1969) showed that hydrogenated amorphous silicon can be obtained by decomposing silane using a glow discharge, representing a breakthrough in plasma-based thin-film formation. Spear et al. (1975) succeeded in controlling the charge of amorphous silicon thin films deposited by glow discharge and discovered that these films could be applied to semiconductor devices. In 1980, the industrialization of amorphous silicon thin-film solar cells was initiated. Around the

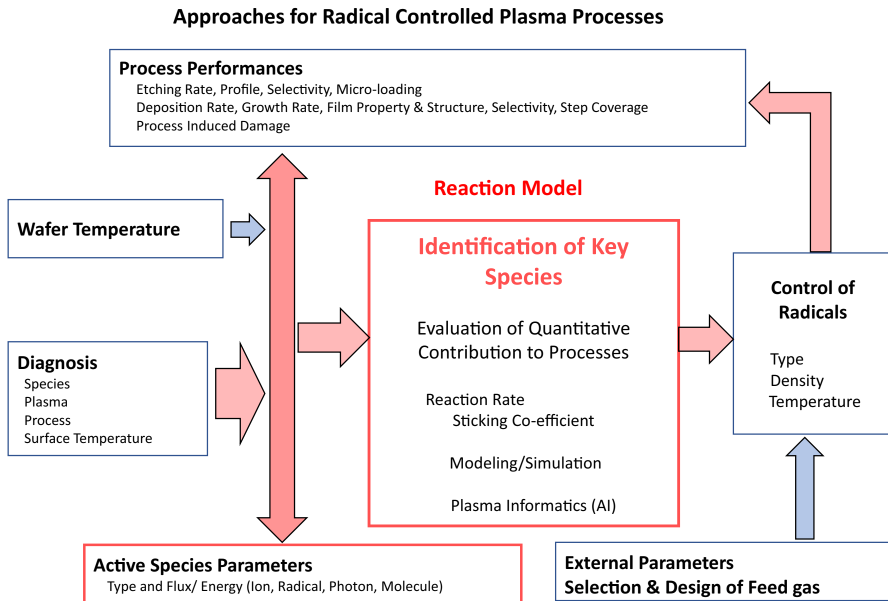

Fig. 8 The particle parameters based on the radicals in the plasma and the approach for radical control in the plasma process

same time, Madan et al. (1979) and Matsuda (2004) discovered that microcrystalline silicon (μc-Si) could be formed at low temperatures by diluting a large volume of hydrogen gas in conjunction with plasma enhanced chemical vapor deposition (PECVD).

This discovery drew attention to the behavior of deposition precursors and hydrogen atoms during deposition in plasma processes using silane and hydrogen gas, and led to the construction of a model for the growth mechanism. This research, in turn, resulted in the production of thin-film silicon devices for solar cells. Subsequently, microcrystalline silicon thin films were also employed in thin-film transistors for liquid–crystal displays, leading to new breakthroughs in electronic devices. However, it remains necessary to improve the properties of amorphous silicon and microcrystalline silicon thin films, and new advances in plasma processes may make this possible. For this purpose, it is necessary to understand the gas-phase and surface reactions of active species in plasmas, especially process-critical radicals, and to construct thin-film deposition models to control critical radicals, as shown in Fig. 8.

Many researchers are working to establish these methods, and the properties of particles in H_2 diluted SiH_4 plasmas are becoming clearer. Based on correlations between thin-film properties and experimentally observed radical behavior, the radicals acting as precursors for thin-film deposition (e.g., SiH_3) have been identified and their densities and surface adhesion coefficients determined. Other radicals, such as H, that are considered to be important during thin-film deposition by etching and the chemical termination of surfaces have also been identified. The densities and surface adhesion coefficients for such active species have also been clarified.

Observations of various radicals in plasma processes and investigations of the surface attachment coefficients for these radicals have provided important insights into the most important species involved in such processes (Perrin 1998; Hori 2007). Recently, it has also become possible to predict process performance using simulations predicated on these basic parameters. Artificial Intelligence (AI)-based machine learning using large experimental data sets has been employed to derive important parameters for such processes. In fact, models of radical behavior constructed from assessments of the gas phase and surface reactions of these radicals have shown that SiH_3 are the most important species serving as precursors for the fabrication of defect-free microcrystalline silicon thin films involved in the formation of high-quality amorphous silicon (a-Si) and μc-Si thin films. Such studies have examined the spatial distributions of densities of SiH_3 using IRLAS (Infrared diode laser absorption spectroscopy) (Itabashi et al. 1988, 1990) and have also clarified the densities of H (Takashima et al. 2001), which play an important role in promoting the surface reactions of SiH_3 in the process plasma. The reactions of these radicals have been found to be dependent on the surface temperature (Matsuda et al. 1990). A surface reaction model for radicals at relatively low pressures has been proposed by Perrin (1991), as shown in Fig. 9 and established, based on the accumulation of many measurements of radicals in silane plasmas (Matsuda 2004).

Interestingly, Abe et al. (2013)) determined the density and extinction times for H in a SiH_4/H_2 plasma at room temperature using VUV absorption spectroscopy (VUVAS) with a micro hollow-discharge cathode lamp (MHCL) (Takashima et al. 1999) and found that the surface loss probability for H varied from 0.01 to 0.32 as the flow rate of SiH_4 was adjusted. This probability was also greatly affected by the interaction between the surface and deposited species, such as SiH_3, acting as thin-film precursors. Furthermore, it was found that the surface loss probability for H becomes 1 at a substrate temperature of 200 °C even after deposition. These results indicated that SiH_3 and H were important active species that had a significant impact on thin-film formation.

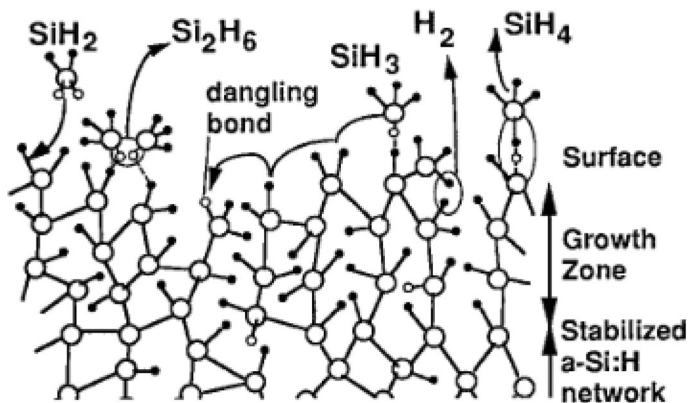

Fig. 9 Plasma induced surface reactions during a-Si:H film growth (Perrin 1991)

Regarding behaviors of radicals at a low pressure in the high-density plasma, the densities of Si, SiH and SiH_3 radicals in the electron cyclotron resonance (ECR) SiH_4/H_2 plasma, where SiH_4 feed stock gas was much depleted were measured as a function of microwave power and total pressure, using IRLAS and ultraviolet absorption spectroscopy (UVAS). It was clarified that Si, SiH and SiH_3 densities in the $SiH_4(50\%)/H_2$ ECR plasma were 3.6×10^9, approximately 1×10^9 and 1.7×10^{10} cm^{-3}, respectively, at the microwave power of 400 W and the total pressure of 1.3 Pa and SiH_3 densities were decreased comparing with those of RF plasma (Yamamoto et al. 1994).

However, the mass production of a-Si and μc-Si thin films has been performed at relatively high pressures (approximately 1200 Pa) for obtaining higher deposition rates. Therefore, the information on the density of SiH_3 and H in the high-pressure region was needed. Abe et al. (2017) quantitatively evaluated the contribution of these radicals to thin films in a PECVD system for the production of actual solar-cell devices. The absolute densities of H and SiH_3 were measured under mass-production processing conditions while forming μc-Si thin films using a mixture of SiH_4 and H_2 gases at 1200 Pa in a 60 MHz very high frequency (VHF) parallel-plate plasma CVD system. These trials established the contributions of these species to thin-film formation. This work was highly valuable, since it represented the first investigation of the radicals active in the mass production of thin films for solar cells at high pressures.

In this study, the absolute density of H was measured by a two-photon resonance four-wave mixing technique in conjunction with VUV laser absorption spectroscopy (VUVLAS) and a Lyman-α light source emitting at 121.6 nm, employing the apparatus shown in Fig. 10 (Abe et al. 2012). The density of SiH_3 radicals was ascertained by cavity ring down spectroscopy operating at wavelengths of 220 and 280 nm under the same conditions, using the apparatus shown in Fig. 11 (Abe 2013).

Figure 12 plots the variations in the cavity losses at wavelengths of 220 and 280 nm in this system over time. At 220 nm, absorption due to SiH_3 was observed along with losses due to scattering by nanoparticles, while at 280 nm only light scattering and absorption by nanoparticles was evident. At 2 ms after plasma ignition, a cavity loss at 220 nm was observed but not at 280 nm, while at 3 ms absorbance at 280 nm appeared and increased rapidly. After 8 ms, the values of both signals were almost the same. Interestingly, at a pressure of 1200 Pa, particles were produced within only 3 ms after plasma ignition. This result indicates that, following ignition, the number of fine particles generated in the plasma increased rapidly as a result of gas phase reactions between SiH_4 and short-lived SiH_2. Therefore, the difference between these two values of 220 nm and 280 nm could be used to estimate the density of SiH_3 (Abe et al. 2017).

Figure 13 summarizes the variations of SiH_3 and H densities as the SiH_4 flow rate is varied at a H_2 gas flow rate of 470 sccm and at 1200 Pa, which are typical conditions for device production. Based on these radical measurements and the actual deposition rates, the quantitative contribution of SiH_3 to thin-film formation was evaluated based on Eq. (2.10). Using a sticking probability (s) of 0.09 (Itabashi et al. 1990) and a radical temperature of 473 K, this contribution was found to be 45%. When evaluated using Eq. (2.11), the contribution was at most 59% when employing

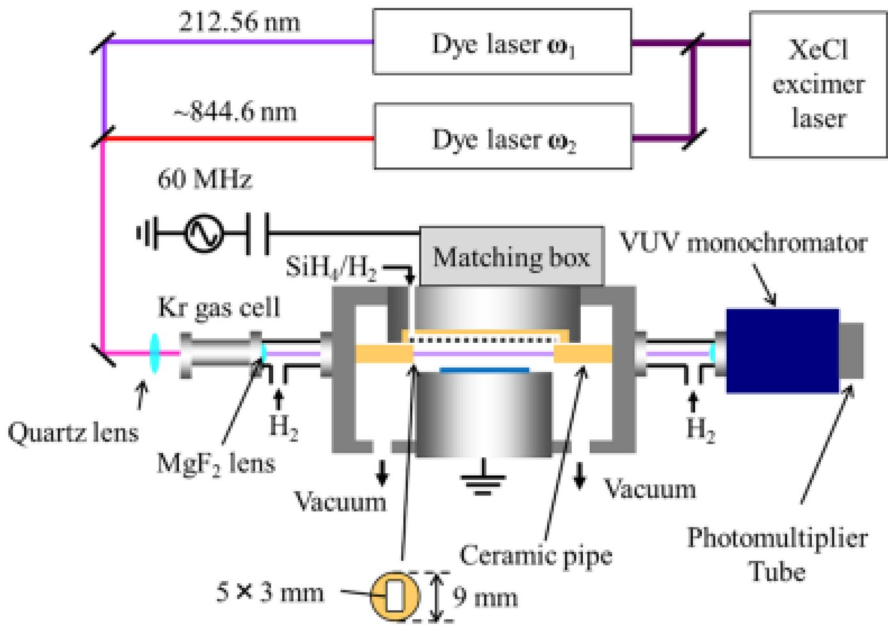

Fig. 10 The measurement system for the absolute density of H by two-photon resonance four-wave mixing technique using VUVAS with Lyman-α light at 121.6 nm (Abe et al. 2012)

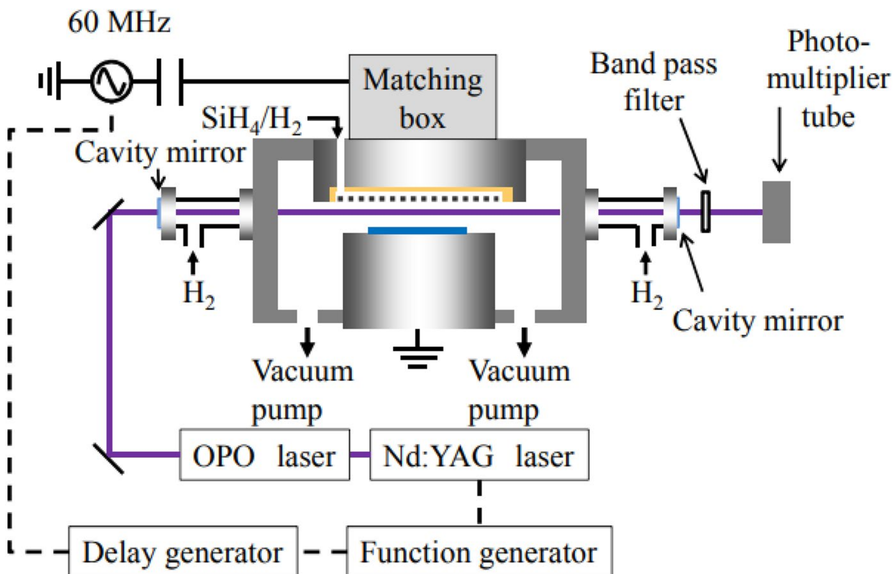

Fig. 11 The measurement system for the absolute density of SiH_3 by CRDS using wavelengths of 220 nm and 280 nm (Abe 2013)

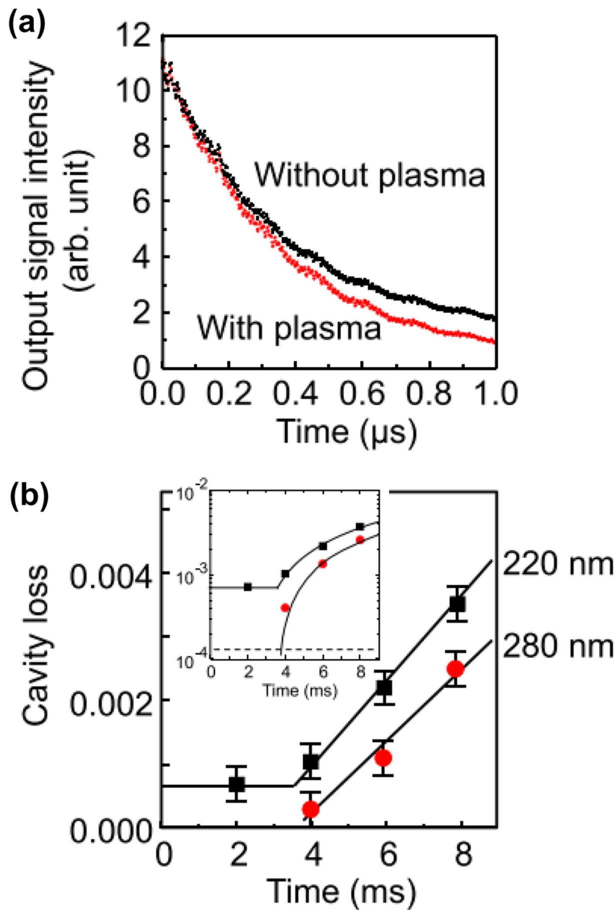

Fig. 12 **a** Typical CRDS cavity decay profiles with and without plasma. **b** Time-evolution of cavity loss after plasma ignition at wavelengths of 220 and 280 nm. The lines are guides for the eye. Inset figure shows a logarithmic plot. The dashed line is a limit of detection (Abe et al. 2017)

a total loss probability (β) of 0.5 (Matsuda 2004). These results demonstrate that the contribution of SiH_3 to the formation of high-quality thin films is on the order of 50%, with the remainder of the process supported by short-lived radicals (such as Si, SiH and SiH_2), higher order radicals and fine particles.

The relationships between the properties of the deposited thin film, the actual contributions of the precursors and the proportion of the H flux contributing to the surface reactions are shown in Fig. 14 (Abe et al. 2012). The φ_c, I(220)/(111) and N_d (10^{16} cm^{-3}) values indicate the results obtained by evaluating the thin-film crystallinity using Raman spectroscopy, assessing the degree of crystalline orientation, (220)/(111), by Xray diffraction and examining the defect density by ESR, respectively. As noted earlier, the surface loss probability, s, for H in Eq. (2.10) is reported

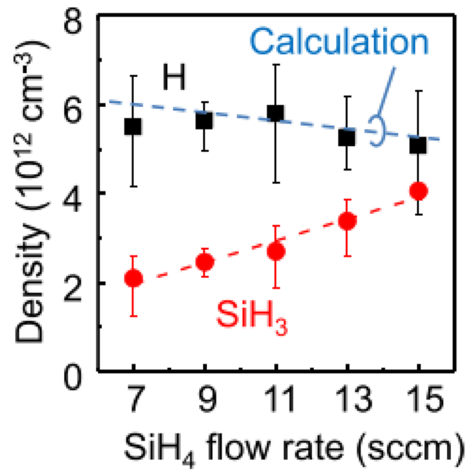

Fig. 13 SiH_3 density as a function of SiH_4 flow rate. The dashed lines through the data are a guide for the eye. For reference, the H density from (Abe et al. 2012) is also reproduced here. The dashed line shows the calculated H density (Abe et al. 2017)

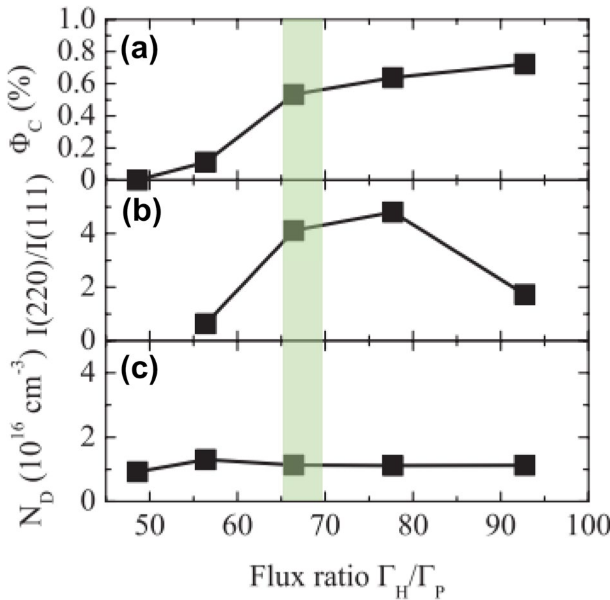

Fig. 14 Film properties interpreted in terms of the flux ratio Γ_H/Γ_p (Abe et al. 2012)

to be 1 when the substrate temperature is 200 °C (Abe et al. 2013). The contribution of all precursors can be estimated from the deposition rate using the equation:

$$\Gamma_p = \frac{R_d \rho}{m_{Si}}, \tag{4.1}$$

where R_d is the deposition rate, ρ is the film density (2.18 g cm^{-3}) and m_{si} is the atomic mass of silicon (4.69×10^{-23} g). Therefore, the flux values represent the relationships between all deposition precursors and the H during the reactions associated with thin-film formation. These relationships in turn determine the thin-film properties, as shown in Fig. 2, and provide a key information regarding radical control during plasma processing, as shown in Fig. 8. In practice, the fabrication of high-quality thin films requires a crystallinity of approximately 50 to 60%, a preferential < 110 > orientation and a low defect density ($<10^{17}$ cm^{-3}). In addition, the flux of precursors and H must be controlled to be within the range of 65–70, which is understood to be located in the transition region from a-Si to μc-Si. As a result, to obtain higher quality thin films with greater deposition rates, it is important to optimize the process using internal parameters to further increase the SiH_3 contribution together with that of H so as to maintain a flux ratio of 65–70.

In summary, during plasma CVD of amorphous silicon thin films and microcrystalline silicon thin-film devices, SiH_3 and H are important active species and are vital to the formation of high-quality thin films. It is, therefore, crucial to evaluate the densities and surface attachment coefficients (that is, the surface reaction constants) for both radicals under conditions conducive to mass production processes. The proportional contributions of these radicals to thin-film formation must also be estimated. On this basis, the properties of the resulting thin films can be predicted using an internal parameter known as the radical density ratio. Evaluating these radical-based internal parameters in a stepwise manner while clarifying their relationships with plasma processing characteristics will allow the control of radicals leading to various innovations. The systematic accumulation of large data sets concerning the behavior of radicals in the gas phase via real-time measurement and diagnostic techniques and subsequent data analysis using AI is also expected to identify important active species and improve the plasma processes by allowing control of these species.

5 Radical-controlled plasma etching, thin-film deposition and growth processes

5.1 Design of feedstock gases for SiO_2 etching

When the material to be etched is known, the possible reaction products can be carefully investigated on the basis of their binding energies and volatilities/vapor pressures. Subsequently, the associated reaction processes, reactive gases and necessary processing temperature/energy values can be estimated. The first step in controlling the radicals in a plasma is the selection of the feedstock gas, as shown in Fig. 6. Table 1 provides the gases used in the etching of typical materials along with the properties of the radicals produced by these gases. Based on the pressure applied during processing, a gas with sufficient vapor pressure must be introduced, and so the boiling point of the gas is important. The chemical binding energies of the elements in the gas are also included in this table and the types of radicals that are expected to be produced are indicated.

As an example, fluorocarbons are generally used in the selective etching of SiO_2 films and CF_2 is known to be an important radical in the etching process (Takahashi et al. 1996a). During etching, these radicals are transported to the bottoms of high-aspect-ratio holes because of their relatively low attachment coefficients and rapidly etch SiO_2 in conjunction with ion impact processes according to the reactions:

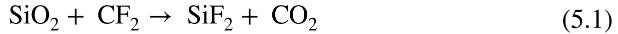

$$SiO_2 + CF_2 \rightarrow SiF_2 + CO_2 \quad (5.1)$$

and

$$Si + CF_2 \rightarrow SiF_2 + C. \quad (5.2)$$

Although CF_2 instantaneously generates SiF_2 on Si with a high vapor pressure by ion impact, C remains on the surface to prevent etching of the Si, such that film formation occurs and etching stops, as discussed in Sect. (5.2). Evidently, CF_2 is important for the selective etching of SiO_2 on Si. Figure 6 demonstrates that the initial step of designing an etching process is to select the feedstock gas. As an example, in selective etching of SiO_2 films against Si and Si_3N_4 films, fluorocarbon gases are used. In early work, CF_4 gas was employed but a greater variety of such compounds is now used. These include fluorocarbons having linear structures (such as C_2F_6, C_3F_8 and C_3F_6), cyclic structures (such as C_4F_8 and C_5F_8) and containing different atoms (such as CHF_3 and C_3F_6O). In plasmas using these gases, the electron density, electron temperature, and the type and density of active species will differ depending on the type of gas. Therefore, it is necessary to systematically measure the plasma parameters and clarify their physicochemical properties before constructing a radical-controlled process.

In Fig. 6, we consider a plasma process going from the bottom of the figure to the top to obtain the desired processing characteristics shown at the base of the diagram. To obtain the desired processing characteristics, the various particle parameters for the gas phase must be selected so that the radicals that are most effective cause the desired reactions on the solid surface in synergy with the ions. The ionization and dissociation reactions of the feedstock gas should selectively generate radicals and ions that are effective during the process. To achieve the desired process, it is necessary to select an appropriate feedstock gas and to control the particles in the plasma reaction vessel. Figure 15 shows the results of systematic measurements of the absolute densities of fluorocarbon gases and radicals in C_4F_8, CF_2F_6 and CHF_3 plasmas using infrared diode laser absorption spectroscopy (IRLAS) (Miyata et al. 1996). It is evident that a high density of CF_2 radicals can be obtained using C_4F_8 to generate the plasma, indicating that the desired radical species and density can be controlled by selecting the gas type and input power. In fact, C_4F_8 gas is now often used, because it efficiently produces CF_2 radicals that perform well during SiO_2 etching.

Shibano et al. (2008) showed that CF_3 ions provide the highest SiO_2 etching rates (Fig. 16). Hayashi et al. (1999) investigated the radical composition produced by the ionization of C_4F_8 gas and demonstrated that light fluorocarbon ions CF^+ and CF_2^+ and heavy fluorocarbon ions such as $C_3F_5^+$ and $C_4F_7^+$ were generated (Fig. 17). In addition, CF_2 radicals were found to be primarily obtained from the dissociation of $C_4F_{8,}$ while F was the main product generated by the dissociation of CF_2 following

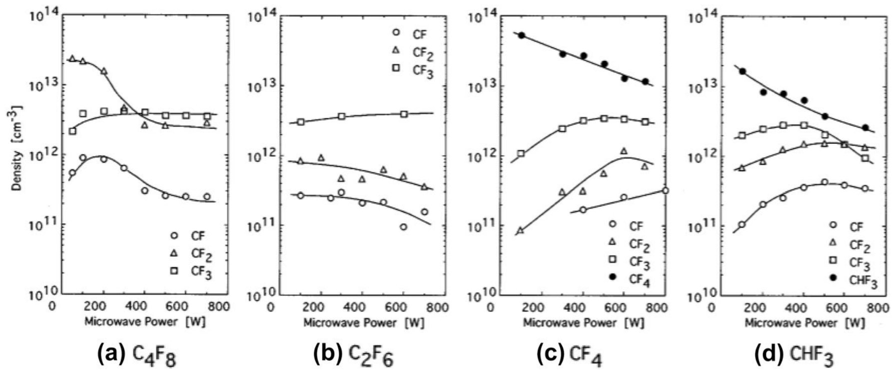

Fig. 15 CF_X (1–3) densities in ECR plasmas employing **a** C_4F_8, **b** C_2F_6, **c** CF_4 and **d** CHF_3 gases as a function of microwave power. The pressure and the flow rate are fixed at 0.40 Pa and 3.0 sccm, respectively (Miyata et al. 1996)

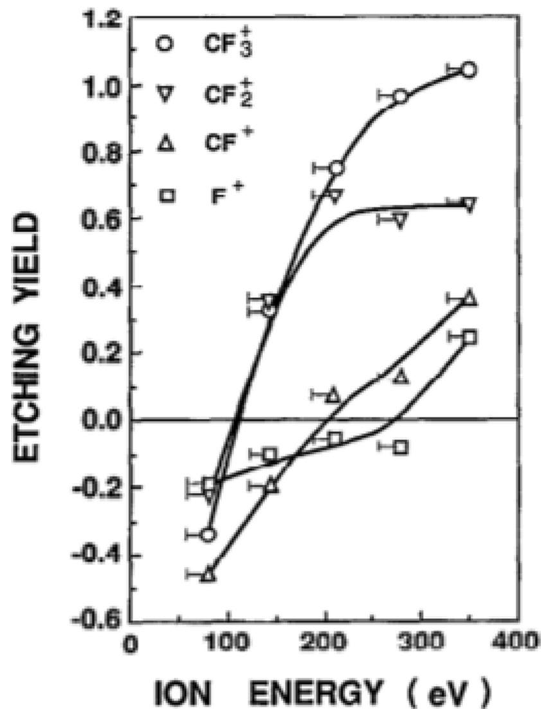

Fig. 16 Etching yields of SiO_2 as a function of CF_x^+ and $F.^+$ ion energy. Angle of incidence was 15°. Negative values mean increases of film thickness caused by deposition of some film on the SiO_2 surface. The error bars show the uncertainty of the actual energy of incident ions, which is caused by charging of the SiO_2, surface (Shibano et al. 2008)

electron impact and was found to be removed by pumping. This prior work estimated that the C_2F_4 density was roughly comparable to the densities of CF and CF_3 and that the surface loss probability for C_2F_4 increased with increasing electron density. These results suggest that C_2F_4 might play an important role in the etching because of its polymerization characteristics. Therefore, gases that efficiently generate CF_2 and/or C_2F_4 and CF_3^+ ions in the plasma would be expected to provide the optimum performance during the high-aspect-ratio etching of SiO_2.

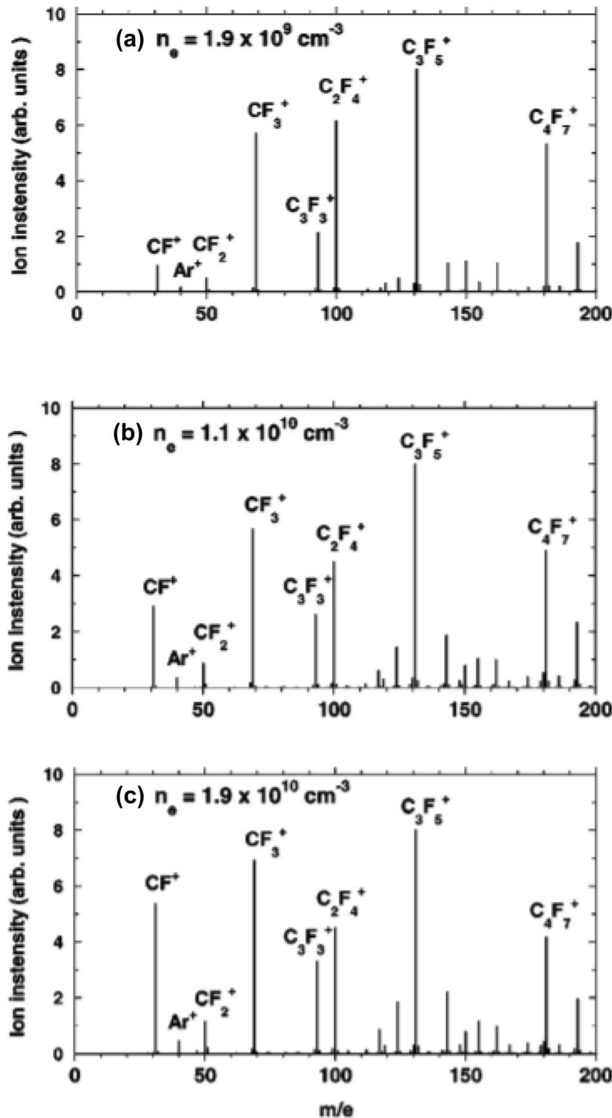

Fig. 17 Mass spectrum for positive ions extracted from the plasma at electron densities of **a** 1.9×10^9, **b** 1.1×10^{10}, and **c** 1.9×10^{10} cm.$^{-3}$. The ions with the energy corresponding to the time-averaged plasma potential were measured (Hayashi et al. 1999)

While researching the optimal radicals for etching, Nagai et al. (2006) developed an environmentally benign gas with low global warming potential: $C_5F_{10}O$ ($CF_3CF_2CF_2OCFCF_2$). This compound efficiently produces radicals and CF_3^+ ions in response to electron impact and so could be used to replace the fluorocarbons having high global warming potential that are conventionally used for SiO_2 etching. The dissociative ionization cross section for CF_3^+ ions obtained from gaseous $C_5F_{10}O$ is much higher than that for other ionic species (more than ten times that

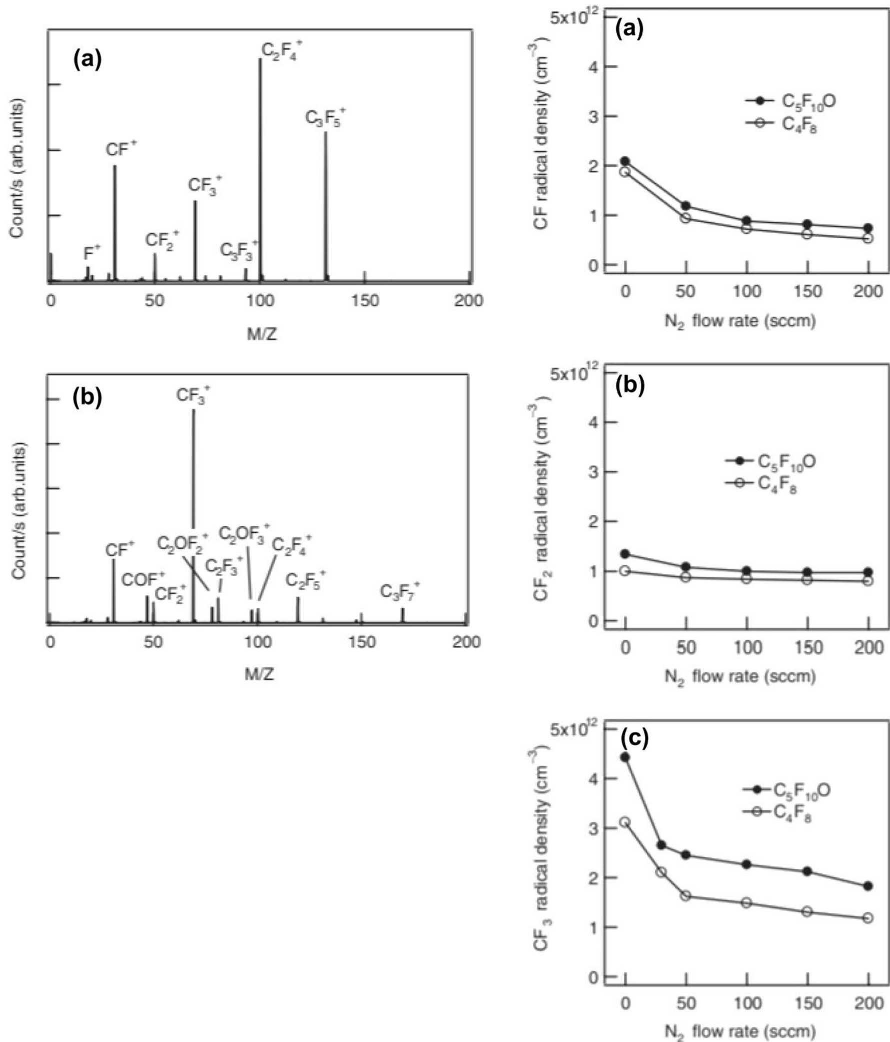

Fig. 18 Left diagram: mass spectra of **a** C_4F_8 and **b** $C_5F_{10}O$ at electron energy of 70 eV. Right diagram: CF, CF_2, and CF_3 radical densities as functions of N_2 flow rate in Ar/C_4F_8/N_2 or Ar/$C_5F_{10}O$/N_2 plasma under conditions of pressure of 10 Pa, gas flow rate of Ar/C_4F_8/N_2 = 1000–x /10/x or Ar/$C_5F_{10}O$/N_2 = 1000-x/10/x sccm, and 60 MHz power of 1200 W (Nagai et al. 2006)

for C_4F_8), as shown in Fig. 18. This is important, because CF_3^+ is the most effective ion in terms of improving the etching rate of SiO_2. This compound was found to generate several radicals in relative quantities of $CF_3 > CF_2 > CF$. Diluting this gas with N_2 or Ar was shown to decrease the densities of CF_3 and CF in the plasma but had no effect on the density of CF_2. Consequently, the relative proportion of CF_2, which provides advantageous etching properties, could be increased. In this manner, by controlling the densities of ionic and radical species via careful selection of the feedstock gas, improved etching characteristics could be achieved. As an example,

the etching rate of a SiOCH film using an $Ar/C_5F_{10}O/N_2$ plasma was approximately 1000 nm/min, which was much higher than the rate obtained using an $Ar/C_4F_8/N_2$ plasma. This pioneering study confirmed that the generation of specific desirable radicals and ions is possible based on tuning the feedstock gas.

5.2 Dilution by noble gases

5.2.1 Silane plasmas

During plasma processing, the pressure affects various key parameters, such as the gas density, electron temperature, vapor pressure, mean free path and gas residence time. Thus, there is typically an optimal pressure, and dilution of the feedstock gas represents an effective means of controlling the radical density. Equation (2.5) indicate that the radical density is directly related to the density of the feedstock gas. Consequently, the radical density can be adjusted by diluting the feedstock with a noble gas that does not contribute directly to any chemical reactions. He, Ne, Ar, Kr and Xe are the most commonly used diluent gases and the ionization energies of these elements are 24.58, 21.55, 15.75, 13.96 and 12.12 eV, respectively. The electron temperature and electron density of the plasma are affected by the ionization energy as well as the ionization cross section of the noble gas. As an example, diluting the feedstock gas with Xe, which has a low ionization energy and a large ionization cross section, increases the electron density and decreases the electron temperature. As discussed in Sect. 4, once the radical species that are involved in thin-film formation are identified, it is vital to control these species. Experiments concerning the fabrication of thin-film solar cells using a SiH_4/H_2 gas plasma have shown that SiH_3 are important precursors.

Nomura et al. (1994) determined the absolute density of SiH_3 using IRLAS and investigated the effect of dilution with noble gases on these radicals. The SiH_3 density in the plasma was ascertained using a 13.56 MHz RF parallel-plate system at a low pressure of 4.0 Pa in conjunction with H_2/SiH_4, He/SiH_4, Ar/SiH_4 or Xe/SiH_4 gas mixtures. The density was found to decrease with increasing dilution rate for all gas mixtures, as shown in Fig. 19, although the number of SiH_3 generated per SiH_4 molecule increased significantly when Xe was used as the diluent. The SiH_3 density increased when a low electron temperature was achieved by diluting the feedstock with Xe, because SiH_3 were selectively produced in conjunction with a relatively large dissociative cross section at low electron energies. In addition, the diffusional annihilation of radicals was reduced by Xe dilution, as shown in Fig. 20.

In the case that SiH_2 or SiH and Si are incident on the surface of an a-SiH thin film, these species generate a columnar surface morphology with a porous, rough texture as they are inserted into SiH bonds with an attachment coefficient (equal to the total loss probability) of approximately 1. Kawasaki et al. (1997) also established that SiH_2 are responsible for the nucleation of particles based on reactions with Si_nH_{2n+2} ($n=1, 2, 3, \ldots$) to form polymerized species. This contribution to particle nucleation may affect the film deposition rate when the particle radius increases above approximately 10 nm, and so it is important to clarify the behavior of such

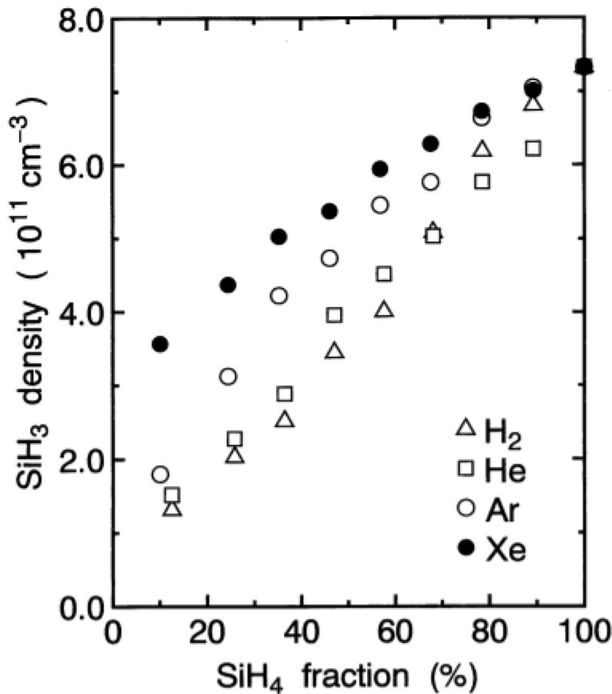

Fig. 19 SiH_3 radical density vs the SiH_4 fraction in rf plasma using H_2/SiH_4, He/SiH_4, Ar/SiH_4, and Xe/SiH_4 gas mixtures. The total gas pressure was 4.0 Pa and the input rf power was 200 W (Nomura et al. 1994)

radicals in the gas phase. Kono et al. (1995) investigated SiH_2 in a plasma based on SiH_4 gas diluted with various noble gases and with H_2, using LIF, with the results presented in Fig. 21. It is apparent that SiH_2 was produced in these systems primarily by the reaction:

$$SiH_4 + e \rightarrow SiH_2 + \left(H_2 \text{ or } 2H\right) + e. \tag{5.3}$$

In contrast, in the case of dilution with Xe or Ar, the formation of SiH_2 was found to be promoted by the reaction of SiH_4 with metastable Xe* or Ar* species according to the reaction:

$$SiH_4 + X^* \rightarrow SiH_2 + \left(H_2 \text{ or } 2H\right) + X. \tag{5.4}$$

Figure 22 shows the data obtained from analyses of SiH_x (x = 0–3) species in a parallel-plate electrode RF SiH_4/Ar plasma (Hori et al. 2006; Goto 2001; Kono et al. 1993; Sakakibara et al. 1991; Nomura et al. 1994). The densities of Si, SiH and SiH_2 were found to increase following dilution with Ar, while that of SiH_3 decreased. The lifetimes of SiH_3, which act as precursors for the fabrication of high-quality a-Si and μc-Si thin films, were found to be as long as several ms, whereas those of Si, SiH and SiH_2 were less than 100 μs. These short lifetimes are attributed to reactions with

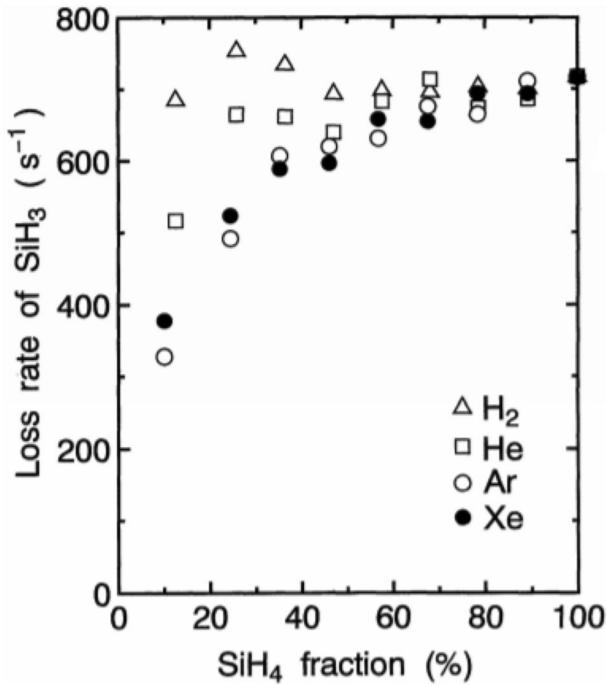

Fig. 20 SiH_3 loss rate as a function of SiH_4 fraction in the afterglow of H_2/SiH_4, He/SiH_4, Ar/SiH_4, and Xe/SiH_4 gas mixture plasmas. The total gas pressure was 4.0 Pa and the input rf power was 200 W (Nomura et al. 1994)

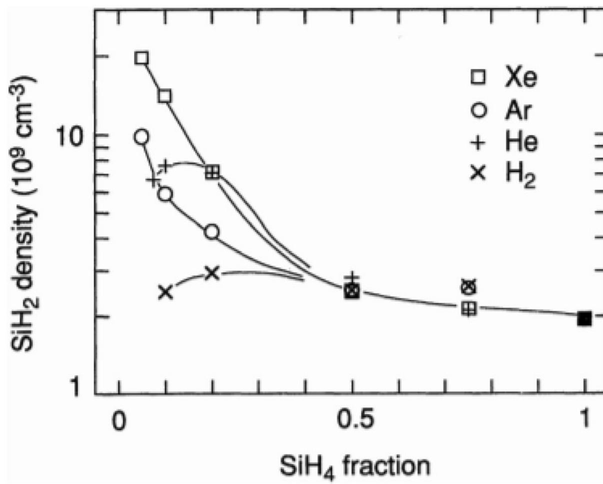

Fig. 21 Comparison of the SiH_2 densities in 40 W, 40 mTorr plasmas using SiH_4/Xe, SiH_4/Ar, SiH_4/He and SiH_4/H_2 gas mixtures (Kono et al. 1995)

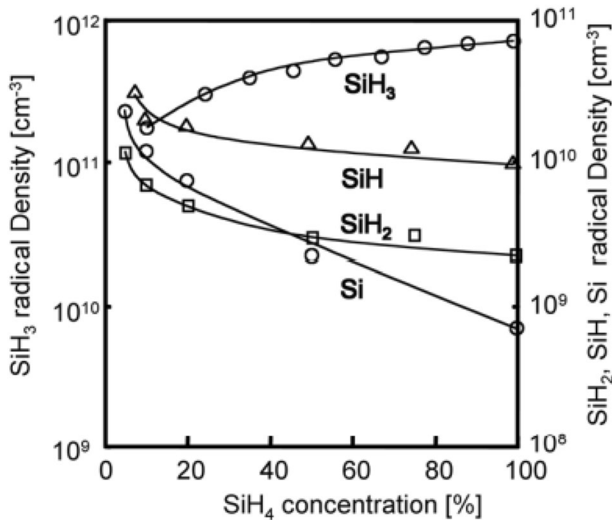

Fig. 22 Systematic measurement results of Si, SiH, SiH_2 and SiH_3 in a parallel-plate electrode RF SiH_4/Ar plasma (Goto 2001; Hori et al. 2006; For reference, the SiH_3 density from Nomura et al. 1994; SiH_2 density from Kono et al. Si density from Sakakibara et al. 1991)

the SiH_4 feedstock to produce larger molecules (Si_2H_6 and Si_2H_5) responsible for the appearance of defects. The gas-phase reactions of these short-lived radicals with heavier molecules also produced fine particles that were a factor in the formation of defects in the thin films. Therefore, it is necessary to remove these molecules before they reach the surface of the film (that is, to control the gas residence time). SiH, Si and SiH_2 all have large surface attachment coefficients ranging from 0.7 to 1.0. Naturally, short-lived radicals generate defects during the surface reaction process that make it challenging to fabricate high-quality thin films. Therefore, it is very important to control not only SiH_3 but also these short-lived radicals.

As noted above, to obtain high-quality a-Si and μc-Si thin films, the density of SiH_3 must be as high as possible relative to those of Si, SiH and SiH_2 and larger molecules. The density of SiH_3 can be increased in an undiluted SiH_4 plasma but the removal of heavier molecules by an exhaust pump or other means is necessary. In the case that the plasma is diluted with Ar gas, the SiH_4 density decreases such that the formation of larger molecules is suppressed, while the densities of Si, SiH and SiH_2 increase. The latter effect is disadvantageous with regard to the formation of high-quality thin films. As shown in Fig. 6, dilution with noble gases may be an important aspect of controlling the formation and disappearance of radicals to realize radical-controlled plasma processes.

The electron temperature can also be controlled by noble gas dilution, and so is a very important factor with respect to adjusting the generation of radicals. Ishijima et al. (2008) reported changes in the electron temperature in a plasma based on 10% C_4F_8 mixed with different noble gases (He, Ne, Ar, Kr and Xe) as a result of measurements using an absorption probe. The addition of noble gases having different ionization potentials into the reaction gas allowed the electron temperature to be

tuned, the F, CF, CF_2 and CF_3 densities to be systematically controlled, and the final radical composition to be modified. From these studies, it is apparent that the dissociation of the source gas can be adjusted by dilution with a noble gas having a low ionization potential to give a lower electron temperature. Thus, careful selection of the noble gas diluent allows the radicals generated in the plasma to be controlled.

5.2.2 O_2 plasmas

SiO_2 is a very important insulating film in ULSIs but must be fabricated at relatively low temperatures (below 550 °C). For this reason, low-temperature oxidation of silicon using plasmas has attracted much attention. Itoh et al. (1999) reported that radical oxidation is a very promising approach to controlling SiO_2 uniformity and reliability, because O is able to oxidize Si to produce atomically flat SiO_2/Si interfaces. It is also evident that the O oxidation mechanism is different from the conventional dry oxidation mechanism. The addition of Kr as a diluent in this plasma-based low-temperature oxidation process has been reported to result in the formation of a high-quality silicon oxide film with a low leakage current (Ueno et al. 2000; Sekine et al. 2001; Tanaka et al. 2003; Goto et al. 2003). The incorporation of Kr at a dilution ratio of 97% or higher is believed to promote collisions between metastable Kr atoms and oxygen molecules to generate excited state O ($^1D_2$) in addition to ground-state oxygen atoms. These O ($^1D_2$) contributes to the formation of high-quality oxide films. Takeda et al. (2007) reported the first-ever assessment of the absolute densities of O ($^3P_{j=0,\,1,\,2}$) and O ($^1D_2$) as well as O_2^+ in a surface-wave excited plasma in which oxygen was highly diluted with Kr. The O (^3P_j) density was measured using VUVAS in conjunction with MHCL. Figure 23 demonstrates that the density of O ($^3P_{j=0,\,1,\,2}$) decreased with increasing Kr gas dilution ratio. The O ($^1D_2$) density was ascertained using VUVAS based on the 3 s $^1D_o-2p$ $^1D_2$ transition at 115.22 nm and was determined to be almost constant over the Kr dilution range of 0 to 30%. However, above 30%, the density increased drastically with further increases in the

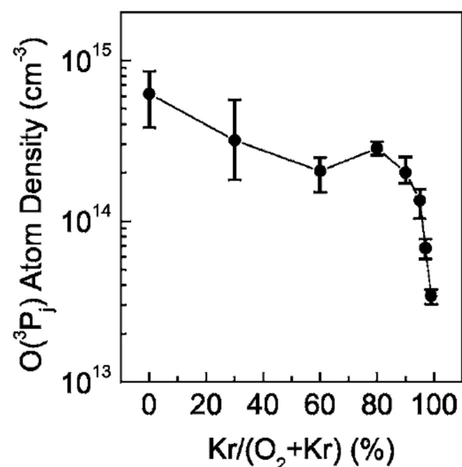

Fig. 23 Absolute densities of O (^3P_j) radical as a function of the Kr gas dilution ratio in O_2/Kr surface wave excited plasma (Takeda et al. 2007)

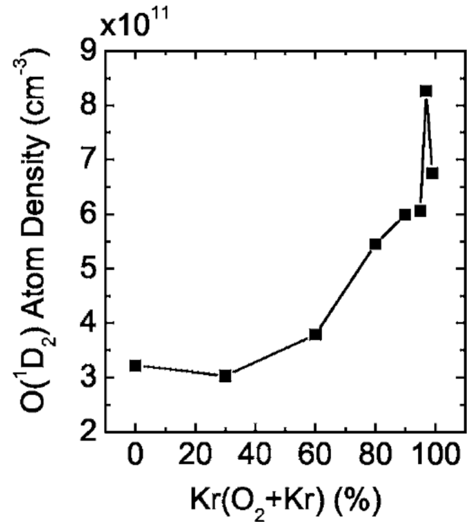

Fig. 24 Absolute densities of O ($^1D_2$) radical as a function of the Kr gas dilution ratio in O_2/Kr surface wave excited plasma (Takeda et al. 2007)

extent of dilution (Fig. 24). The density of this species was also two orders of magnitude lower than that of the O ($^3P_{j=0, 1, 2}$) as a consequence of the reactions:

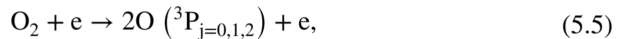

$$O_2 + e \rightarrow 2O\left(^3P_{j=0,1,2}\right) + e, \tag{5.5}$$

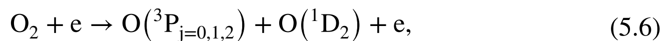

$$O_2 + e \rightarrow O\left(^3P_{j=0,1,2}\right) + O\left(^1D_2\right) + e, \tag{5.6}$$

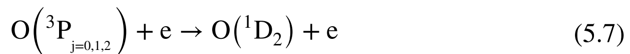

$$O\left(^3P_{j=0,1,2}\right) + e \rightarrow O\left(^1D_2\right) + e \tag{5.7}$$

and

$$Kr^* + O_2 \rightarrow Kr + 2O. \tag{5.8}$$

The generation of O (^3P_j) as a result of electron impact dissociation [Eqs. (5.5) and (5.6)] appears to have been dominant over the collisional dissociation of oxygen molecular with metastable Kr atoms (Eq. 5.8). The formation of O ($^1D_2$) due to electron impact dissociation and excitation [Eqs. (5.6) and (5.7), respectively] was also more pronounced than that stemming from the collisional dissociation of oxygen molecules with metastable Kr atoms. It is noteworthy that O_2^+ ions have been shown to be the primary species even at high Kr dilutions employing quadrupole mass spectrometry (QMS) as shown in Fig. 25. These results indicate effective charge transfer under these conditions according to the reaction equation:

$$Kr^+ + O_2 \rightarrow Kr + O_2^+. \tag{5.9}$$

Significantly diluting the O_2 with gaseous Kr can evidently produce high quality Si oxide films at rapid rates. The associated reaction mechanism is determined

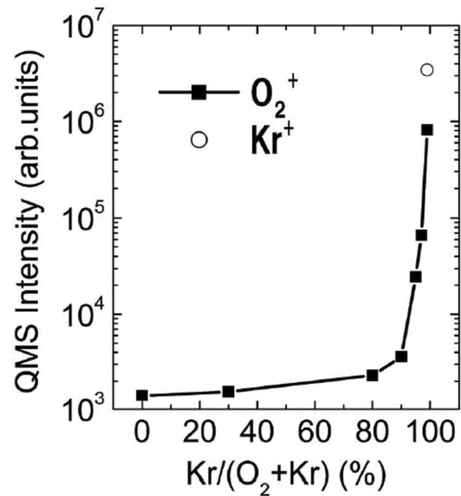

Fig. 25 QMS as a function of the Kr gas dilution ratio in O_2/Kr surface wave excited plasma (Takeda et al. 2007)

both by the presence of O and by the density of O_2^+. Increased dilution of the O_2 with noble gases, especially with Kr gas, results in surface activation of the Si as a consequence of collisions with low-energy O_2^+ that promote the oxidation action of highly reactive O ($^1D_2$).

The effects of Kr and Ar dilution on O_2 gas plasmas have been compared (Takeda et al. 2008) and the data show that O ($^1D_2$) are primarily generated by electron impact and that Ar produces a greater radical density by raising the electron temperature. Based on VUVAS data, the translational temperature of oxygen atoms was estimated to be approximately 2000 K at a pressure of 90 Pa. In the pressure region between 116 and 133.3 Pa, the translational temperature of O ($^1D_2$) during Kr dilution trials was found to be higher than that obtained with Ar dilution (Fig. 26). The radical density and translational temperature data allowed estimation of the radical flux at the substrate surface using Eq. (2.9). These estimates indicated that the incident flux of O ($^1D_2$) was larger in the case of Ar dilution (Fig. 27), meaning that Ar dilution promoted the oxidation of silicon to a greater extent. This finding that the radical flux contributing to oxidation can be controlled by adjusting the temperature of radicals via significant dilution with noble gas is of significant interest.

Taylor and Tynan (2005) systematically examined the electron density, electron temperature and atomic oxygen density in an O_2 gas plasma diluted with He, Ar or Xe. The oxygen radical density was determined by both actinometry and mass spectrometry, while the plasma density and electron temperature were ascertained using Langmuir probes. The oxygen radical density was highest for the O_2/Xe mixture and lowest for the O_2/He mixture (see Fig. 28a). Somewhat surprisingly, increasing the electron temperature at a fixed plasma density ($n_e < 1.33 \times 10^{11}$ cm^{-3}) decreased the O density (Fig. 28b). This effect was analyzed in terms of the dissociation, ionization and diffusion of oxygen radicals and was attributed to variations in the transport of radicals, and not to the actual effect of electron temperature. It is apparent that the control of radicals requires a comprehensive analysis of the behavioral dynamics of

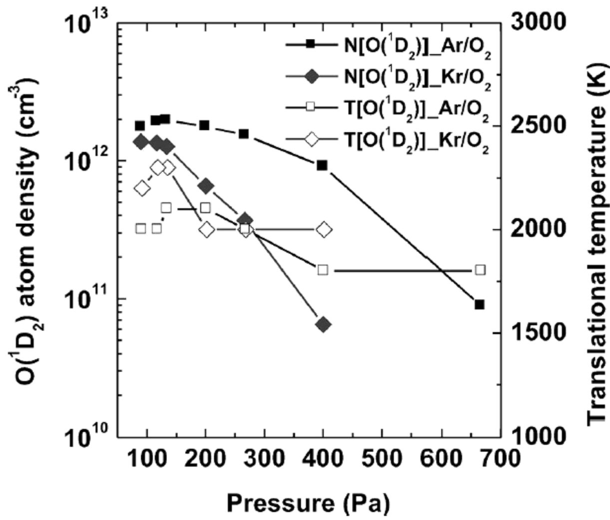

Fig. 26 Absolute densities and translational temperatures of O ($^1D_2$) in Kr/O_2 and Ar/O_2 (Takeda et al. 2008)

such radicals in the reaction equipment and tuning of radical reactions and transport processes. The use of oxygen mixtures expanded the ranges of O and ion densities, while at the same time allowing independent control of these densities.

5.3 High-precision etching with radical control

The composition of radicals in the gas phase is greatly affected by the gas residence time. The flow rate for the gas has a significant effect on the residence time and, as the dissociation of the raw gas proceeds, atomic radicals are increasingly formed,

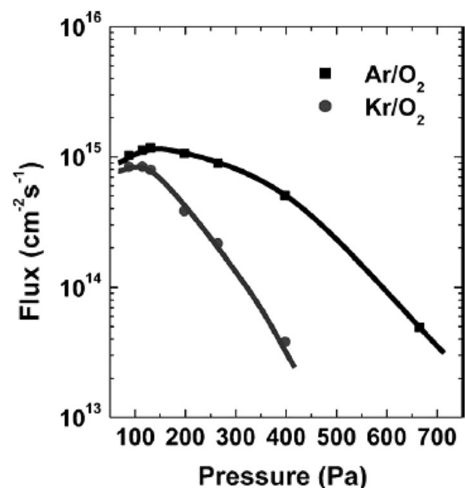

Fig. 27 Fluxes of O ($^1D_2$) in Kr/O_2 and Ar/O_2 surface wave excited plasma (Takeda et al. 2008)

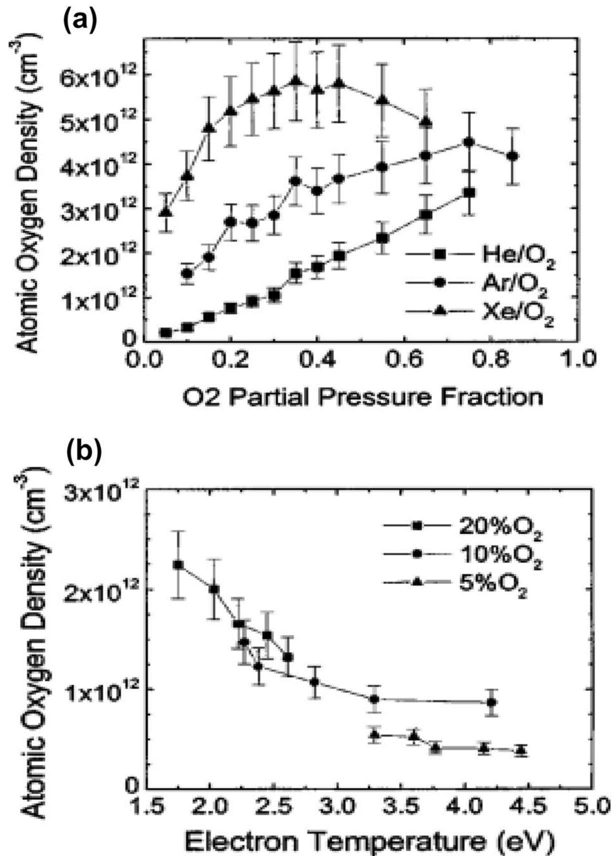

Fig. 28 **a** O density measured by actinometry vs the ratio of O_2 /(He + O_2), O_2 /(Ar + O_2), and O_2 /(Xe + O_2), (**b**) O density variation with electron temperature (Taylor and Tynan 2005)

as demonstrated by Fig. 7. Equation (2.5) also show that suppressing excessive dissociation of the feedstock gas and obtaining the desired radical composition requires shortening the residence time of the gas. Because radicals are also generated when electrons collide with the byproducts generated during etching, a shorter residence time will increase this effect. Therefore, the radical density in the process can be controlled by applying a high level of dilution with a noble gas to control the degree of dissociation of the feedstock gas, and by rapidly removing byproducts without changing the chemical composition of the raw gas. A high-precision etching process requires a plasma chemistry that can selectively generate the radical species serving as precursors for etching by comprehensively controlling internal parameters (Hayashi et al. 1999). This necessitates control of the electron density and gas residence time, as indicated by Fig. 6.

Tatsumi et al. (1997) studied F/CF, F/CF_2 and F/CF_3 controlled by suppressing the excessive dissociation of gaseous C_4F_8 by applying a short gas residence time and high electron density in a mass production equipment for parallel plate plasma

etching. The formation of radicals was tuned by changing the Ar flow rate, pressure and power according to the τn_e term, as shown in Fig. 29. In addition, introducing O_2 gas at an optimum flow rate into the C_4F_8 stream did not change the F density but reduced the high densities of CF and CF_2 that were otherwise deposited on the bottom and sidewalls of the fine pattern and degraded the etching shape. In this manner, the deposition of a fluorocarbon thin film on the surface of the fine pattern was suppressed. The disappearance of F was controlled by placing a Si plate on the top electrode of the parallel plate. As a result, deep contact hole with a high aspect ratio (pore diameter: 0.09 μm, aspect ratio: 11) were successfully fabricated in the SiO_2 film by skillfully controlling the generation and loss processes of radical species important for etching while employing a $C_4F_8/Ar/O_2$ gas mixture (Fig. 30). This work demonstrated that superior etching performance can be obtained by identifying the radical species important for etching and controlling these radicals based on Eq. (2.6).

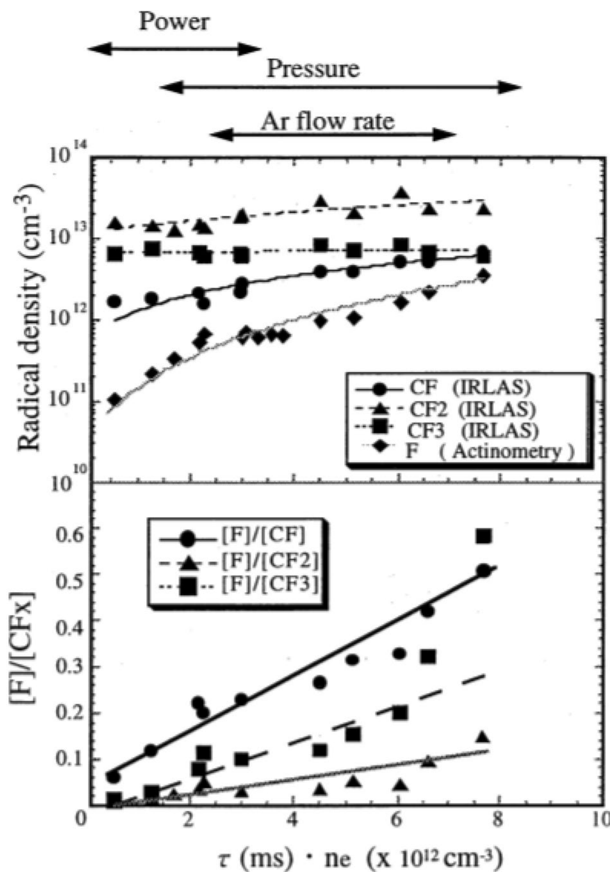

Fig. 29 Comparison of radicals as a function of the number of collisions (Tatsumi et al. 1997)

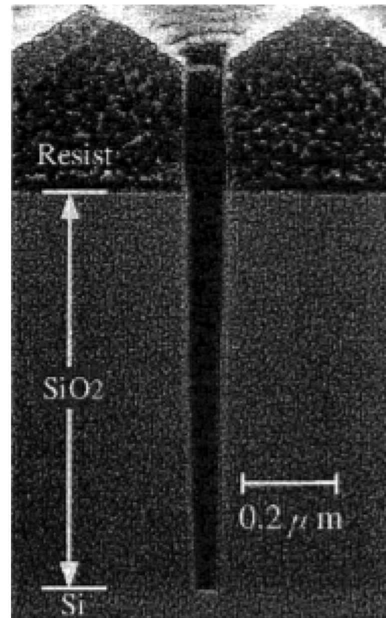

Fig. 30 Optimized etched profile. A 0.09μmΦ contact hole with aspect ratio of 11 was obtained (Tatsumi et al. 1997)

5.4 Design and control of feedstock gases for SiN_x etching

During the etching of Si_3N_4, H promote the removal of N in the Si_3N_4 by producing volatiles, such as NH_x and HCN, and so function as an etchant. Consequently, hydrofluorocarbons such as gaseous CH_2F_2 have been used to achieve the highly selective etching of Si_3N_4 on Si. The dissociation of C–H and C–F bonds in hydrofluorocarbons is important in terms of controlling the density of reactive species, such as ions and radicals. Generally speaking, the F produced by the dissociation of C–F bonds are the main Si etching agent, while the H resulting from the rupture of C–H bonds promote the deposition of fluorocarbon polymers on Si_3N_4 and the etching of Si_3N_4 and polymers. The dissociation of C–F and C–H bonds also produces CH_xF_y that contribute to the deposition process.

The highly selective etching of SiO_2 and SiN in the presence of polymeric Si (poly-Si) has been demonstrated in trials employing fluorocarbon gases containing H, such as CH_2F_2 (Kondo et al. 2015a, b) and CH_2FCHF_2 (Hsiao 2021). Figure 31 shows the SiO_2, SiN and poly-Si etching rates as functions of the flow rate of CH_2F_2 diluted with Ar (Kondo et al. 2015a). It is noteworthy that the etching rate for SiN films became higher than that for SiO_2 films upon increasing the proportion of CH_2F_2. In addition, a polymeric film was deposited on the poly-Si film and no etching was observed. During etching of SiN with a CH_2F_2 plasma, CH_xF_y radicals and ions exhibited unique reaction kinetics, as indicated in Fig. 32 (Kondo et al. 2015b). These data confirm the dependence of the proportional densities of CH_2F and CHF_2 on the Ar/(Ar + Kr) value in the CH_2F_2 plasma. During these trials, the various radicals were monitored using QMS and CH_2F were found to be dominant. This result is attributed to $CH_2F_2 \rightarrow CH_2F + F$ dissociation occurring preferentially rather than

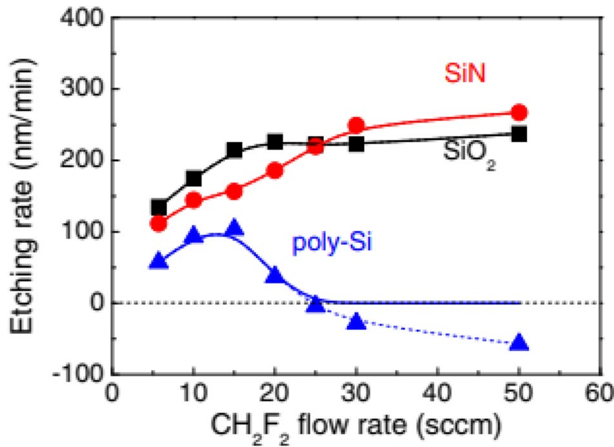

Fig. 31 Dependence of etching rates of SiO_2, SiN, and poly-Si films in Ar-diluted CH_2F_2 plasma on flow rate of CH_2F_2 for Ar (300sccm), electron density of 10^{11} cm.$^{-3}$, 2 Pa, and V_{pp} of − 1000 V) (Kondo et al. 2015a)

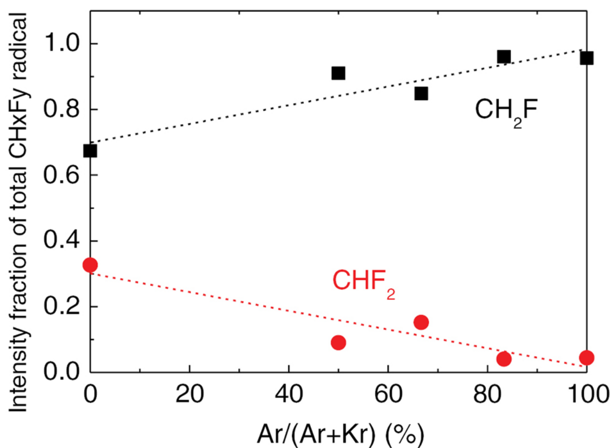

Fig. 32 Dependence of CH_2F and CHF_2 radical fraction on total CH_xF_y radical density over Ar fraction (Ar/(Ar + Kr) flow rates) in CH_2F_2 plasma (Kondo et al. 2015b)

$CH_2F_2 \rightarrow CHF_2 + H$ dissociation. As the Ar/(Ar + Kr) ratio was varied, the densities of CHF_2 decreased and CH_2F conversely increased, indicating that dilution with a noble gas was able to selectively control the radicals. This phenomenon was not ascribed to the variation in electron bombardment associated with the electron temperature change induced by modifying the Ar/Kr ratio, as discussed in Sect. 5.2. Rather, it was suggested that metastable Ar and Kr atoms contributed to the dissociation of the source gas. Using appearance mass spectrometry, the ${CHF_2}^+$ obtained from the dissociation of hydrogen were assessed at a threshold energy of 13.8 eV, while those from the dissociation of fluorine (CH_2F^+) were monitored at a threshold

energy of 15.8 eV. These assessments showed that radical formation comprised [1] dissociative ionization, [2] radical ionization, and [3] Penning [metastable] ionization stages. Using the data cross section and assuming electron temperatures of 3 eV for Ar and 2.6 eV for Kr, the radical production fractions were fit to the experimental results, as shown in Fig. 33. In this manner, the CH_2F/CHF_2 radical density ratios during these three stages were estimated to be 0.3: 0.1: 0.6. Thus, almost half of the density was the result of Penning ionization, suggesting that CH_2F_2 diluted with Kr may produce CHF_2^+, CHF_2 and H, whereas Ar dilution tends to generate CH_2F^+, CHF_2 and F.

Figure 34 demonstrates that CHF_2^+ and CH_2F^+ were very close to the ionization threshold energies for Ar and Kr (16.0 and 14.0 eV, respectively) (Kondo et al. 2015b). Therefore, it is likely that the ionization of CH_2F_2 is modified in plasmas diluted with noble gases. In the case that a CH_2F_2 plasma is diluted with Ar or Kr, either CHF_2^+ or CH_2F^+ ions may be selectively produced, along with H and F. These ions are preferentially generated based on the dissociative ionization pathways associated with charge exchange collisions, via the reactions:

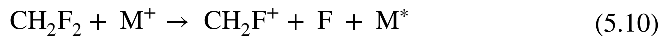

$$CH_2F_2 + M^+ \rightarrow CH_2F^+ + F + M^* \tag{5.10}$$

and

$$CH_2F_2 + M^+ \rightarrow CHF_2^+ + H + M^* [M = Ar, Kr]. \tag{5.11}$$

Significant dilution with a noble gas increases the density of noble gas ions due to the large ionization cross sections of these elements. In addition, at higher pressures, the density of active species ions increases due to charge exchange caused by collisions between the noble gas ions and the feedstock gas or other active species. This charge exchange process is also seen in Kr^+–O_2 gas mixtures [Eq. (5.9)].

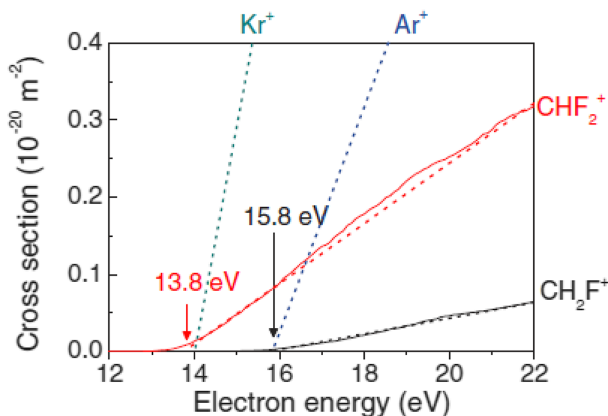

Fig. 33 Dependence of CH_2F and CHF_2 radical fraction on total CH_xF_y radical density over Ar fraction (Ar/(Ar + Kr) flow rates in CH_2F_2 plasma (Kondo et al. 2015b)

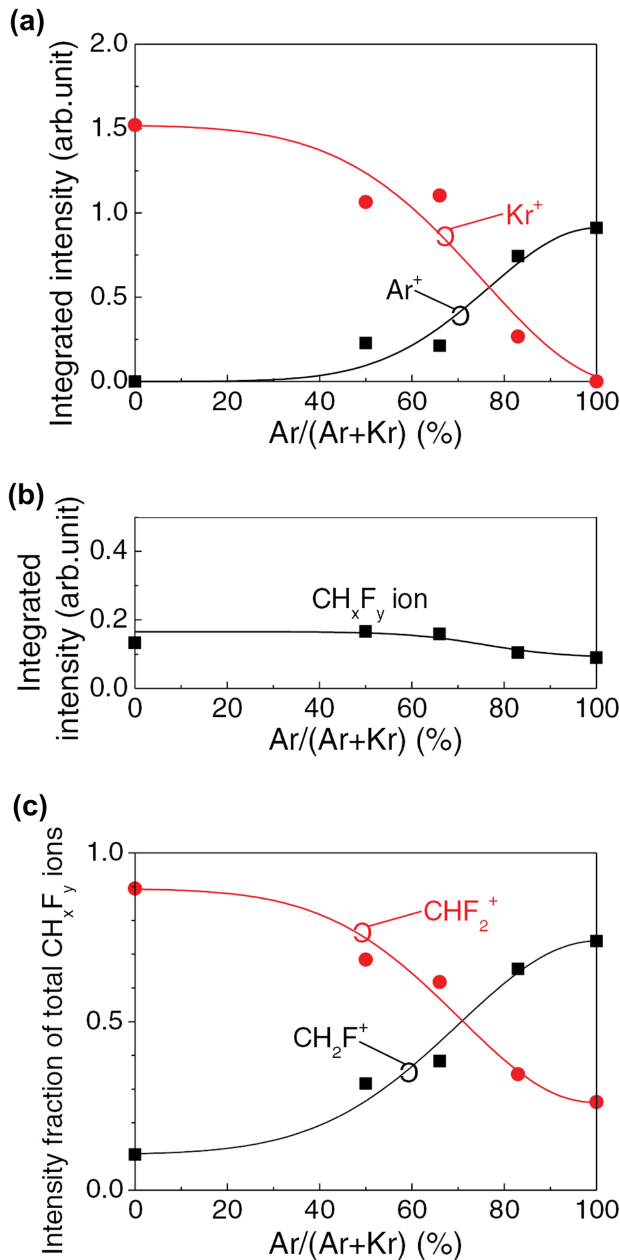

Fig. 34 Dependence of **a** Ar^+ and Kr^+ ion densities, **b** total CH_xF_y ion density, and **c** individual CH_2F^+ or $CHF_2.^+$ ion fraction on total CH_xF_y density over Ar fraction (Ar/(Ar + Kr) flow rates in CH_2F_2 plasma (Kondo et al. 2015b)

Recently, an interesting approach to the etching of SiN films by CF_4/D_2 gas mixtures has been proposed. The etching rates using this plasma were found to be

superior to those obtained from a CF_4/H_2 plasma. A model incorporating hydrogen abstraction by deuterium indicated a greater probability of reactions between the etchants (F, C or D) and Si or N dangling bonds, as shown in Fig. 35 (Hsiao et al. 2021). The different masses of D and H will promote reactivity by modifying the vibrations of chemical bonds. Thus, the use of isotopes may have a role in radical-controlled plasma processes.

5.5 Short pulse modulation etching

The physicochemical properties of various plasmas, such as electron density, electron temperature, plasma potential and active species densities, can be altered by applying time modulation to the plasma power. Of particular interest is the ability to change the electron temperature by applying a short pulse modulation. Chinzei et al. (1996) reported the CF, CF_2 and CF_3 densities in a helicon wave plasma generated

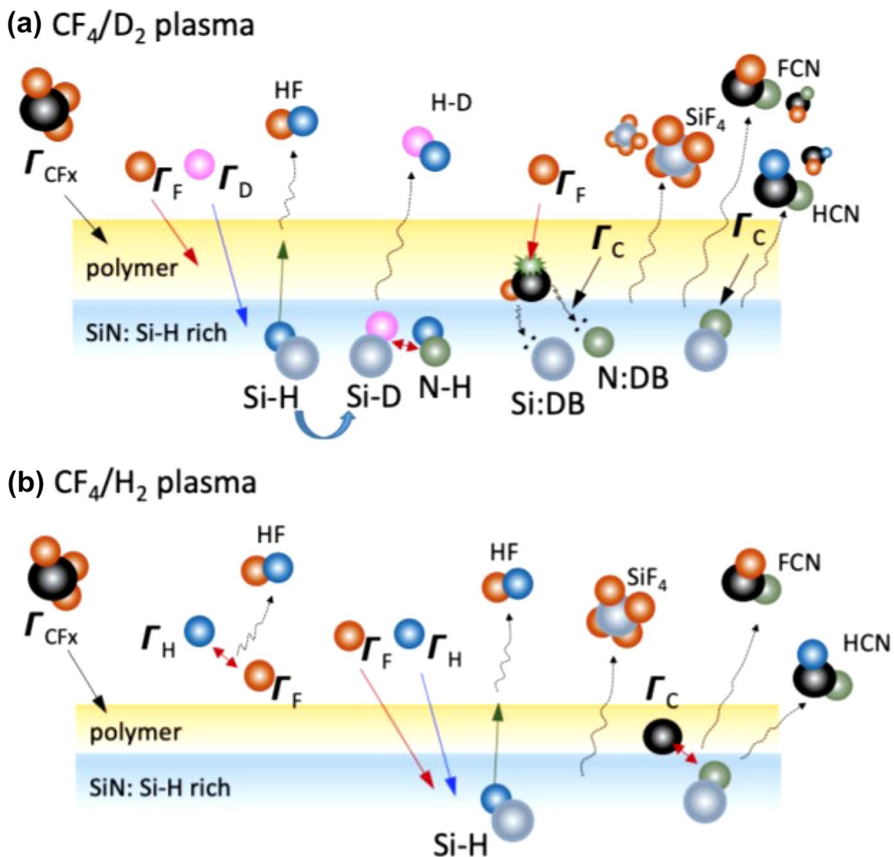

Fig. 35 Schematic illustration of the proposed etching mechanism of the SiN film etched by the **a** CF_4/D_2 plasma and **b** CF_4/H_2 plasma (Hsiao et al. 2021)

using a C_4F_8/H_2 gas mixture when a 10 μs pulse modulation was applied at a duty ratio of 50%. By systematically measuring the densities of CF, CF_2 and CF_3 with an appearance mass spectrometry and monitoring changes in the density of F via emission spectroscopy, it was shown that the radicals could be controlled by pulse modulation. Figure 36 confirms that the electron temperature was lowered and gas dissociation was suppressed by pulse modulation. In addition, the proportion of CF (the precursor radical for deposition) to F (the precursor radical for etching) was increased. During etching, CF was deposited on Si to prevent the etching of SiO_2/Si, thereby improving the etching selectivity.

A short-pulse modulation plasma has also been applied to etching processes and has been analyzed by various diagnostic and simulation methods (Ahn et al. 1996;

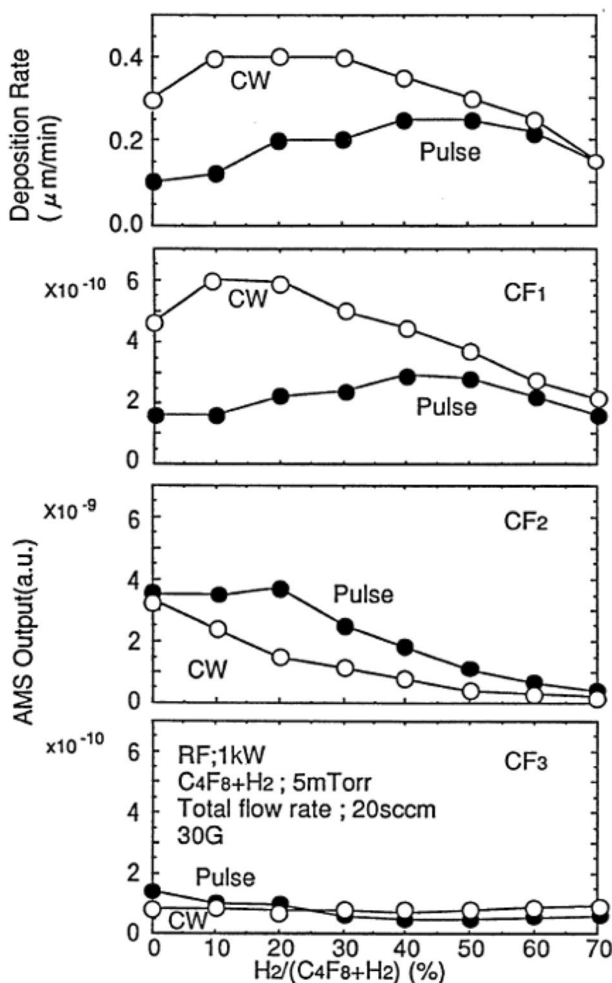

Fig. 36 Comparisons of the deposition rate and radical densities for pulse and CW discharges. The source Power of 1 kW is the instantaneous value in the pulse (Chinzei et al. 1996)

Lieberman and Ashida 1996). Sugai et al. (1997) systematically measured the electron density, electron temperature and chlorine radical densities in inductively coupled plasmas generated using chlorine gas in conjunction with a short pulse modulation of 100 μs and a duty ratio of 50%. Pulse modulation was found to control the dissociation of the chlorine gas and to vary the chlorine radical density by changing the electron temperature over time. Figure 37 summarizes the relationships between electron density and electron temperature with modulation time and demonstrates that the electron temperature increased at the start and end of the pulse but decreased after the power was turned off (Sugai et al. 1997). Figure 38 provides data related to the densities of chlorine radicals and ions over time. Note that the absolute density of chlorine radicals was determined using time-resolved laser-induced fluorescence spectroscopy (Sugai et al. 1997). When the power was turned off, negative ions and chlorine radicals were generated by the dissociative attachment of low-energy electrons to chlorine gas: $Cl_2 + e \rightarrow Cl^- + Cl$. On the application of power, there was no significant change in the density of chlorine radicals, but spikes in the density of these radicals occurred in conjunction with power-on and power-off events. Specifically, at – 40 μs, the chlorine radical density increased due to the dissociation reaction shown above as a result of electron impact because of the high electron temperature. The peak at 20 μs indicated that the chlorine radical density was increased because of dissociative attachment caused by the decrease in electron temperature. These results confirm that the chlorine radical density changed along with the electron temperature, meaning that the radical density could be controlled by pulse modulation.

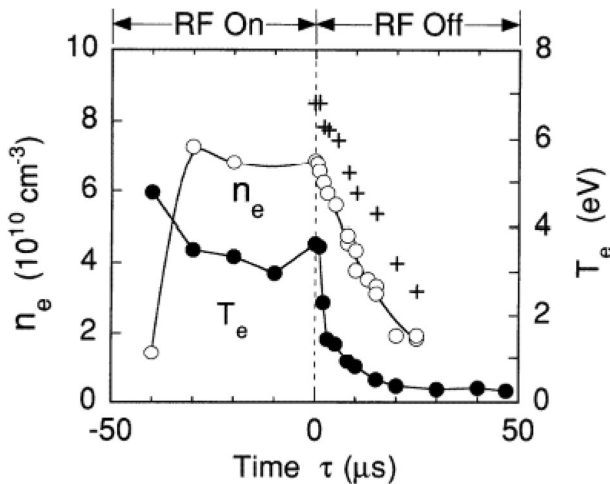

Fig. 37 Temporal variations in electron density ne (open circles) and electron temperature T_e (closed circles). The crosses indicate the total electron density including photodetached electrons. The instantaneous RF power is 400 W with 100 μs period and 50% duty cycle at 8 mTorr of Cl_2 (Sugai et al. 1997)

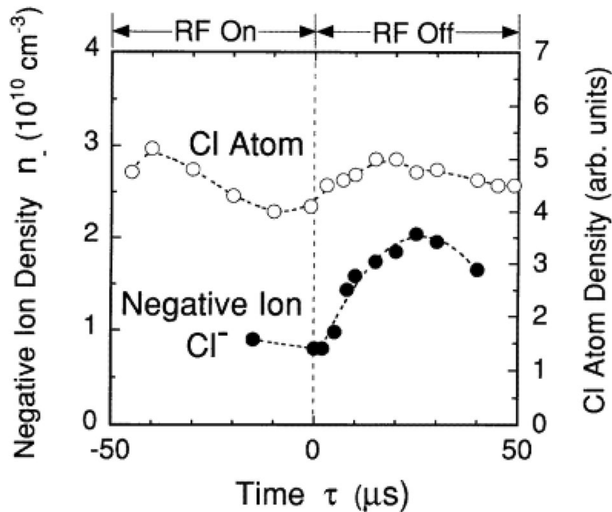

Fig. 38 Time variations in chlorine atom density and negative-ion density in the 400 W pulsed discharge in 8 mTorr Cl_2 (Sugai et al. 1997)

5.6 Long time span pulse modulation

Time-modulation processes in which the plasma is turned on and off for tens of ms or longer have been reported to allow tuning of the plasma process, leading to high-quality thin-film deposition and etching processes. Boswell and Henry (1985) reported that a low-pressure resonant RF discharge with SF_6 gas gave a selectivity value greater than 100 during the etching of Si and SiO_2 at high repetition rates. These experiments used a pulsed discharge on the order of several tens of ms for the anisotropic profile etching. Because the F in a plasma have long lifetimes, pulse modulation allowed the etching properties to be improved by controlling the flux of fluorine and ions via time modulation.

Watanabe et al. (1988) found that both the deposition rate and quality of a-Si thin films could be improved by square-wave modulation of a high-frequency discharge using silane diluted with a rare gas at a low frequency of 40 Hz. The powder concentration in the discharge space was also greatly reduced. This work reported that a modulated discharge can increase the electron density and SiH_3 density, which is advantageous when generating high-quality thin films. The SiH_3/SiH_n ($n=0$–2) ratio could be controlled by modulating the plasma, because the lifetime of SiH_3 was much longer than those of SiH_n species. When the plasma was turned on, the short-lived radicals were removed by surface and gas phase reactions, whereas when the discharge was off, only SiH_3 was present. As such, thin-film formation with SiH_3 radicals as precursors could be achieved throughout the process.

Takahashi et al. (1993, 1994) assessed CF, CF_2 and CF_3 densities in a CHF_3 electron cyclotron resonance (ECR) plasma using IRLAS while varying the on–off period of the microwave source and also when using a continuous wave (CW) power source. The ratio of CF and CF_2 densities to the CF_3 density was successfully

controlled through variation of the duty cycle in conjunction with a constant pulse width, allowing modification of the fluorocarbon film deposition rate, as shown in Fig. 39. Furthermore, the gas-phase reactions of CF, CF_2, CF_3, and F by on–off modulation of O_2-added CHF_3 ECR were elucidated and their relationship with surface reactions was clarified, demonstrating the effectiveness of controlling plasma processes by on–off modulation (Takahashi et al. 1996b).

5.7 Down-flow processes

Horiike and Shibagaki (1976) reported a radical-controlled etching process referred to as down-flow etching, as shown in Fig. 40, and named chemical dry etching (CDE). Long-lived active species were controlled in this system by generating radicals via a discharge and transporting these radicals to the reaction region, where the samples were etched. These radicals survived long enough to contribute to reactions on a wafer to realize chemical dry etching of SiO_2 and poly-Si without any damage due to charged particles or photons. On the basis of a mass spectrometric analysis, it

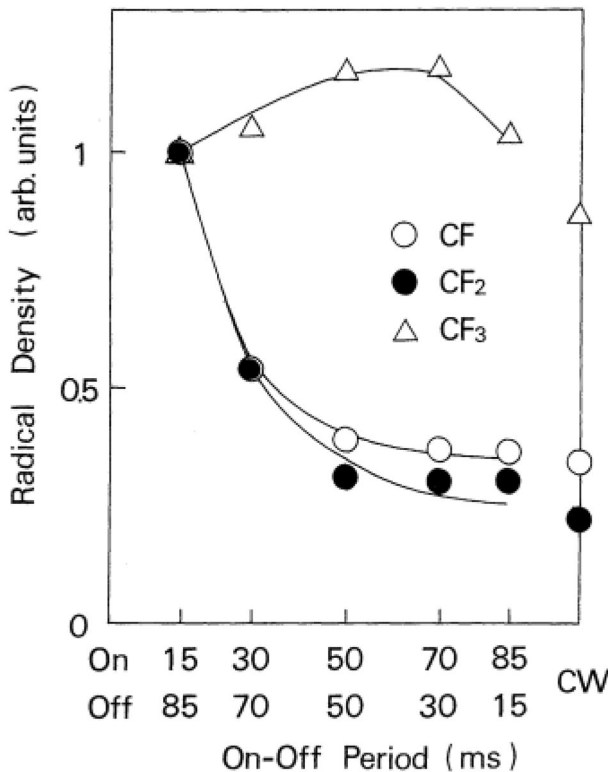

Fig. 39 CF_x (X = 1–3) radical densities as a function of the on–off period of microwave at the CHF_3 pressure of 0.4 Pa and the microwave power of 300 W in the ECR plasma. The densities are normalized to unity at an on-period of 15 ms (Takahashi et al. 1993)

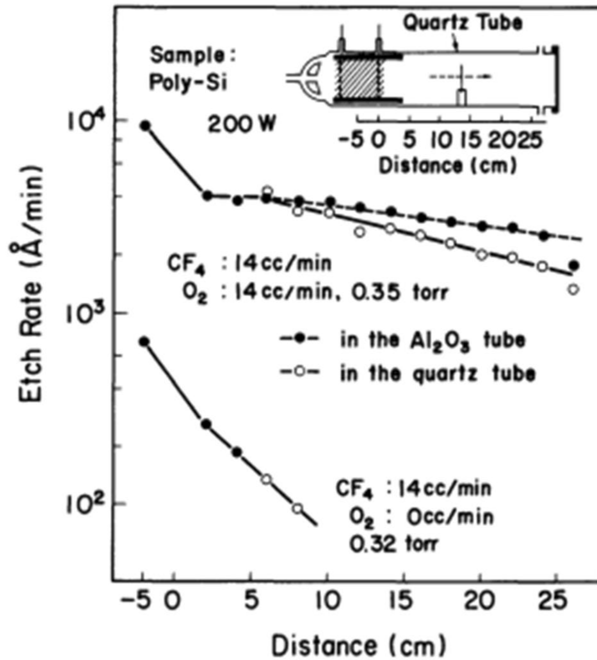

Fig. 40 Etch rate as a function of distance from the electrode. –●– shows etch rate of poly-Si when an Al_2O_3 tube is inserted inside the quartz tube (Horiike and Shibagaki 1976)

was concluded that F reacted on the sample surface. However, the lifetime of these radicals was very short and so those radicals formed in the discharge region could not have been transported to the reaction region. Consequently, the following reaction mechanism was proposed.

(1) The active species was COF, which transported F in the form of stable COF_2 molecules according to the equation:

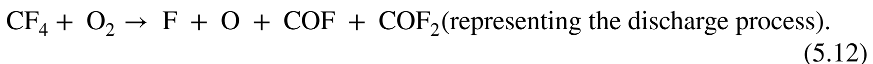

$$CF_4 + O_2 \rightarrow F + O + COF + COF_2 \text{(representing the discharge process)}. \quad (5.12)$$

(2) The COF underwent dissociation at the surface to generate F that provided the actual etching via the equations:

$$COF \rightarrow F + CO \text{ (representing the surface process)}, \quad (5.13)$$

$$F + Si \rightarrow SiF, \quad (5.14)$$

and

$$F + COF \rightarrow COF_2. \quad (5.15)$$

In this manner, using chemical reactions occurring downstream of the plasma, relatively long-lived radical species could be transported to regions, where there

were no charged particles, such that radical-induced reactions took place on the material surface. This system allows reactions to be performed without damage from charged particles or radiation. In recent ULSIs processes, etching and deposition reactions in atomic layers have been accomplished by transporting active species into complex 3D structures and deep holes, and these chemical reaction processes using radicals have attracted much attention.

5.8 Wall temperature controlled processes

The reactions at the walls in a plasma system are among the most important factors affecting the radical density and the overall reliability of the process. Using appearance mass spectrometry, Ito et al. (1994) reported that heating of the entire plasma etching chamber to 230 °C generated CF_3 and CF_2 densities in the reactor two to three orders of magnitude higher than those in a conventional reactor heated to 30 °C, as shown in Fig. 41. Sugai et al. (1995) monitored the density of F using actinometry with wall heating and found essentially no change. This heating was found to effectively control the etching process by enhancing the formation of carbon-containing radicals and, in particular, could increase the SiO_2/Si selectivity ratio.

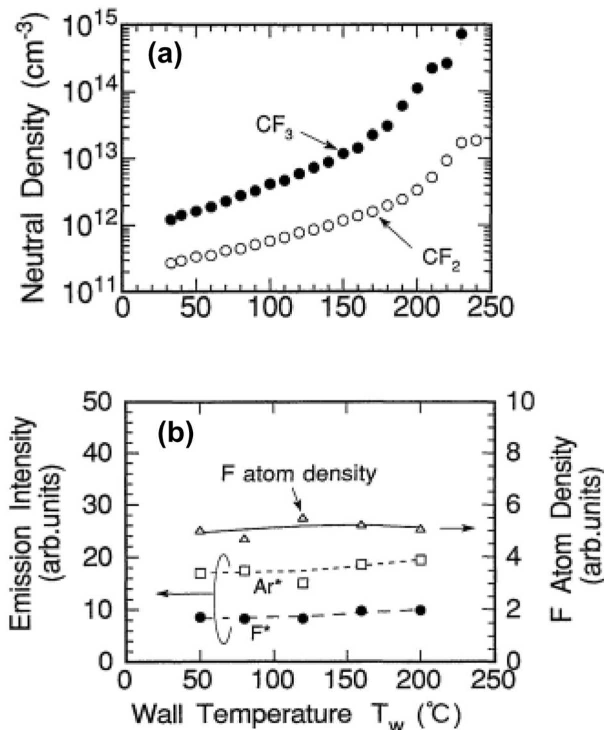

Fig. 41 **a** CF_2 and CF_3 densities and **b** F density as a function of temperature of the inner wall. 100mTorr CF_4 and 100 W RF power (Ito et al. 1994)

5.9 Control of dipole radicals by Coulomb force

Sekine et al. (1993) achieved the selective etching of Si/SiO_2 at substrate temperatures below 0 °C using a Cl_2-based magnetron plasma reactor. In this etching process, the products formed by the reaction of chlorine with silicon were decomposed in the gas phase to form SiCl, oxides and other unsaturated molecules. Radicals such as oxychloride species have a large dipole moment and thus a greater probability of attachment to SiO_2 than to Si. This is because the SiO bonds on SiO_2 are also polar and, therefore, attract dipole molecules based on Coulomb forces. As a result, only the SiO surface was covered with silicon chloride or oxychloride and this protected the surface from etching by chlorine ions. It was proposed that this protective film inhibited etching of the SiO_2 and resulted in a high poly-Si/SiO selectivity ratio. As such, the polarization of radicals could be used to control their reaction adhesion coefficient by selective deposition or other means.

5.10 Radical injection

5.10.1 Carbon nanowall growth by H injection

In general, the types and density of radicals are determined by the choice of gas species, the shape of the plasma device, the gas pressure and the applied power, as shown in Eq. (2.7). When mixing multiple gases to control the types and densities of various radicals, it is difficult to simultaneously control the densities of multiple radicals, because the radical species produced by each gas and their densities depend on the dissociation cross sections specific to each gas, as is evident from Eq. (2.5). To address this problem, the radical species can be generated in advance in different plasma sources and injected into the actual processing equipment so that the densities of multiple radical species can be controlled independently. This method was first proposed by Hori and Hiramatsu and has been used for high-precision etching and thin-film formation processes.

Hiramatsu et al. (2004) fabricated 2D carbon nanowalls using a capacitively coupled RF PECVD method with H injection. This work represented the first time that carbon nanowalls were grown on Si, SiO_2 and sapphire substrates without any catalyst. The growth of these nanowalls was also found to be independent of the substrate material (Fig. 42). The relationship between the growth of the carbon nanowalls and manufacturing conditions such as the type of feedstock gas was investigated. A C_2F_6/H_2 system was determined to generate vertically aligned carbon nanowalls on the substrate, while the nanowalls grown using a CH_4/H_2 system were wavy and as thin as 10 nm (Fig. 43). In contrast, when no H was injected, carbon nanowalls were not formed. When using gaseous C_2F_6 as the feedstock, CF_3 was dominant, while the use of CH_4 provided CH_3 as the main active species, although the surface sticking probabilities for both radicals under these conditions were not ascertained. Interestingly, depending on the feedstock gas, the precursors for the formation of carbon nanowalls were different. These results indicated that the shape of the carbon

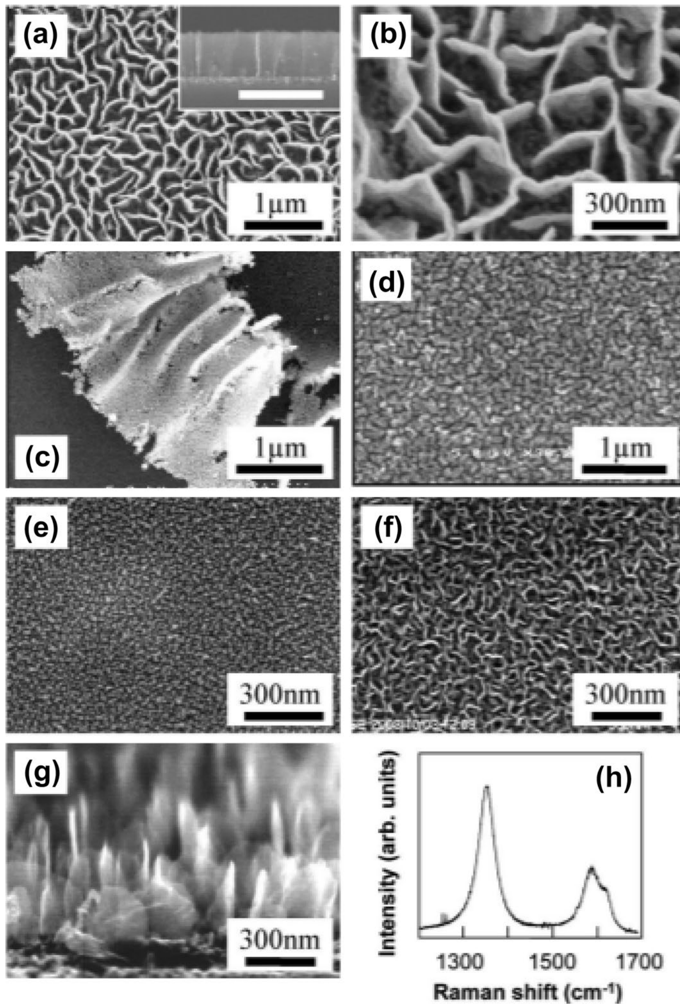

Fig. 42 Scanning electron microscope (SEM) images of the carbon nanowalls grown on Si substrate using C_2F_6 rf-CCP assisted by H injection for 3 h; **a** top view and **b** closeup view. Inset in **a** is a cross-sectional view. **c** SEM image of carbon nanowall mat grown for 8 h, which was scratched out from Si substrate. **d** SEM image of deposits formed using the C_2F_6 /H_2 system without ICP for 3 h. SEM images of carbon nanowalls grown for **e** 15 min, **f** 30 min, and **g** 1 h. **h** Raman spectrum for carbon nanowalls in (**a**) (Hiramatsu et al. 2004)

nanowalls could be modified by controlling the H density and the CF_x and CH_x based on H injection.

Hiramatsu et al. (2006) also investigated the growth of carbon nanowalls by injecting H generated by an inductively coupled plasma (ICP) into a parallel-plate plasma CVD system together with a C_2F_6/H_2 gas mixture. Carbon nanowalls were found to form as the amount of injected H was increased by increasing the ICP power level. The H in this system was measured by VUVAS, while the CF, CF_2

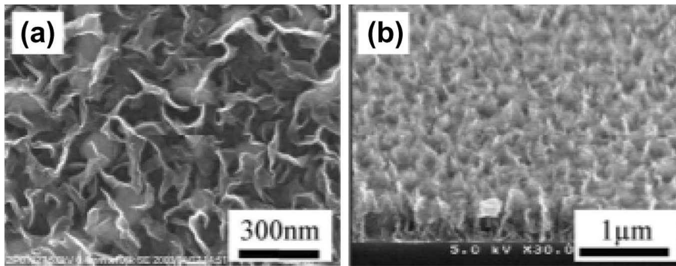

Fig. 43 SEM images of the carbon nanowalls grown on Si substrate using CH_4 /H_2 system for 3 h; **a** top view and **b** tilted view (Hiramatsu et al. 2004)

and CF_3 were monitored using appearance mass spectrometry. The results confirmed that the formation and shape of the carbon nanowalls could be adjusted by controlling the density of CF_x relative to the density of H (Fig. 44).

Figure 45 shows a tandem type of radical injection plasma CVD system capable of large-area radical-controlled processing. At the top of this equipment is a microwave plasma generator providing surface wave excitation that can generate a high electron density over a wide pressure range. At the base is a parallel-plate plasma equipment capable of 100 MHz excitation that can generate a high-electron-density plasma at a relatively low electron temperature. By connecting these two devices via multiple slits, the radicals generated in the upper part can be uniformly injected into the device in the lower part. In particular, the upper plasma source can introduce H_2 gas to generate high-density H, while the lower plasma source can introduce a feedstock gas to provide radical species that are effective during processing at a

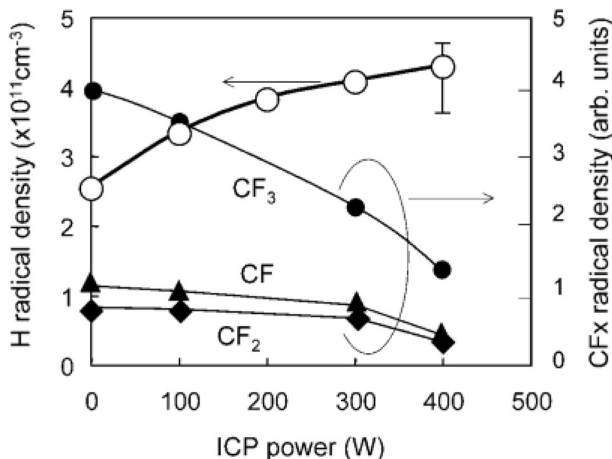

Fig. 44 H density in the capacitively coupled plasma region employing C_2F_6/H_2 system measured using VUVAS technique as function of rf power of remote H_2 inductively coupled plasma (ICP), together with behaviors of relative densities of CF_3, CF_2 and CF measured by appearance mass spectrometry (Hiramatsu et al. 2006)

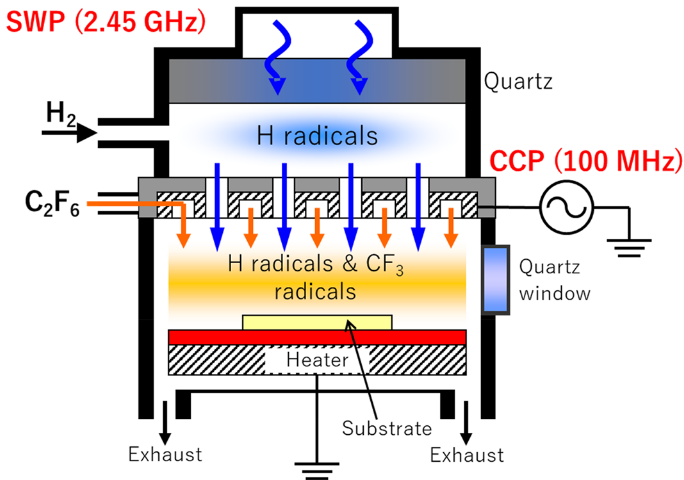

Fig. 45 Schematic illustration of the tandem type of Radical Injection Plasma Enhanced Chemical Vapor Deposition (RIPECVD) (Kondo et al. 2008)

low electron temperature while preventing excessive gas dissociation. By controlling both plasma parameters independently, H can be injected into the lower plasma chamber to control the density of H and radical species during deposition or etching (Kondo et al. 2008).

Using this system, Kondo et al. (2009) introduced O_2 gas in addition to H and CF_x radicals to control the appearance of O. Figure 46 presents Raman spectra of carbon nanowalls made with and without the introduction of O_2 gas, and demonstrates that the intensity ratios of the G-band (IG) to the D-band (ID): IG/ID ratio could be increased by injecting O. As a result, carbon nanowalls consisting of high-quality graphene with few defects were successfully synthesized by controlling the formation of H, CF_x and O. During the growth of these carbon nanowalls, the reaction rate for O with unconnected bonds was high, and such reactions could potentially generate defects in the graphite network. However, because these bonds were etched by the O, few defects appeared in the graphite.

Cho et al. (2014) found that there is a linear relationship between wall density and H density of carbon nanowalls, which can be controlled by the H density in the plasma. They showed that the relative composition in CH and H atoms is at least an indicator of film quality control.

While studying the injection of H into CH_4 gas for the synthesis of amorphous carbon films, Sugiura et al. (2018) investigated the relationship between the behavior of radicals and the resulting film compositions. Figure 47 plots the CH_3 density as a function of residence time along with the proportion of sp^2 hybridized carbon in the film based on trials using plasma-based CVD with a CH_4/H_2 gas mixture and the injection of H. When the residence time was decreased from 18 to 6 ms, the CH_3 density determined by mass spectrometry increased from 9.6×10^{10} to 1.6×10^{11} cm^{-3}. The sp^2 proportion of the a-C film reached a minimum of 46% at a residence time of 6 ms, at which point the CH_3 radical density was at its maximum.

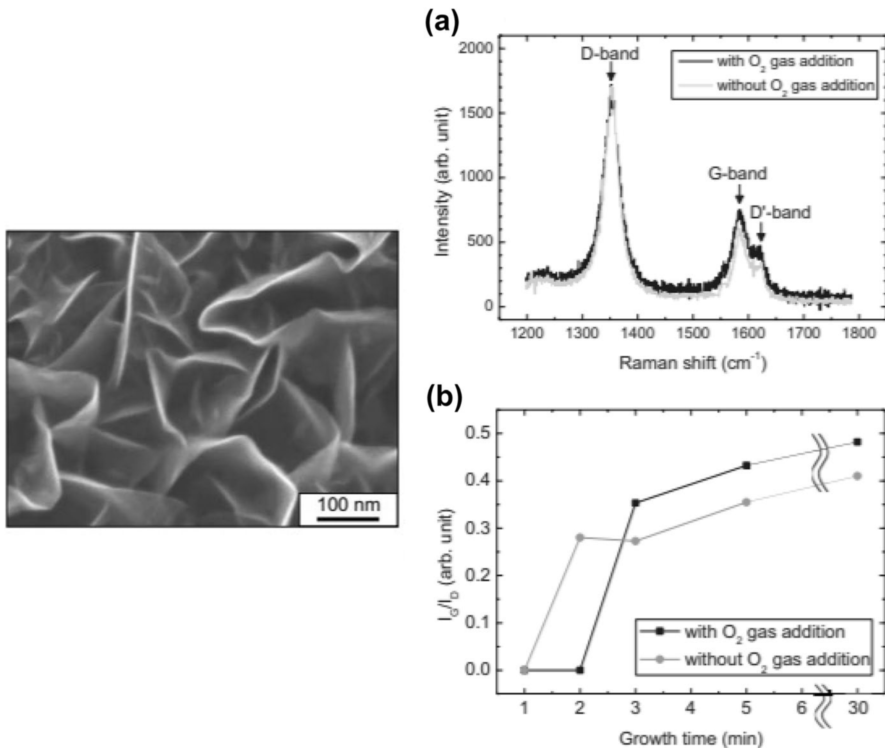

Fig. 46 Left diagram: top-view SEM image of a carbon nanowall film synthesized for 30 min with O_2 gas addition at 5 SCCM. Right diagram: **a** a Raman spectra of carbon nanowalls synthesized for 5 min with and without O_2 gas addition. **b** I_G /I_D ratios of CNWs synthesized with and without O_2 gas addition as functions of growth time (Kondo et al. 2009)

At longer residence times, the degree of CH_4 dissociation increased, while the C_2H_4 density decreased owing to the dissociation and recombination of precursors, leading to the lowest sp^2 proportion in the a-C films. These data indicate that the chemical bonding in a-C films, which are important for a variety of applications, could be modified by controlled radical injection. This knowledge improves our understanding of the formation mechanism and bonding structures of such films. Furthermore, such research is expected to eventually allow precise tuning of the electronic properties of a-C films.

5.10.2 Deposition and etching by CF_2 injection

Takahashi et al. (1996a) succeeded in injecting CF_2 into downstream ECR plasmas using Ar and H_2/Ar mixtures. IRLAS confirmed that only CF_2 radicals were produced from the thermal decomposition of hexafluoropropylene oxide (HFPO; CF_3CFOCF_2) and the deposition rates for fluorocarbon films were measured while varying the microwave power at a constant CF_2 density using the radical injection method. The results showed that CF_2 was important precursors for the formation of

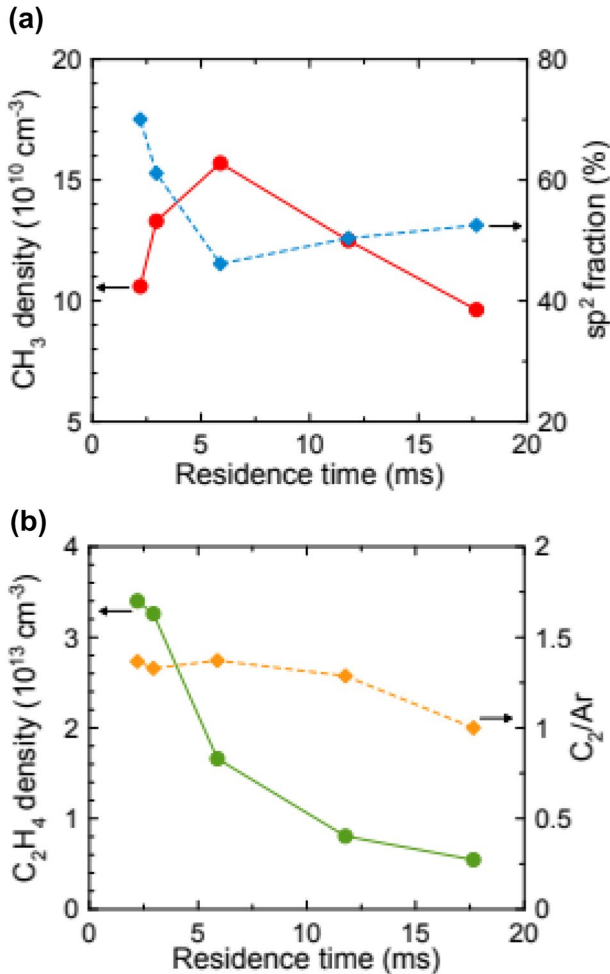

Fig. 47 **a** Dependence of CH_3 density (circles) on residence time. sp^2 fractions (diamonds) are also plotted in the right axis. **b** Dependence of C_2H_4 density (circles) on residence time. C_2/Ar ratios (diamonds) normalized by that at τ of 18 ms are also plotted (Sugiura et al. 2018)

fluorocarbon films in conjunction with surface activation by plasma irradiation. H atoms and CF_2 in the plasma were also found to play important roles in the formation of carbon-rich fluorocarbon films and to provide highly selective SiO_2 etching with the application of a bias to the substrate. Furthermore, a H_2/Ar ECR plasma with the downstream injection of CF_2 radicals exhibited highly selective SiO_2 etching.

Inayoshi et al. (1998) injected only CF_2 together with Ar gas at the downstream position of an ECR plasma and observed the reactions between these radicals and the substrate surface using in situ Fourier transform infrared (FTIR) spectroscopy. These reactions were evidently accelerated by Ar ion irradiation such that thin films with high concentrations of CF_2 could be produced (Fig. 48). The effect of Ar ions

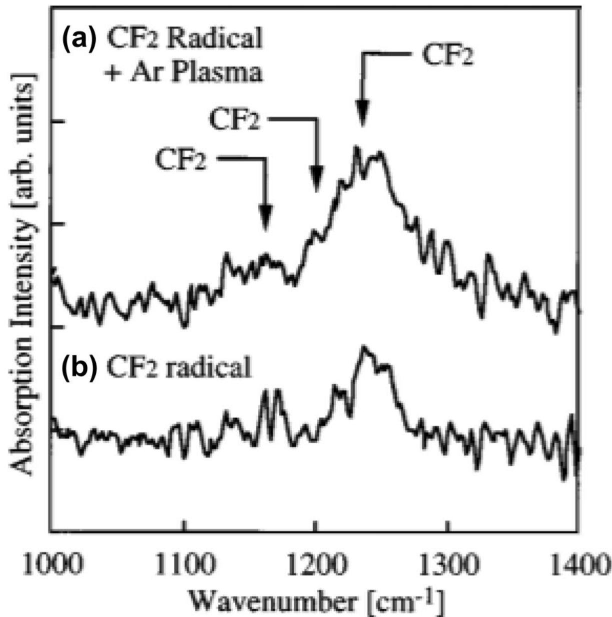

Fig. 48 FTIR spectra of **a** the fluorocarbon film formed on the a-Si surface in the ECR Ar downstream plasma with CF_2 injection and **b** the fluorocarbon film formed on the a-Si surface by CF_2 injection without the ECR Ar downstream plasma exposure (Inayoshi et al. 1998)

on the formation of fluorocarbon thin films was also evaluated by installing a pair of permanent magnets in the processing chamber to ensure that Ar ions did not contact the Si substrate. Under these conditions without ion bombardment, CF_2 did not result in thin-film formation. The results show that CF_2, an important precursor of polymer films, reacts with the substrate only under ion irradiation. Thus, by selectively injecting specific radicals into the plasma, the surface reactions of the radicals could be ascertained and a monochromatic radical process was realized.

6 Autonomously controlled radical processes

6.1 Autonomous time-evolving radical control

Hori and Goto (2006) reported the design of an autonomous plasma production equipment capable of self-diagnosis, self-determination and self-control. This apparatus used a small light source to monitor atomic radicals using VUVAS. The behavior of atomic radicals in the plasma was ascertained in real time and the data were fed back to the device to ensure that the processing conditions remained optimal. It was proposed that this device could realize nanoscale microfabrication of thin films by controlling radicals in the plasma in a time-resolved manner. In addition, the effectiveness of this concept was demonstrated by controlling H and N during plasma etching of organic low-k thin films (Nagai et al. 2003).

Figure 49 shows the variations in the patterns etched onto organic low-k films using various proportions of H and N and different substrate temperatures (Yamamoto et al. 2012). During the etching of organic thin films, H contribute to the actual etching while N form a protective film on the sidewalls of the etched pattern. This prevents the pattern from becoming bowed due to undercutting by H. It is also known that, when the density ratio of N to H is increased, the thickness of the sidewall protection film layer consisting of C–N bonds increases and the pattern changes to a tapered shape, as shown in Fig. 50. Thus, by precisely controlling the H and N, it is possible to form fine patterns with vertical shapes. The ratio of these radicals can be adjusted by monitoring their densities in plasmas generated using mixtures of H_2 and N_2 by VUVAS and controlling the relative flow rates for the two gases based on these data. In this manner, the fine pattern shape of an organic low-k thin film can be controlled. However, the loss probability (that is, the reaction coefficient) for H and N at the organic thin film varies greatly as the substrate temperature is changed, as shown in Fig. 49. Throughout the plasma etching process,

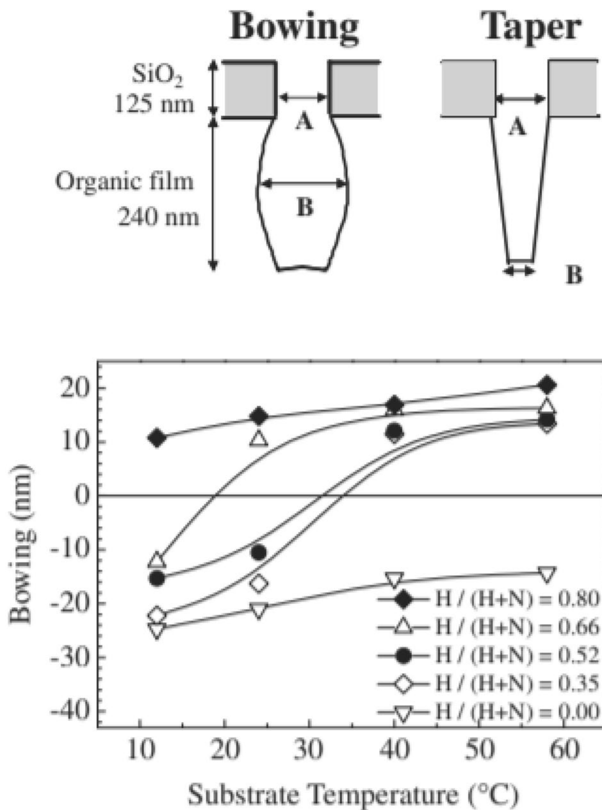

Fig. 49 Amount of bowing on sidewall of trench pattern as a function of substrate temperature (Yamamoto et al. 2012)

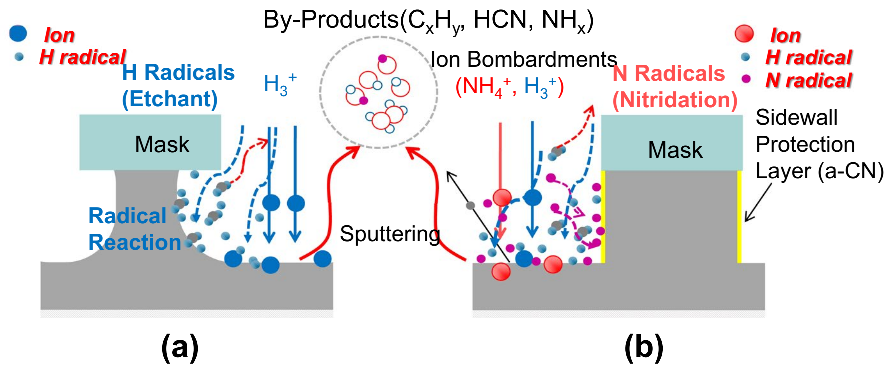

Fig. 50 **a** Etching of organic film by H_2 plasma, **b** Etching of organic film by H_2/N_2 plasma The sidewall protective layer consisting of carbon nitride film formed by N protects the etching reaction from H. On the other hand, the carbon nitride film formed on the bottom surface is etched by ion impact, resulting in the etching of a vertical shape

the substrate temperature rises due to the energy released by the collisions of ions. Yamamoto et al. (2012) found that vertical fine pattern shapes could be successfully obtained by changing the H/N ratio as the substrate temperature varied, as demonstrated in Fig. 51. As an example, a H/H + N ratio of 0.8 produced a pattern having a significantly bowed morphology, because the reaction rates for H radicals increased along with the substrate temperature, such that precise vertical shapes could not be obtained (Fig. 51a). A H/H + N ratio of 0.5 was used in an attempt to prevent this bowing but did not yield a highly precise pattern because of increases in the substrate temperature (Fig. 51b). It is apparent from such studies that ultra-high precision nano-scale etching requires the plasma conditions to be reoptimized as the etching pattern evolves. To achieve this, it will be necessary to create an autonomous plasma process in which the device itself identifies the optimal conditions while executing the etching process. Such technology is expected to lead to new types of semiconductor plasma processing.

Takahashi et al. (2012) developed an autonomously controlled plasma etching system (Fig. 52) that integrates a compact radical monitor based on VUVAS, an MHCL, a highly accurate Si substrate temperature monitoring device, a spectroscopic ellipsometer and an FTIR reflection absorption spectrometer attached to a chamber. This apparatus was able to perform contactless measurements of the substrate temperature during plasma processing in real time. The primary internal parameter for this system was the radical density ratio, while the external parameters were the VHF power of the top electrode, the RF power of the bottom electrode, the gas flow rate ratio and the pressure. The film thickness and composition were additional inputs to this process.

The system was equipped with feedback control that adjusted the radical density ratio. That is, a target value was selected for the radical density ratio (H/H + N) and the actual values were determined based on the mixed gas ratio or other external parameters. Using this apparatus, the etching rates for organic low-k films were autonomously controlled by monitoring the H and N densities and adjusting the gas

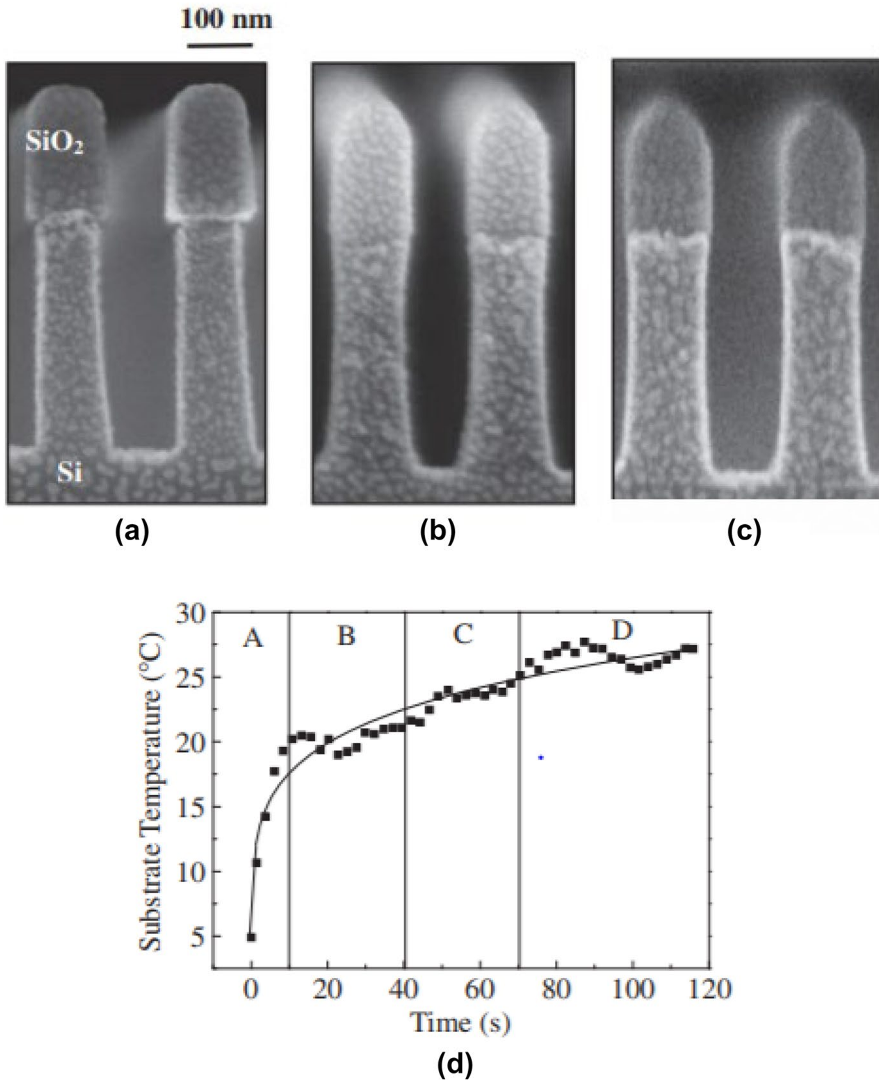

Fig. 51 SEM images of etched profile of organic film: **a** H/(H + N) = 0.80, **b** H/(H + N) = 0.52, **c** after new plasma process. Substrate temperature during new plasma processes in which radical density ratio varied as a function of plasma exposure time **d** (Yamamoto et al. 2012)

mixture ratios using a feedforward and feedback compensation mechanism (Fig. 53). Figure 54 presents the results obtained from the autonomous control of the H/H + N ratio. The target values were 0.4 between 0 and 65 s, 0.6 between 65 and 130 s and 0.4 after 130 s. The sampling interval for the radical density measurements was set to 1 s for the two radical density monitors, and the red line in Fig. 54 shows the radical density ratio as determined by these monitors. It can be seen that this value was almost equal to the target value. This result indicates that the radical density

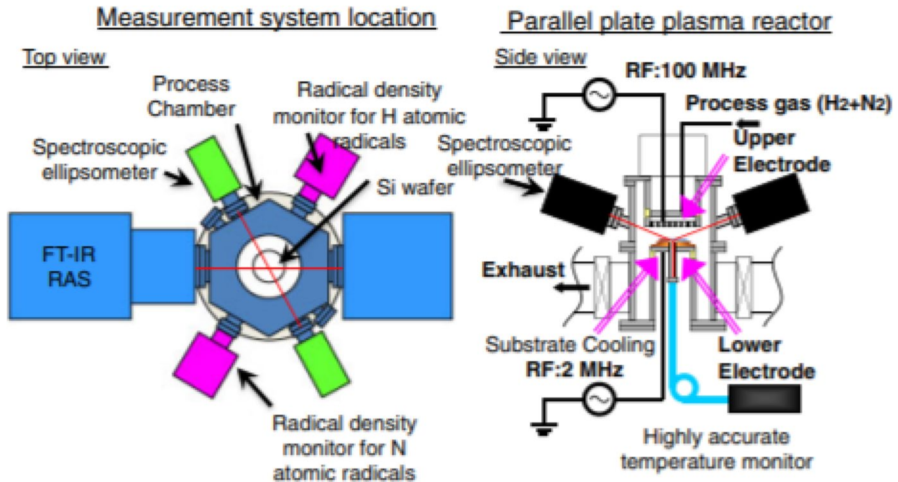

Fig. 52 Schematic diagram of autonomously controlled plasma etching system (Takahashi et al. 2012)

ratio could be controlled autonomously by changing the mixed gas flow rate ratio via computer according to optimal values obtained in advance using radical density data generated by the radical monitors. Using this system, the autonomous control of the etching for organic low-k films was successfully achieved.

6.2 Ultra-high precision etching with autonomous control of radicals and temperature

In general, even if attempts are made to maintain a constant substrate temperature using an electrostatic chuck or other apparatus, this temperature will increase due to the injection of high-energy ions during plasma processing. Especially during etching, the effect of ion irradiation on the substrate temperature cannot be ignored, because etching proceeds via the mutual reactions of fast ions and radicals. Even so, it has traditionally been difficult to accurately measure the substrate temperature in real time during plasma processes. Tsutsumi et al. (2013, 2015a) developed an interferometer using an incoherent light source to allow in situ substrate temperature monitoring during plasma processing. This device was able to measure the temperature of a Si wafer at 50 ms intervals using an autocorrelation-type frequency-domain low-coherence interferometer with a precision of 0.04 °C. Figure 55 presents the relationship between the etching shape and temperature based on the results of real-time measurements of the substrate temperature with an interferometer while maintaining the H/H + N ratio at 0.52 during the etching of organic low-k thin films (Yamamoto et al. 2012). At low substrate temperatures, a tapered etching shape was obtained, whereas higher temperatures resulted in a bowed shape. It is apparent that obtaining a vertical shape (A–B = 0) with a pattern size variation on the order of 1 nm required the substrate temperature to be controlled within 1 °C. As noted, the present technology available for controlling radical ratios in real time

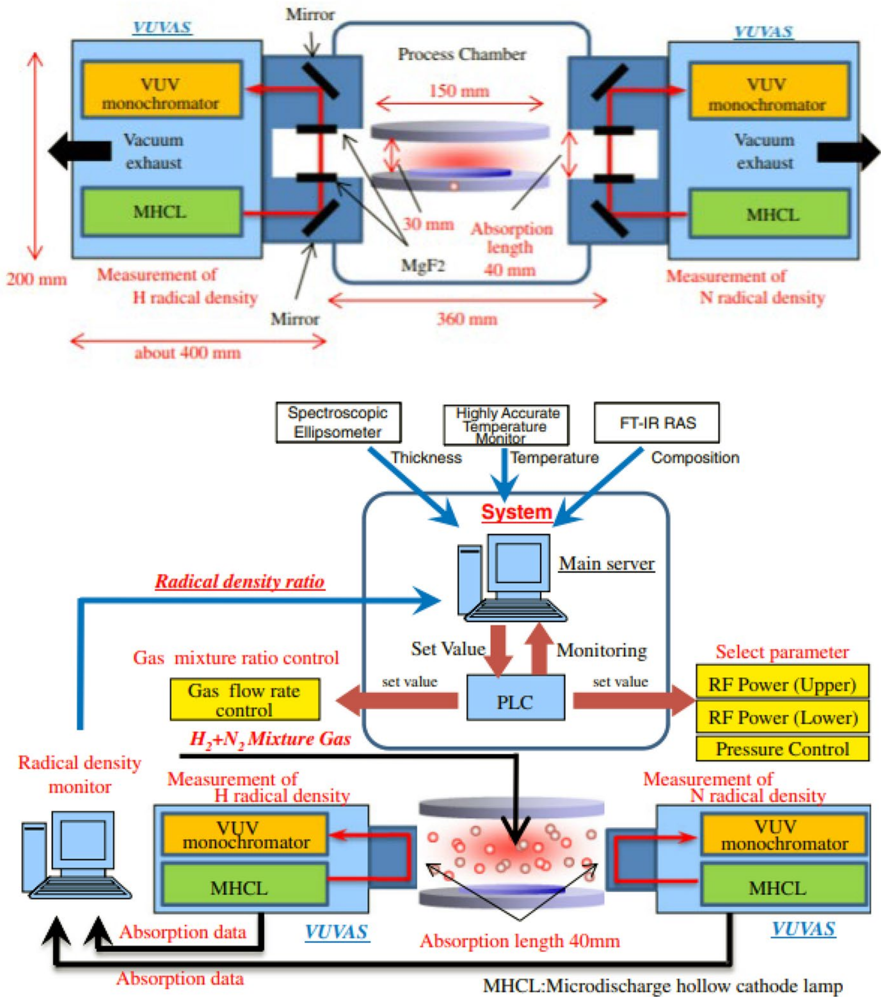

Fig. 53 Schematic diagram of feedback control system for radical density ratio H/(H + N) (Takahashi et al. 2012)

is not sufficient to allow nano-scale etching with ultra-high precision, and so new methods are needed. As a means of addressing this problem, a technology has been developed that provides a constant substrate temperature by controlling the on/off state of the plasma source. In the autonomous etching system described above, the temperature data acquired using the interferometer are sent to a server in real time and these data are used to adjust external parameters associated with the etching system, such as valves and power supplies. Tsutsumi et al. (2015b) reported highly accurate control over the temperature of a Si wafer based on varying the on/off times of the power supplies to the top and bottom electrodes, which in turn was predicated on real time temperature data.

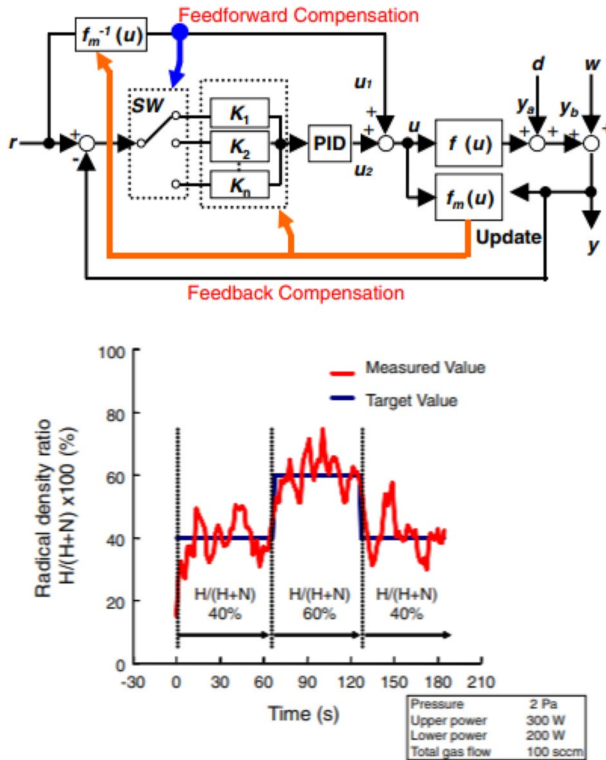

Fig. 54 Temporal control of radical density ratio H/(H + N) by autonomous system with controlling the gas mixture ratio using a feedforward and feedback compensation system. (Takahashi et al. 2012)

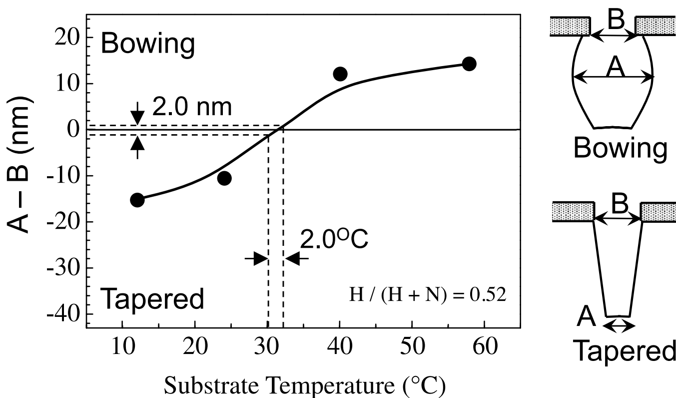

Fig. 55 Evaluation of pattern dimensional variation from vertical direction due to substrate temperature variation, taken from Fig. 49 (Yamamoto et al. 2012)

The data in Fig. 56 demonstrate that the temperature of the wafer was kept stable within a few degrees during etching of organic films with a H_2/N_2 plasma by autonomously turning the power supply to the upper electrode on and off at the optimum pulse duty ratio in response to the rise in wafer temperature caused by ion irradiation. In a typical etching system, the wafer is held by an electrostatic chuck and cooled by refrigerant and/or He gas from a chiller. In addition to the ion irradiation, the temperature rise of the components around the wafer also contributes to heating of the wafer, such that the wafer temperature during etching changes in a complicated manner. However, as shown in Fig. 56b, the duty ratio per discharge was automatically and gradually decreased, such that the wafer temperature was maintained

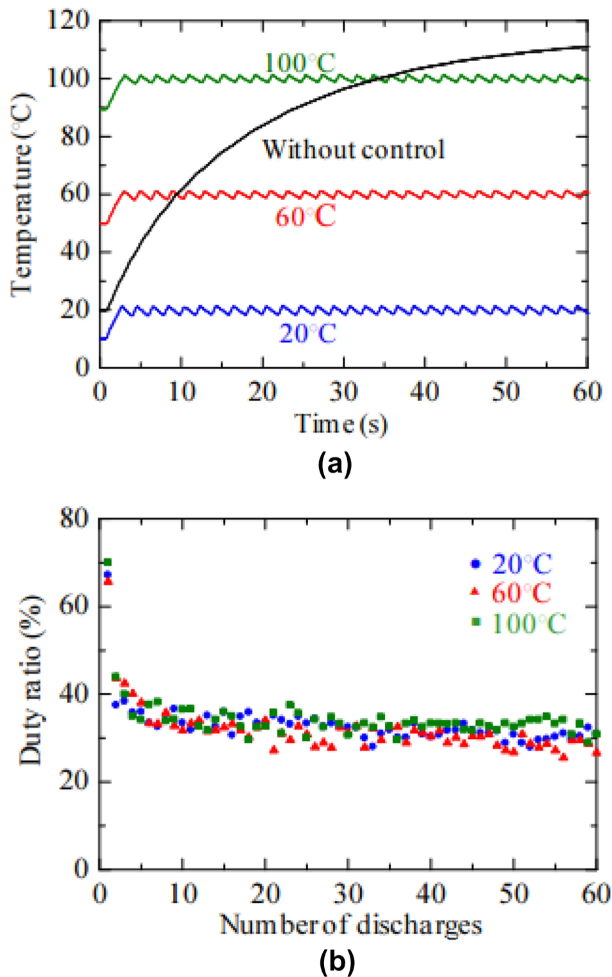

Fig. 56 **a** Temporal variations of wafer temperature during plasma processes with and without wafer temperature control. **b** Duty ratio variations per discharge in plasma processes with wafer temperature control (Tsutsumi et al. (2015b)

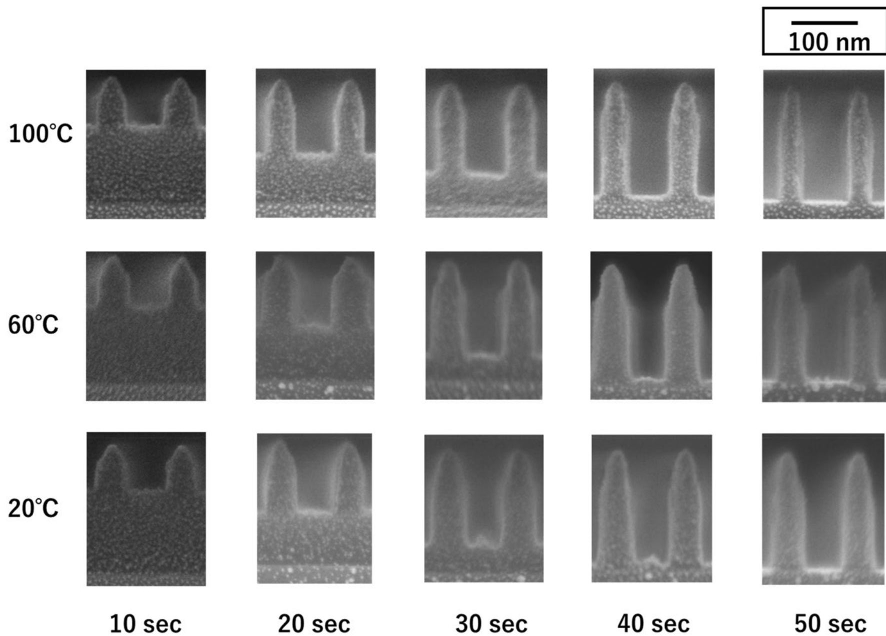

Fig. 57 Cross-sectional SEM images of organic film etched features for wafer temperatures and cumulative discharge time (Tsutsumi et al. 2015b)

at a constant value. Using this feedback system, wafer temperatures of 20, 60 or 100 °C could be maintained during etching. Figure 57 shows the results obtained from the etching of organic low-k thin films using hydrogen and nitrogen plasmas with the radical ratio maintained at 0.51. These trials likely represent the first-ever etching with the substrate temperature kept constant. The figure shows the film morphologies that were obtained as the wafer temperature was varied. As the temperature was increased, the trench width etched into the organic film became larger. This width was determined by the balance between the etching reaction and the effect of temperature on the formation of the protective film on the trench sidewalls. Consequently, the use of autonomous adjustment of the substrate temperature and radical ratio allowed the etching of 3D micropatterns with an exceptional degree of control over dimensional fluctuations (Tsutsumi et. 2015b).

7 Radical control in atmospheric-pressure plasma processing

Kanazawa et al. (1988) and Okazaki et al. (1989) succeeded in generating a glow plasma under atmospheric pressure. This pioneering research led to the development of industrial applications for atmospheric-pressure low-temperature plasmas, and also created new research trends in the field of plasma physics and chemistry (Kogelschatz 2003). The development of high-speed etching and surface treatment techniques would be highly beneficial with regard to the manufacturing of

microscale mechanical elements such as micro-electromechanical systems and in the surface modification of roll-to-roll polymer sheets. Traditionally, low-pressure, high-density plasma processes have been used to treat these materials but do not provide sufficient throughput. In addition, more than half of the manufacturing process takes place in a reactive gas atmosphere in a vacuum. As a result, the associated equipment and facilities have become more complex and larger and the accompanying cost increases have become a serious problem. A non-equilibrium atmospheric-pressure plasma process has been proposed as a means of addressing these issues. The electron density in this plasma is approximately 10^{13}–10^{17} cm^{-3}, which is more than three orders of magnitude higher than those in conventional vacuum plasmas. In addition, the electron temperature is approximately 1 eV lower than those for standard systems, and because a vacuum is not required, the cost and processing time can be reduced.

Using this plasma, ultrahigh density radicals and ions can be injected into the substrate surface. In addition, because it is a low-temperature plasma, the process can be designed based on the knowledge previously accumulated from conventional low-pressure plasma processes. In general, the density of radicals in atmospheric-pressure low-temperature plasmas is more than three orders of magnitude higher than that in a conventional vacuum plasma, while the gas temperature ranges from around room temperature to a few thousand degrees C. The mean free paths of particles in atmospheric-pressure plasmas are on the micrometer scale and the ultra-dense radicals generated in these systems are instantly annihilated by particle collisions. Furthermore, atmospheric-pressure plasmas allow the introduction of solutions, and the resulting combination of wet and dry characteristics can provide radicals with unique physical chemistries, leading to new processing technologies.

Atmospheric-pressure low-temperature plasmas can be used for ultra-fast material processing, deposition and surface treatment and can also be applied for the purpose of killing pathogenic bacteria, inducing apoptosis (programmed cell death) in cancer cells, healing of skin diseases and injured tissues, and regeneration of biological tissues. Thus, research regarding the medical applications of plasmas has become of interest worldwide. Plasmas are also being applied in agriculture and fisheries, such as to promote the growth of plants and fish, and may, therefore, represent one aspect of addressing a future food crisis. On this basis, atmospheric-pressure, low-temperature plasmas may result in the establishment of a new interdisciplinary field that integrates the science and engineering of plasmas with medicine, agriculture and fisheries, and molecular biology. It should be noted that these advances will require the development of techniques for monitoring and controlling radicals in such plasmas.

7.1 Radical controlled atmospheric-pressure plasmas for industrial applications

Kono et al. (2001) developed a microwave-excited atmospheric-pressure low-temperature plasma incorporating a micro-gap, while Yamakawa et al. (2004) used the microwave-excited atmospheric-pressure low-temperature plasma system to etch SiO_2, employing gaseous He with NF_3 and H_2O. The extent of SiO_2 etching was

found to depend on the NF_3 flow rate and the distance between the plasma and the substrate. Increasing the NF_3 flow rate increased the etching rate and rapid etching of approximately 14 µm/min was obtained at a distance of 5 mm. This etching rate was close to one order of magnitude greater than that obtainable with conventional low-pressure high-density plasmas. This etching process exhibited minimal Si etching and so provided a very high SiO_2/Si selectivity ratio of more than 200. The etching mechanism was investigated using FTIR spectroscopy to examine particles in the plasma. Approximately 60% NF_3 dissociation was observed and a peak between 3800 and 4200 cm^{-1} indicated the formation of HF. These results suggested that HF was produced by the reaction between H_2O and fluorine radicals in the NF_3 plasma.

Figure 58 provides a diagram of this ultrafast and highly selective etching reaction processes using He, NF_3, H_2O and He, NF_3 systems (Yamakawa et al. 2005a). Analyses employing emission spectroscopy found that N, F, H, O, OH and N_2 were present in the former plasma, while N, F and N_2 were generated in the latter. These are considered to be the active species in the vicinity of the electrode. At d = 5 mm (that is, near the electrode), both SiO_2 and Si could be rapidly etched, such that the SiO_2/Si selectivity ratios for these two systems were as low as 5.1 and 1.2, respectively. The associated reactions are believed to have been

$$SiO_2 + 4F \rightarrow SiF_4 + O_2 \tag{7.1}$$

and

$$Si + 4F \rightarrow SiF_4. \tag{7.2}$$

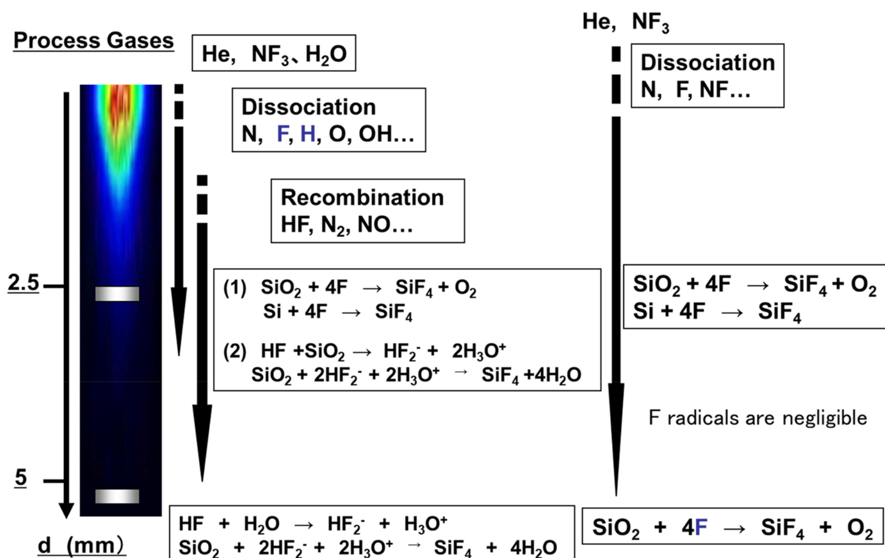

Fig. 58 Etching model for microwave-excited nonequilibrium atmospheric pressure plasma (Yamakawa et al. 2005a)

In contrast, the addition of H_2O caused the F radicals to collide with other particles at a distance of 5 mm from the electrode as described above, resulting in the generation of more HF. Because the SiO_2/Si selectivity ratio was more than 200 under these conditions, the F radicals capable of etching the Si appear to have rarely reached the substrate, indicating that the etching was mainly caused by HF. In the presence of water, it has been reported that HF and SiO_2 undergo the reactions:

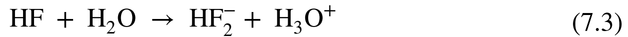

$$HF + H_2O \rightarrow HF_2^- + H_3O^+ \tag{7.3}$$

and

$$SiO_2 + 2HF_2^- + 2H_3O^+ \rightarrow SiF_4 + 4H_2O. \tag{7.4}$$

Without the addition of H_2O, the etching rate was very low and the selectivity ratio was as low as 2, suggesting that only a small number of F reached the substrate. As discussed above, the addition of H_2O caused a rapid decrease in the number of F and promoted the formation of HF. Controlling the densities of F, HF and H_2O was found to be important with regard to obtaining a high selectivity ratio during high-speed etching. The data from this system indicated that, in the case of atmospheric-pressure plasmas, the mean free path is very small (less than 1 μm) and so many radicals react in the gas phase and are inactivated (Yamakawa et al. 2005a).

Iwasaki et al. (2006) achieved a high etching rate by introducing water during the etching of SiO_2 by an atmospheric-pressure CF_4/Ar gas plasma generated by a dielectric barrier discharge in conjunction with a pulsed electric field (Fig. 59). A SiO_2 etching rate of 400 nm/min could be obtained with the addition of a small amount of

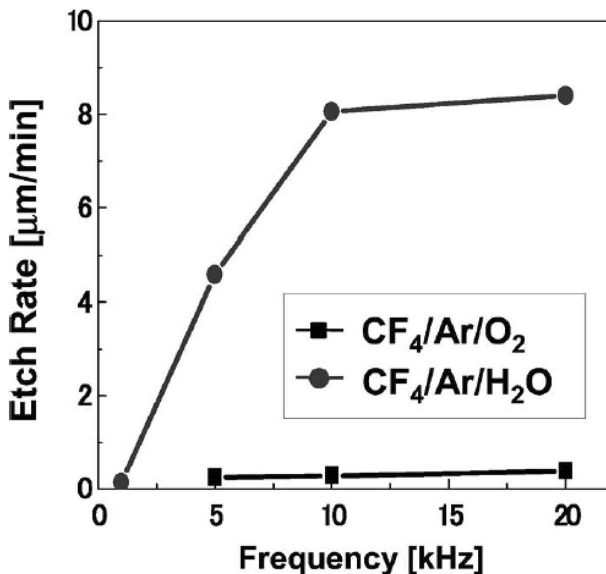

Fig. 59 Characteristics of the SiO_2 etch rate with H_2O gas or with O_2 gas in the atmospheric-pressure pulsed plasma (Iwasaki et al. 2006)

oxygen gas, indicating that the etching of SiO_2 was promoted by chemical reactions in the atmospheric-pressure plasma even without high-energy ion bombardment. Furthermore, upon adding H_2O, an ultrafast SiO_2 etching rate of more than 8 μm/min was obtained at 20 kHz. This SiO_2 etching in association with H_2O addition was found to be highly dependent on the presence of HF. The behavior of fluorocarbon-based molecules and higher order radicals with and without the addition of water together with the characteristics of SiO_2 etching were investigated by Li^+ ion attachment mass spectrometry (IAMS). Figure 60 provides the IAMS spectra of the gases discharged from the plasma source without and with added H_2O (Iwasaki et al. 2006). These experimental results suggest that SiO_2 etching with H_2O addition was greatly affected by variations in the HF concentration. The results obtained using a CF_4 plasma also confirmed the validity of the HF etching model proposed by Yamakawa et al. (2004). Certain gases could be discharged from the plasma source without any molecular fragmentation, including CF_4Li^+, $C_2OF_4Li^+$, $C_3HF_5Li^+$, $C_3F_6Li^+$ and $C_3HF_7Li^+$, while $C_3F_6Li^+$, $C_3HF_7Li^+$, $C_4F_8Li^+$ and $C_4HF_9Li^+$ could be used for calibration. These results demonstrated that the formation of both C_3HF_7 and C_3F_6 was drastically reduced when H_2O was added to the CF_4. In addition, CF_2 and CF_3 generated in the plasma were found to be recombined by a three-body collision

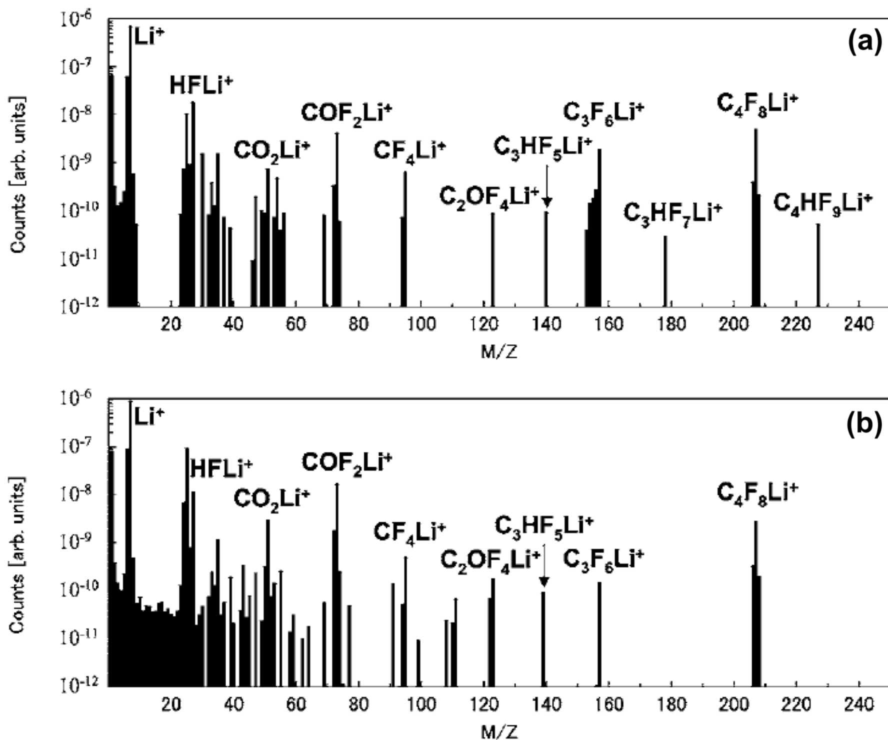

Fig. 60 Mass spectrum of the gases exhausted from the plasma **a** without addition of H_2O and **b** with addition of H_2O to CF_4 (Iwasaki et al. 2006)

reaction to generate heavier species in the remote plasma region. Higher order radicals are well known as precursors to the formation of protective layers that reduce the etching rate for SiO_2, and the generation of higher order radicals such as C_3HF_7 and C_3F_6 was significantly suppressed by H_2O addition such that the etching rate was improved. The proportion of stable COF_2, which is thought to be generated by the reactions of lower molar mass radicals, such as CF_2, CF_3 and O, was also increased with the addition of H_2O.

Using the non-equilibrium atmospheric-pressure plasma excited by microwaves, Yamakawa et al. (2005b) successfully etched a film made of the organic material FLARE™ at a high rate of 24 m/min using He and O_2 gases (Fig. 61). In other trials using a substrate temperature of 325 °C, the etching rate of the organic film was an ultrafast 315 m/min. The etching rate was found to increase as the distance, d, from the electrode to the substrate was decreased, as shown in Fig. 61a. The density of O, as estimated from the O/Ar emission intensity ratio, increased as d decreased, while the ozone density decreased (Fig. 61b). These results are the opposite of those obtained during the etching of organic films. The activation energy for organic film etching was estimated to be 0.53 eV from an Arrhenius plot, and this value is almost

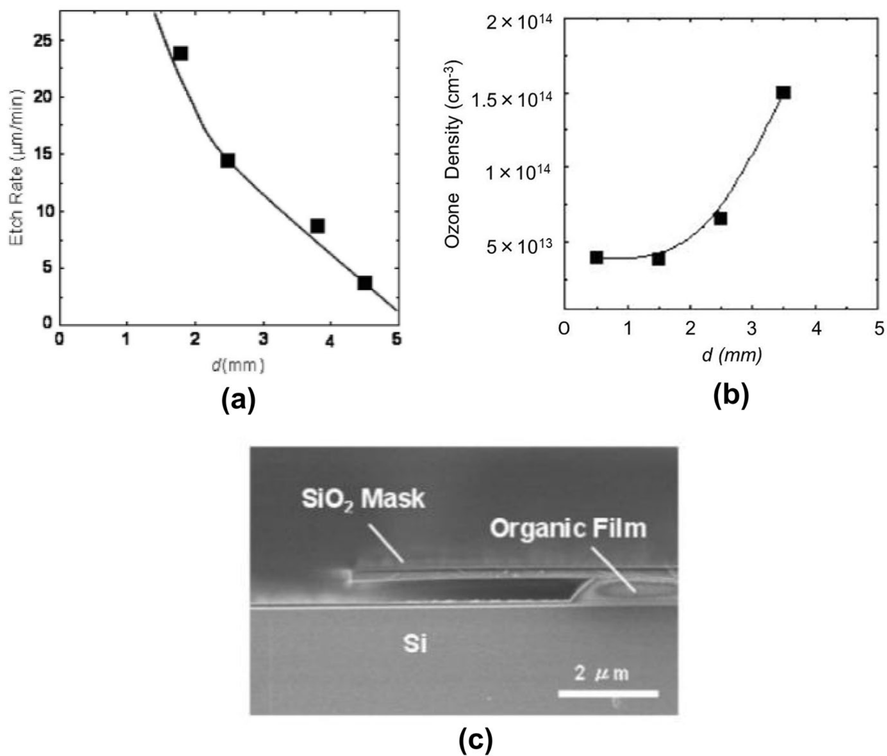

Fig. 61 Etching rate of organic film as a function of distance from electrode (**a**). The ozone density as a function of from electrode (**b**). Cross-sectional scanning electron microscope SEM image of the etched profile of the organic film (**c**) (Yamakawa et al. 2005b)

equal to that for etching by O. Consequently, O is believed to be the main organic film etching species in this plasma system.

This process suggests new approaches to the high-speed microfabrication of organic films in a variety of applications (Fig. 61c). One of the most important industrial applications of atmospheric-pressure plasmas is surface treatment, including the preparation of glass substrates for liquid–crystal devices, removal of metal oxide films in plating systems and pretreatment prior to the bonding of dissimilar materials. In these cases, ultra-high processing speeds are desirable and there is a need for ultra-high density atmospheric-pressure plasmas capable of broadband processing.

Iwasaki et al. (2008) developed an apparatus in which the current between two electrodes was alternated to provide broadband, high-speed processing using an ultra-high density atmospheric-pressure low-temperature plasma (Fig. 62). The rotational temperature in this plasma was estimated from the emission spectrum of the N_2 second positive system ($C^3\Pi_u$–$B^3\Pi_g$), while the electron density was calculated by fitting the hydrogen Balmer series optical emission spectrum (H_β: 486.17 nm) using a Voight function considering Doppler, pressure, instrumental and Stark broadening. Figure 63 shows that the electron density in this plasma was on the order of 10^{16} cm^{-3} at a 1% O_2/Ar gas flow rate of 15 standard liters per minute and that this density was increased by the addition of O_2 gas. The $O(^3P_j)$ radical density was ascertained using VUVAS and found to be extremely high at 1.6×10^{15} $cm^{-3,}$ while the gas temperatures were in the range of 1800–2150 K. The O density increased along with the O_2/Ar ratio up to a ratio value of 1%, above which the density decreased, as shown in Fig. 64. The O density obtained at atmospheric pressure was also much higher than the values found in low-pressure plasmas. The O was determined by the reaction:

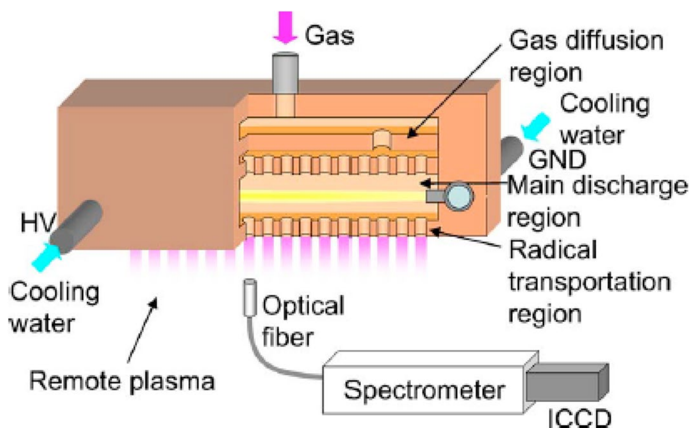

Fig. 62 Schematic illustration of nonequilibrium atmospheric pressure plasma excited by a 60 Hz ac power supply and optical emission spectroscopy (OES) system (Iwasaki et al. 2008)

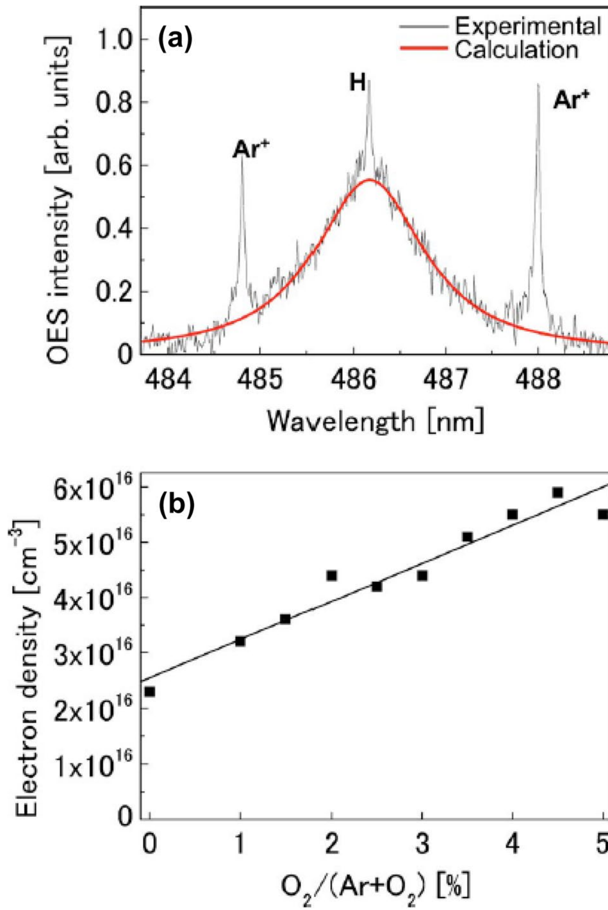

Fig. 63 Optical emission spectrum of H as observed in the measured and calculated spectra (Iwasaki et al. 2008)

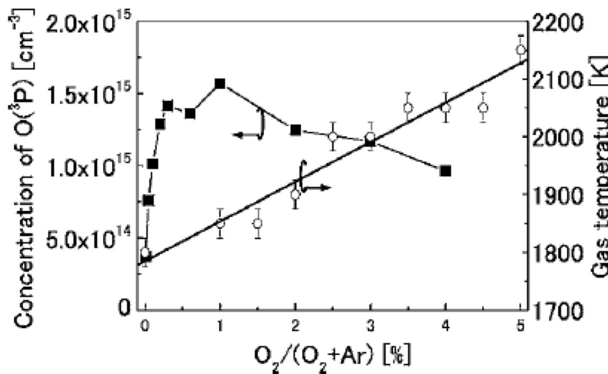

Fig. 64 Ground-state oxygen radical O (^3P_j) concentration and the gas temperature in the main discharge as functions of the O_2 /Ar mixing ratio(Iwasaki et al. 2008)

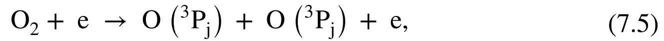

$$O_2 + e \rightarrow O\left({}^3P_j\right) + O\left({}^3P_j\right) + e, \quad (7.5)$$

along with the recombination reactions

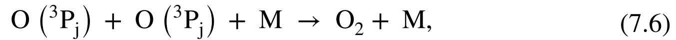

$$O\left({}^3P_j\right) + O\left({}^3P_j\right) + M \rightarrow O_2 + M, \quad (7.6)$$

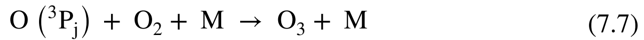

$$O\left({}^3P_j\right) + O_2 + M \rightarrow O_3 + M \quad (7.7)$$

and

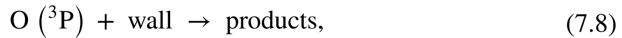

$$O\left({}^3P\right) + \text{wall} \rightarrow \text{products}, \quad (7.8)$$

where M is a species such as Ar that participates in three-body reactions. The rate constants for Eqs. (7.6) and (7.7) were determined to be 1.47×10^{-34} and 2.0×10^{-35} $cm^6\ mol^{-2}\ s^{-1}$, respectively, when using Ar at a temperature of 2,000 K.

In this system, the dissociation reaction of O_2 induced by electron impacts occurred more frequently as the amount of O_2 added to the Ar was increased, as a result of the greater electron density according to Eq. (7.5). That is, a high density of O was generated in conjunction with a high electron density. The recombination reactions in Eqs. (7.6) and (7.7) were evidently the primary reactions in the plasma, because the O densities were measured in the remote plasma region. Especially, the O in the plasma was transported to the downstream region by the gas flow, during which frequent collisions resulted in the production of O_3. The O density decreased at O_2 proportions in the Ar flow greater than 1%.

An untreated glass substrate exhibited a contact angle of 50° due to the presence of organic matter on its surface but this value was reduced to less than 10° after 23 ms plasma irradiation in the case that O_2 was added to the Ar plasma at 1% or more. Interestingly, the density of O was found to reach a maximum at a level of 1% and decreased at higher concentrations. This discrepancy between the cleaning properties of the plasma and its O density can possibly be ascribed to the effects of gas temperature and UV radiation on the cleaning performance, both of which would be associated with increases in electron density due to the addition of O_2.

In atmospheric-pressure plasmas, the radical density and temperature are highly dependent on the loss processes, because the mean free path of radical species is less than 1 μm. In particular, the addition of O_2 significantly increases the temperature of the O and promotes surface chemical reactions.

Inui et al. (2010) reduced copper oxides using the atmospheric-pressure low-temperature plasma excited with a 60 Hz alternating current and having an ultra-high electron density of over 10^{16} cm^{-3}, employing a H_2/Ar gas mixture. The gas temperature and electron density data obtained from these experiments are presented in Fig. 65 and can be seen to differ from the values for an O_2/Ar plasma shown in Fig. 64. Figure 66 provides the H densities, which were determined to be on the order of 10^{12} cm^{-3} using VUVAS. This approximate density is three orders of magnitude smaller than the value obtained with an O_2/Ar atmospheric-pressure plasma using the same equipment (Fig. 64). The density was also found to increase with

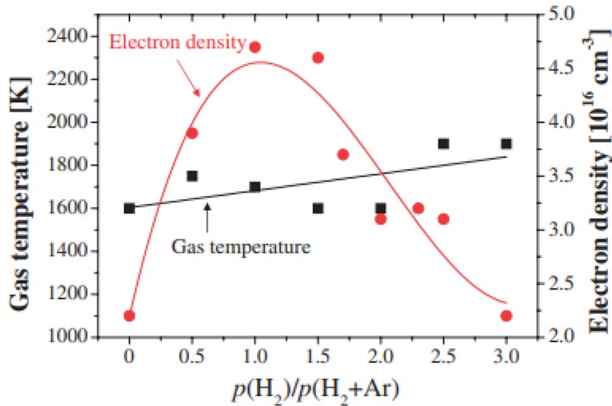

Fig. 65 Gas temperature and electron density as functions of H_2 / (H_2 + Ar) (Inui et al. 2010)

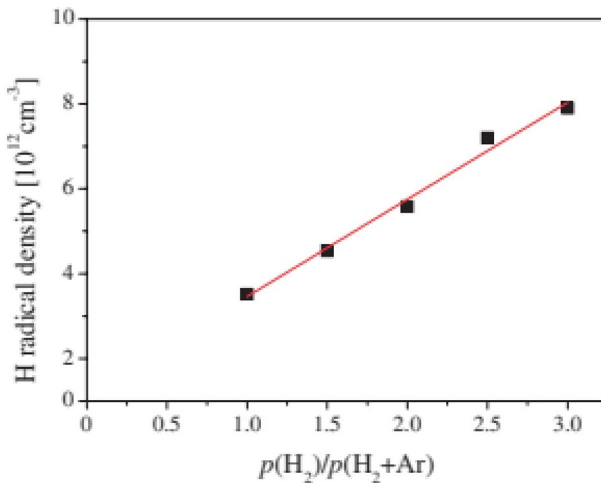

Fig. 66 H density in the remote plasma region as a function of H_2 /(H_2 + Ar) gas (Inui et al. 2010)

increasing H_2 addition. Therefore, the H density exhibited different behavior from that of the O density, which increased as the amount of O_2 was increased up to 1% but decreased with the further addition of O_2. O were lost rapidly in this system, while the rate of H recombination was lower. Using the H_2 plasma, neither CuO nor Cu_2O could be reduced in the vicinity of 200 °C although exposure to H reduced these copper oxides at 90 °C. The associated reactions involving H may have been

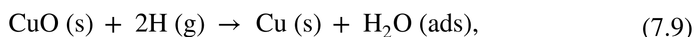

$$\mathrm{CuO\ (s) + 2H\ (g) \rightarrow Cu\ (s) + H_2O\ (ads)}, \tag{7.9}$$

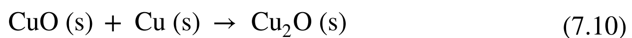

$$\mathrm{CuO\ (s) + Cu\ (s) \rightarrow Cu_2O\ (s)} \tag{7.10}$$

and

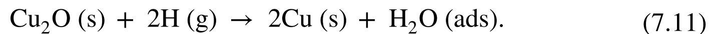

$$Cu_2O\ (s) + 2H\ (g) \rightarrow 2Cu\ (s) + H_2O\ (ads). \tag{7.11}$$

Figure 67 shows the thicknesses of copper oxide specimens after the H_2/Ar plasma treatment (Inui et al. 2010). Here, sample 1 was processed at a rate of 1 mm/s, while samples 2 and 3 were treated at 0.1 mm/s. Note also that samples 2 and 3 were exposed to the same treatment but the process was repeated five times in the case of sample 3. The thicknesses of the copper oxide layers (which consisted of CuO and Cu_2O) decreased as the duration of exposure to the H radicals in the remote plasma was increased. CuO was evidently reduced to Cu_2O when using a rate of 1 mm/s, while both CuO and Cu_2O were further reduced at the treatment speed of 0.1 mm/s to the point that they were completely reacted. Under these experimental conditions, the effects of ions on the sample surface were considered to be negligible, because the sample was situated relatively far from the plasma. The increase in the amount of Cu_2O observed in conjunction with a processing rate of 1 mm/s can be attributed to the reaction of CuO with Cu. Therefore, the increase in the amount of underlying Cu_2O indicates that reduction occurred both at the CuO surface and at the CuO/Cu_2O and Cu_2O/Cu interfaces due to the interdiffusion of H, CuO_x ions and Cu ions. The effect of H exposure on the reduction of Cu oxides in these trials was qualitatively estimated. As shown in Fig. 66, the H density was on the order of 10^{12} cm^{-3} and the H flux at the copper oxide surface was estimated to be 5×10^{16} $cm^{-2}\cdot s^{-1}$. Consequently, the rate of reduction of CuO at ambient temperature was determined to be approximately 4×10^{14} $cm^{-2}\cdot s^{-1}$ based on changes in the CuO thickness and density. From these data, the ratio of the amount of CuO reduced to the H flux was calculated to be approximately 0.008. It is apparent that a large number of H is necessary for the reduction of copper oxides. These trials also indicate that a high-density atmospheric-pressure plasma employing a H_2/Ar gas mixture can effectively reduce CuO.

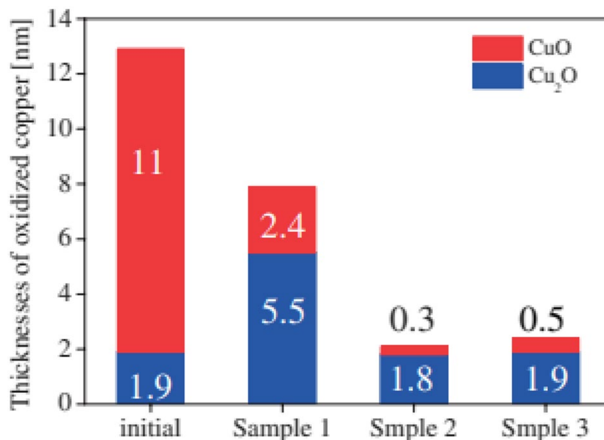

Fig. 67 Thicknesses of copper oxides after the H_2 /(H_2 + Ar) gas treatment (Inui et al. 2010)

7.2 Atmospheric-pressure low-temperature plasmas for biological applications

Atmospheric-pressure low-temperature plasma technology has made it possible to irradiate liquids and living organisms with plasma and the cross-reaction field between plasmas and living organisms has attracted much attention. Graves (2012) reviewed reactive oxygen and nitrogen species in redox biology and indicated some applications to medicine and biology. Lu et al. (2016) provides a systematic overview of particle production, transport and bio-implications related to atmospheric pressure non-equilibrium plasmas. The exposure of living organisms to plasma (direct irradiation) or injections of plasma-activated solutions into living organisms (indirect irradiation) have been found to produce unique phenomena, such as the selective destruction of cancer cells, non-invasive hemostasis, wound healing and immunotherapy. Furthermore, these techniques can effectively kill pathogenic bacteria, inactivate viruses, and promote plant growth and function. It is also known that the chemically active species generated in a plasma can have a significant effect on living tissues. Figure 68 summarizes the chemical and biological reactions that occur when living organisms or liquids are exposed to a plasma. Because of the presence of liquid on the surfaces of living tissues, a chemical reaction field is generated and it is important to clarify and control the reactions between the plasma and liquid. There are a wide variety of radicals among the chemically active species produced by a plasma, which can be classified into short-lived radicals and

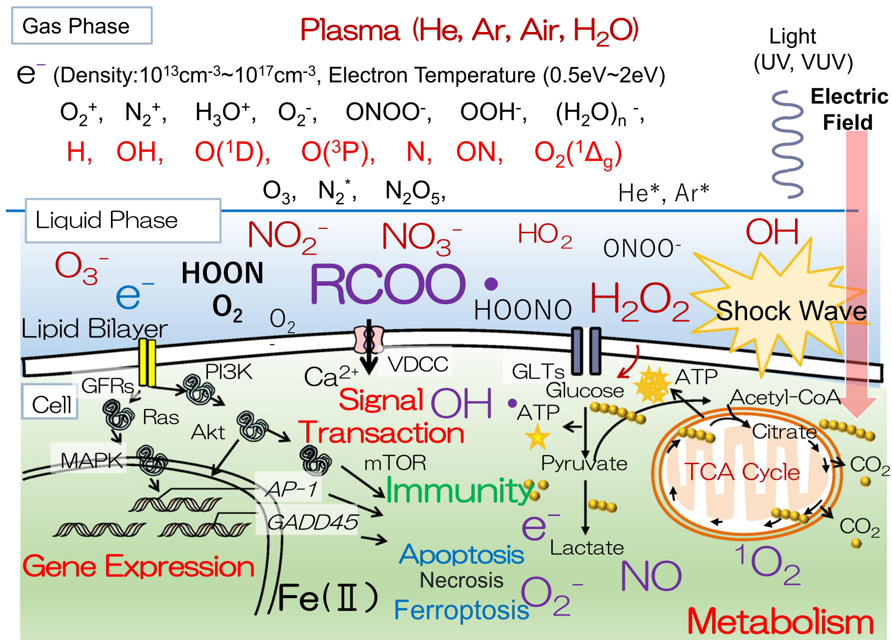

Fig. 68 Chemical and biological reactions that occur when living organisms or liquids are exposed to a plasma

medium-to-long-lived radicals. During direct irradiation, short-lived reactive species, electric fields, shock waves and radiation can interact with living organisms.

In the case of indirect irradiation, the short-lived active species disappear due to reactions with other molecules, while the chemical and biological effects of the medium- and long-lived active species are maintained. The inorganic and organic species generated by plasma irradiation can induce various signaling events in cells and cause the emergence of super-biological phenomena. During the application of atmospheric-pressure and low-temperature plasmas to living systems, ROS, RNS and RONS can be obtained in conjunction with the use of gaseous helium or argon along with the addition of air or water. These species react with water, cell culture media and living organisms to produce additional new reactive species, such as by undergoing chemical reactions (including bond cleavage and oxidation) that affect biological tissues and various signaling circuits in cells. As shown in the figure, the typical inorganic reactive species are OH and O_2^-, both of which are short-lived, and H_2O_2, NO_2^-, NO_3^- and $ONOOH^-$, which are medium- and long-lived reactive species.

In recent years, it has become clear that organic compounds can induce the expression of super biofunctions following the irradiation of cell culture media with these active species, and the identification of organic radical species has attracted significant interest (Tanaka et al. 2021).

Normally, ROSs in living tissues are constantly metabolized by various enzyme systems. O_2^-, H_2O_2, HO, ClO^-, singlet oxygen ($O_2(1\Delta g)$) and O_2^- all have short lifetimes and many such species are highly reactive and will attack lipids, proteins, nucleic acids and carbohydrates.

8 Control of direct irradiation of living organisms with radicals

8.1 Quantitative analysis of interactions of radicals with living organisms

The direct irradiation of living organisms with plasma has been used for sterilization and the destruction of microorganisms, since von Siemens first reported the concept of plasma-generated ozone (O_3) treatments in 1857. As noted in the previous chapter, the Okazaki group reported the formation of a glow-like discharge plasma using helium gas under atmospheric pressure in 1988 (Kanazawa et al. 1988). This atmospheric-pressure low-temperature plasma was applied to the irradiation of living organisms in the 1990s, because it represented a low-cost sterilization process. As an example, several studies have assessed the degradation of bacteria on plants, fruits and other foods using plasmas. In these processes, active oxidizing species such as OH, $O_2(1\Delta g)$ and O_3 together with UV light at wavelengths ranging between 200 and 400 nm emitted from excited nitrogen and nitric oxide molecules are considered to be the key factors providing a sterilization effect.

Iseki et al. (2010) have worked on the inactivation of mold spores (P. digitatum) via direct treatment with a high-density atmospheric-pressure plasma having an electron density on the order of 10^{15} cm^{-3}. Although Ar was used as the carrier gas, the spores were irradiated with ROS and UV light due to air entrainment. The

active species that were effective in inactivating mold spores were investigated by irradiating the spores independently using an ozonizer. During these trials, the density of ozone was measured using UV absorption spectroscopy. The inactivation of a fungus was found to be significantly affected by the distance between the plasma and the fungus. At an irradiation distance of 10 mm, the decimal reduction time (*D* value; based on the number of surviving spores after treatment) was found to be 1.7 min in the presence of 2 ppm ozone, while a value of 6.1 min was obtained using 600 ppm ozone generated by the ozonizer. The effect of UV light was ascertained by irradiating the spores with a quartz glass plate on top of the specimen. This trial gave *D* values of 26.2 and 3.8 min with and without the plate, respectively. These results indicated the presence of an active species with a degree of inertness two orders of magnitude higher than that of ozone, and that oxygen radicals were an important ROS that contributed to the inactivation of mold. The mechanism by which P. digitatum spores were inactivated was studied by Iseki et al. (2011).

This work developed an atmospheric-pressure oxygen radical source that provided only neutral O to avoid the effects of UV light and charged species. A diagram of this device is provided in Fig. 69 (Hashizume et al. 2013). This apparatus generated only atomic oxygen ($O(^3P_j)$) and excited molecular oxygen ($O_2(^1D_g)$) by removing charged particles and light from an atmospheric-pressure plasma using a mixture of Ar and oxygen gases. The densities of these species were also determined using VUVAS to allow a quantitative analysis of their behavior. The densities of the $O(^3P_j)$ and $O_2(^1D_g)$ (which were both considered to be highly reactive oxidation species) as obtained using VUVAS at different distances from the radical source are shown in Fig. 70 (Hashizume et al. 2013). The D values in this system were evaluated and found to increase from 1.2 to 19.8 min with increasing exposure distance. When the exposure distance was changed from 10 to 20 mm, the $O(^3P_j)$ density decreased sharply, from 2.3×10^{14} to 1.3×10^{13} cm^{-3}, while the $O(^3P_j)$ density also decreased with increasing exposure distance. Using an argon gas plasma at atmospheric pressure, the lifetime of the $O(^3P_j)$ was approximately 0.5 ms and the inactivation rate of spores was on the order of 10^{-17} cm^3 s^{-1}. In contrast, the lifetime of the $O_2(^1D_g)$ was more than several tens of ms and the spore inactivation rate was less than 10^{21} cm^3 s^{-1}. Quantitative evaluation of the inactivation rate of neutral oxygen species indicated showed that $O(^3P_j)$ played an important role. Because the O_3 concentration was determined to be below the VUVAS detection limit of approximately 2.5×10^{13} cm^{-3}, it was evident that $O_2(^1D_g)$ and O_3 played only a minor role. This study provided quantitative information concerning oxygen radicals and mold inactivation kinetics and confirmed that highly efficient mold inactivation could be achieved by controlling the oxygen radicals.

It is particularly important to consider the mechanism by which oxygen radicals react with cells to inactivate mold spores, based on morphological changes. As an example, the intracellular nanostructures of the spores were observed by transmission electron microscopy (TEM), with the results shown in Fig. 71 (Hashizume et al. 2015). In the control (untreated) cells, intracellular organelles such as nuclei and mitochondria were clearly observed (Fig. 71a), while these intracellular organelles were degraded after exposure to an $O(^3P_j)$ dose of 7.0×10^{19} cm^{-2} or higher, as demonstrated in Fig. 71d–f. Based on these results, a mechanism was proposed

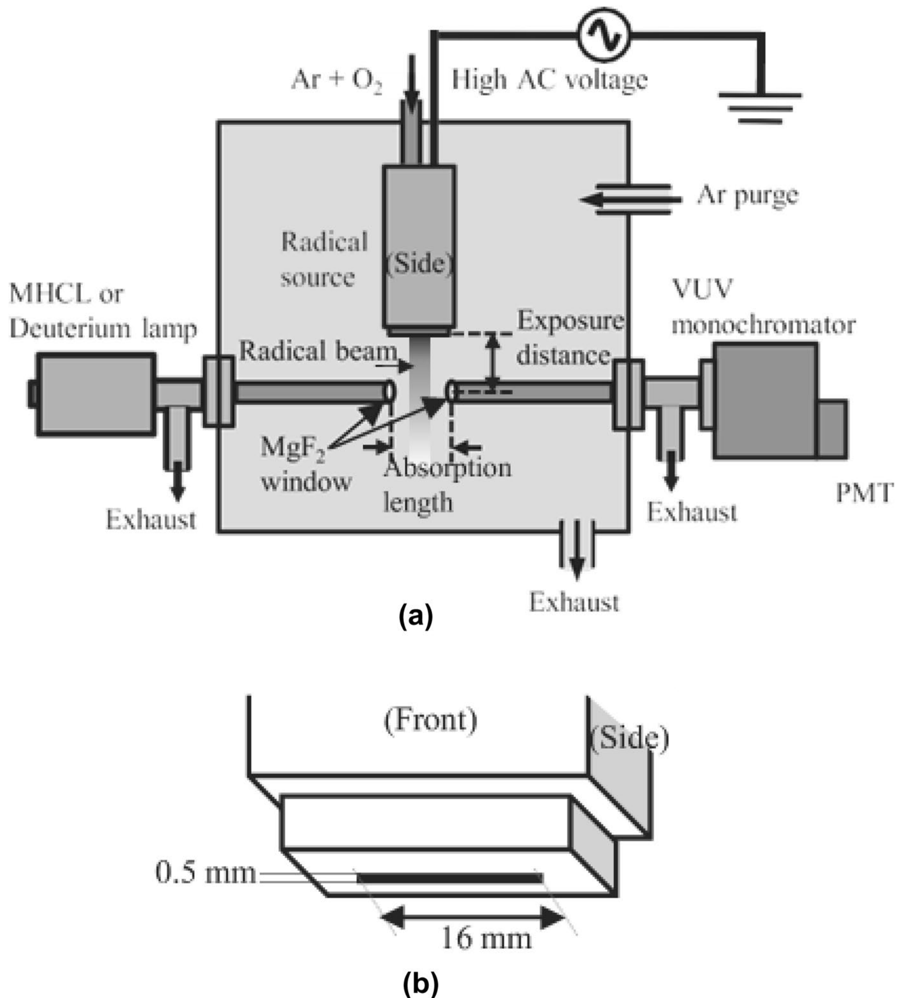

Fig. 69 Atmospheric pressure oxygen radical source that provides only neutral O to avoid the effects of UV light and charged species (Hashizume et al. 2013)

for the inactivation of P. digitatum spores treated with oxygen radicals that were highly diluted with Ar gas. In this mechanism, $O(^3P_j)$ react with the cell walls and membranes of the spores such that low doses (approximately 2.1×10^{19} cm^{-2}) of these radicals significantly inhibit spore function without causing pronounced changes in the ultrafine morphology. Intracellular organelles are also oxidized and degraded and most spores are inactivated at a dose of approximately 1.0×10^{20} cm^{-2}. Finally, at an $O(^3P_j)$ fluence of 2.3×10^{17} cm^{-2} s^{-1}, intracellular organelles (including all membrane structures) are completely degraded at high $O(^3P_j)$ doses above 1.0×10^{20} cm^{-2}. Since the associated D value was 1.8 min, spore function could be

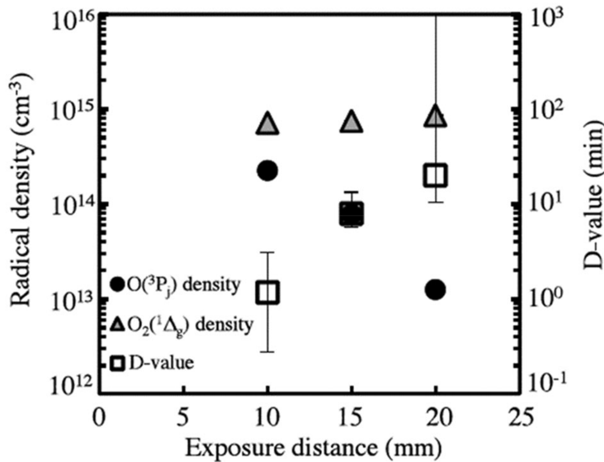

Fig. 70 Densities of $O(^3P_j)$ and $O_2(^1D_g)$ measured by VUVAS at different distances from the radical source, and the evaluated D values (Hashizume et al. 2013)

inhibited without causing serious ultrastructural changes as oxygen radicals interacted with the cell membranes.

8.2 Control of intracellular free radicals by oxygen radicals generated from a plasma

In prior work, the complicated behavior of several radicals generated in plasmas has been analyzed and the interactions between these radicals and solids have been controlled to develop etching, deposition and surface modification processes. Such studies have led to the development of the field of semiconductor plasma processing. In the case of the interactions between radicals generated from plasmas and P. digitatum spores, as discussed in the previous section, it is clear that oxygen radicals contributed to the inactivation. The critical difference between the interactions of radicals with living tissues and with semiconductor materials is that a large number of various radicals will already exist inside living organisms to maintain homeostasis. These radicals will interact with the active species generated by the plasma. In general, free radicals in vivo act to maintain redox homeostasis between donors and acceptors of electrons in living cells. These redox mechanisms are essential to balancing the reduced and oxidized states of cells during metabolic activities. As an example, the respiration of oxygen generates a large number of free radicals for the maintenance of life. Living organisms require enormous amounts of oxygen, which is converted into ROS, such as O_2^-, H_2O_2, HO, ClO^- and $^1O_2$ by enzymes. Among these, O_2^- and HO are short-lived species that can react chemically with lipids, proteins, nucleic acids and carbohydrates in the body, resulting in functional disorders. In particular, H_2O_2 (which is frequently generated in living organisms) generates harmful OH via the Fenton reaction. The reactions between naturally occurring radicals in living tissues and the radicals delivered from a plasma have not

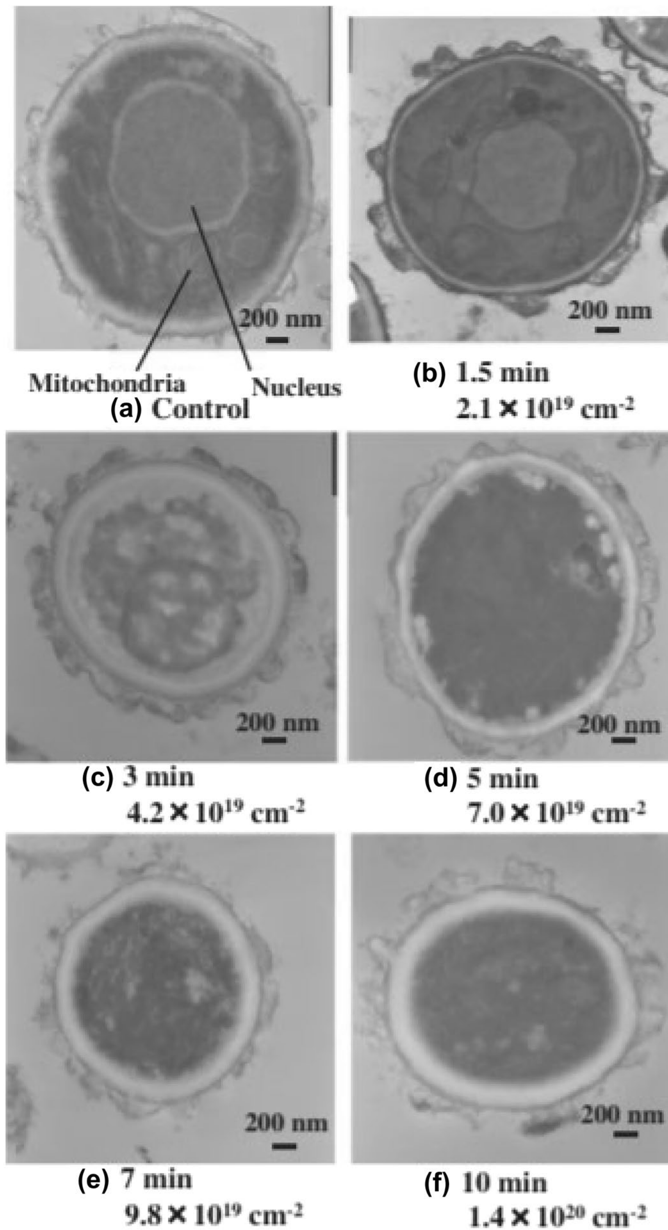

Fig. 71 TEM images of cross sections of P. digitatum spores: **a** control spore and **b**–**f** spores treated with oxygen radicals for 1.5, 3, 5, 7, and 10 min, respectively. The doses of $O(^3P_j)$ for various treatment times are also expressed under a flux of 2.3×10^{17} cm^{-2} s^{-1} (Hashizume et al. 2015)

yet been fully elucidated, and new theories are being created to assess the interactions of these radicals inside and outside of cells. It should be noted that there is also an antioxidant defense system in the body that efficiently decomposes ROS to limit

metabolic dysfunction. Based on this, we can gain insights into the mechanism by which mold spores are killed by oxygen radicals as described in the previous section. As an example, quinone (Q), which comprises two carbonyl groups on a cyclic organic compound, is an electron transfer carrier. The reduced semiquinone radical (QH^-) and the semiquinone anion (Q^-) radical are protected from oxidative stress by transformation to oxidized Q, as shown in Fig. 72.

Ishikawa et al. (2012) used real-time ESR to determine the relationship between oxygen radicals from a plasma and semiquinone radicals in spores. Figure 73 presents a diagram of the apparatus employed to perform real-time ESR measurements and the signals acquired after O exposures. During these trials a drop of a P. digitatum spore suspension was placed on a quartz plate and dried. After this, the plate was transferred to a quartz glass tube and set inside the ESR cavity, which was connected to a plasma discharge zone by a quartz tube. Gaseous oxygen was passed through this tube at a pressure of 15 Pa, while microwaves were supplied to generate a plasma discharge. ESR measurements were performed under this low pressure and showed the formation of gaseous O_2^- and O. A quartz tube was also used to remove ions and radiation generated in the plasma such that only radicals impacted the spores. As shown in the figure, the ESR spectrum of the fungal spores indicated a g value of 2.0040 and a line width of approximately 0.5 mT. Note that the ESR signal of sprouts was significantly weaker.

It can be seen that a signal due to the semiquinone radical appeared at a steady state based on conversion to peroxyl quinone by oxygen radicals. Consequently, the defense mechanism likely involved the semiquinone radical, which was held in the spores. This compound captured and scavenged the ROS generated by incoming oxygen radicals, was transformed into a stable quinone and then oxidized to a peroxyquinone.

Figure 74 provides a diagram summarizing the generation and disappearance of ROS in a living organism. As discussed, the antioxidant defense system in living tissues works to maintain life through the interactions of various enzymes and metals with ROS. Electrons, reactive species (ROS and RNS), radiation, electric fields

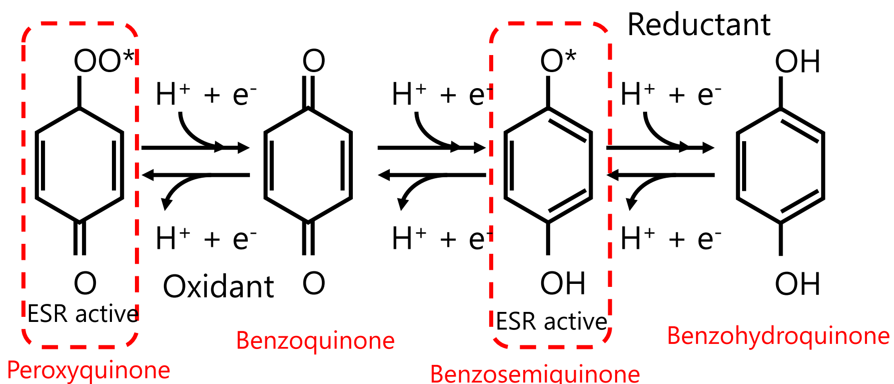

Fig. 72 Chemical scheme of the reaction related to the quinone (Q) structure by the oxidation stress

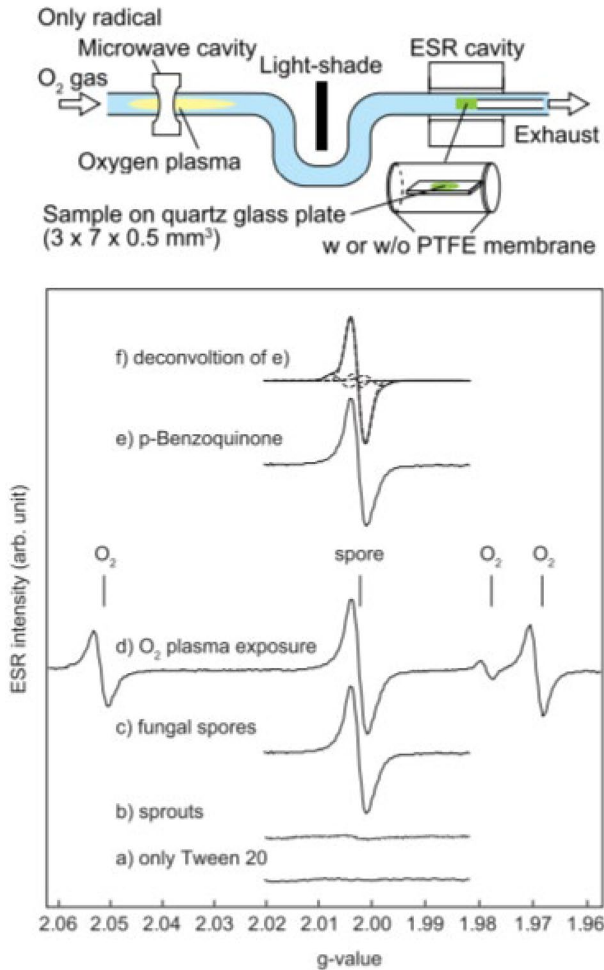

Fig. 73 Schematic diagram of the experimental setup for real-time in situ ESR measurements. Only O can be irradiated (upper), **b** ESR spectra from **a** no signal from Tween 20 only, **b** sprouts of Penicillin digitatum, **c** fungal spores of Penicillin digitatum before plasma exposure, **d**) during O_2 plasma exposure, **e** powder of 1,4-benzoquinone, and **f** deconvolved spectrum of **e** (bottom) (Ishikawa et al. 2012)

and shock waves generated by a plasma may act on these circuits and induce various oxidative stresses on the homeostasis of the organism. These effects could promote existing or novel reactions in the body. ROS are involved in strengthening cell walls via the cross-linking and lignification of structural proteins, peroxidation of lipids, and activation and induction of the expression of genes related to intracellular signaling pathways. In particular, the interactions of ROS with lipids (LH) are a peroxidation process and proceeds via a chain reaction in association with the generation of LOO*. Interestingly, as will be discussed later, the sensitivity to these ROS and

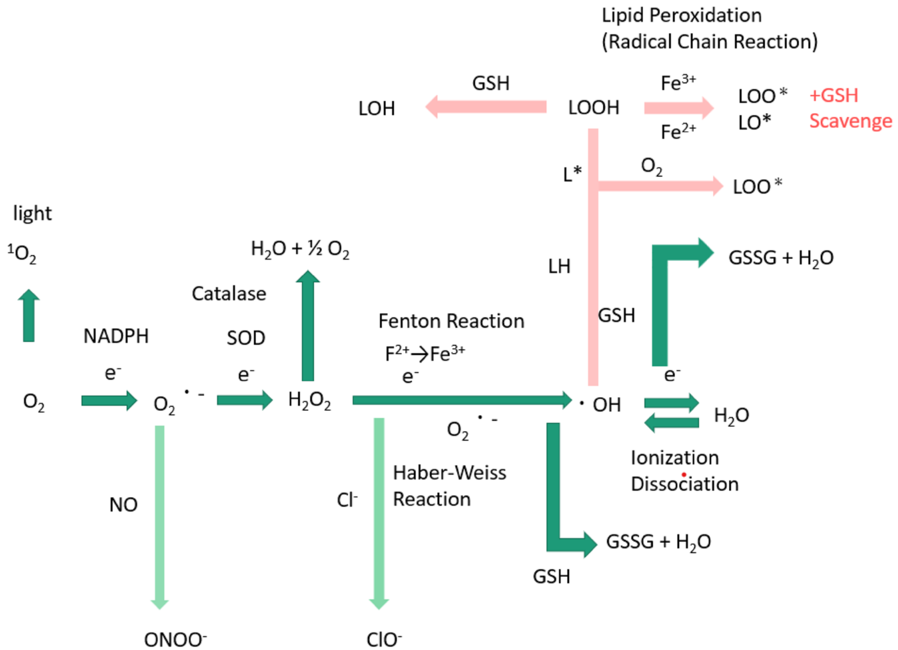

Fig. 74 Typical schematic of the generation and disappearance of reactive oxygen species in a living organism. Here, GSH, GSSG, LH, LOH, LOOH, L*, LO*, LOO*, NADPH and SOD indicate the glutathione, glutathione disulfide, lipid, lipid hydroxide, lipid hydroperoxide, lipid radical, lipid oxidation radical, lipid peroxyl radical, nicotinamide adenine dinucleotide phosphate and superoxide dismutase

other species and the associated mechanisms can greatly differ between different types of cells.

It is important to ascertain the manner in which these intracellular circuits can be controlled by controlling the radicals injected from the plasma. In fact, it has been suggested that it is possible to control radical homeostasis in the body by inducing radicals in vivo through irradiation at various wavelengths. Therefore, controlling in vivo reactions by locally injecting radicals from a plasma may enable tuning of the regeneration and death of various tissues and selective reactions that take advantage of the differences in sensitivity of cell types.

8.3 Measurements of RONS and radiation in atmospheric-pressure plasmas and their effects on medical treatments

In the case of an atmospheric-pressure plasma using pure Ar, ambient air diffuses into the plasma such that many different gas phase RONS are generated. That is, gas phase molecules such as oxygen and nitrogen from the air are excited and dissociated/ionized. Since collisions occur frequently under atmospheric pressure, species such as atomic radicals and metastable molecules are generated by recombination and other processes in the gas phase, and various RONS and ozone are produced.

Eventually, O, N, NO and OH as well high-energy particles in the VUV region emitted from the plasma irradiate materials located downstream region of the plasma. Takeda et al. (2017) determined the spatio-temporal distribution of these species and of VUV radiation using VUVAS, LIF and UV spectrometry (Fig. 75). The results showed that the absolute density of $O(^3P_j)$ decreased as the distance from the gas slit increased, along with the generation of O_3 due to self-recombination. In contrast, the absolute density of $N(^4S^o)$ was almost constant up to a distance of approximately 10 mm and increased above 12 mm. The VUV emission intensity was also found to decrease with increasing distance from the plasma head. The relative density of NO increased with increasing distance up to 10 mm, after which it plateaued, while the OH density decreased significantly from the exit of the plasma head and could only be observed up to a distance of 5 mm. The proportions of the reactive species produced by the plasma varied as a function of distance from the main discharge region. This distance is a very important parameter, and control of the plasma jet reaction in the treatment of biological samples requires maintaining an optimal distance between the plasma and the biological body based on experimental data. Direct irradiation with these radicals and ions has been reported to have hemostatic and therapeutic effects on skin cancer in vivo. Furthermore, these species are also effective in promoting plant growth.

Hemostasis during surgical procedures has to date been achieved by heat using a radiofrequency coagulator, which has raised concerns about localized burns and

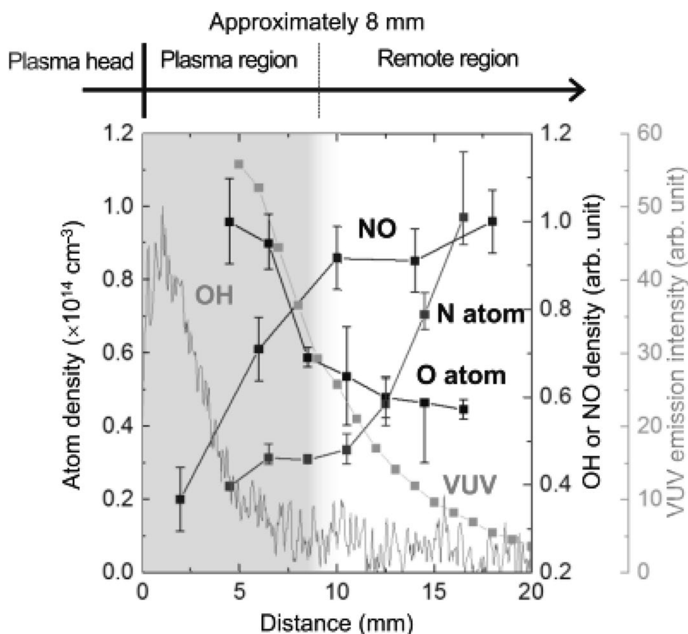

Fig. 75 Relative densities of NO and OH, absolute densities of N $(^4S^o)$ and $O(^3P_j)$ and VUV emission intensity at 174.3 nm due to N as a function of distance from the plasma head gas slit (Takeda et al. 2017)

post-operative damage. Ikehara et al. (2013, 2015) reported that plasma irradiation can coagulate blood in a short time while maintaining the temperature of the irradiated area at body temperature, thus contributing to the realization of minimally invasive surgery. Takeda et al. (2019) systematically evaluated electrical parameters (voltage and current to the target), plasma parameters (gas temperature and electron density, determined by emission spectroscopy), O density in the gas phase, and OH in the liquid phase in the experimental conditions of hemostasis performed by Ikehara et al. Consequently, Miyamoto et al. (2016) clarified the mechanism of erythrocyte coagulation by hemolysis, which is different from thrombus formation by plasma treatment. A series of histological and electron microscopic analyses and plasma current measurements revealed that erythrocyte coagulation is caused by the action of hemolytic proteins. In phosphate-buffered saline (PBS) containing human hemoglobin, aggregation-like clotting occurred 10 s after initial contact with the plasma flare. This suggests that hemolysis is an important step in the coagulation of red blood cells. Furthermore, reducing the current through a target contacting the plasma flare resulted in effective hemolysis and loss of red blood cells. These results indicate that, during plasma hemostasis, the injected current (that is, the number of charged particles) is more closely related to the efficiency of hemolysis than the interaction between radicals from the plasma (Fig. 76).

In an experiment using a melanoma model mouse, Mizuno et al. (2017) found that irradiating the right paw of the mouse with plasma shrank a malignant melanoma in the left paw, and also reported adaptive immune effects, such as an increase

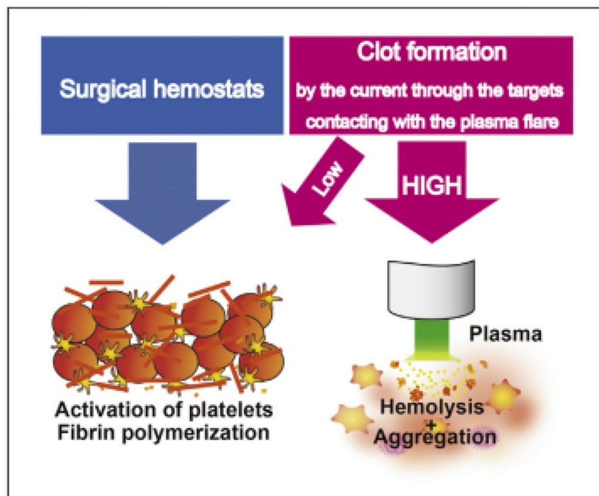

Fig. 76 Schematic illustration of plasma-induced blood coagulations. Plasma treatment induced clot formation coating the surface of wound without heat injury. The plasma can induce clot formation only from red blood cells. The clot formed appears monotonous with membrane-like covering on light and electron microscopy. Meanwhile, the plasma treatment has been considered to promote platelet aggregation and coagulation cascades to form whole-blood clots without hemolysis. These results indicate that clot formations with plasma treatments can be classified into two types, namely, classical (without hemolysis) and alternative (with hemolysis). It is noteworthy that increased plasma current correlated with hemolysis and the ability of serum proteins, such as albumin to aggregate (Miyamoto et al. 2016)

in innate immune response and inflammatory cytokines from spleen cells. However, the specific reactive species from the plasma causing these biological responses and the associated mechanisms are not yet fully understood. Yamato et al. (2021) irradiated the brain surface of adult rats with plasma and examined histological changes in the cerebral cortex, with surprising results. Irradiation resulted in the formation of a three-layered tissue structure in the brain, with high proliferation of resident immature cells and bone-marrow-derived cells. These findings suggest that direct plasma irradiation induces reorganization of cellular and tissue structures, including cell proliferation, in the central nervous system in vivo. Plasma irradiation has potential applications in regenerative medicine of the nervous system.

9 Development of plasma-activated media

In 2013, Tanaka et al. (2013) discovered that, by irradiating a cell culture media with plasma and injecting the activated media into cancer cells and tissues, cancer cells could be killed with higher selectivity than normal cells. This research indicated that cancer cells could be selectively destroyed not by the physical effects of the electric field and charged particles from the plasma, but by the chemicals produced by the interaction between the plasma and the liquid, since the plasma was not directly applied to the living tissue. Thus, by controlling the radicals generated in the plasma, it is possible to synthesize extracellular radicals and active species that induce various biological reactions in the liquid. The active liquid synthesized by plasma irradiation was found to not only selectively kill cancer cells but also to promote plant growth. These results were very unexpected and led to the creation of a new field of study based on indirect irradiation as opposed to the direct application of plasma to living organisms. Consequently, the effects of RONS produced by interactions between plasmas and cell culture media or biocompatible liquids have been researched.

Many studies have investigated the RONS produced by the interactions of water and solutions with oxygen or nitrogen-based plasmas or radicals produced by plasmas (Yan et al. 2017). Here, the behaviors of reactive species in plasma-activated medium (PAM) produced by the interactions of reactive species from plasmas with cell culture media have been intensively examined. PAM exhibit strong anti-tumor effects on various types of cells, including gastric cancer, human lung adenocarcinoma and human breast cancer cells together with age-related macular degeneration (Ye et al. 2015).

As shown in Fig. 77, Utsumi et al. (2013) reported that the introduction of N-Acetyl-L-cysteine (NAC), a scavenger of reactive oxygen species, into PAM greatly reduced the effects of ovarian cancer and anticancer drug-resistant strains of cancer, indicating that intracellular ROS play an important role. The efficacy of PAM has also been reported for both transplanted and anticancer drug-resistant strains of cancer, reducing cancer deposition and extending the lifespan of test mice. Based on the results of these in vitro and in vivo studies, research into the behavior of RONS in PAM and the interactions of these species with cells and organisms has been actively conducted.

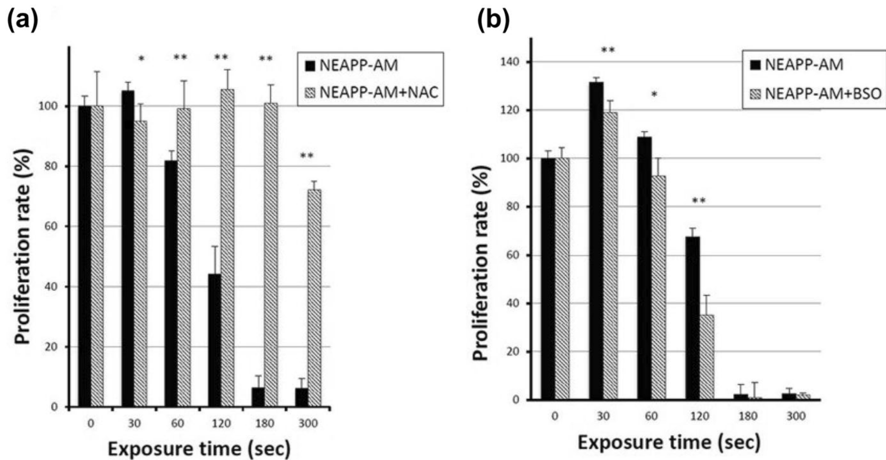

Fig. 77 Role of ROS in the atmospheric pressure low-temperature plasma activated medium (NEAPP-AM). **a**, **b** Influence of intracellular ROS modulation by n-acetylcysteine (NAC) and L-Buthionine-(S,R)-sulfoximine (BSO) on PAM induced cell death. NOS2 cells were pretreated with NAC (4 mM) **a** or BSO (2 m M) **b** for 2 h and then exposed to NEAPP-AM with NAC or BSO for an additional 24 h. The cell viability assay was used for evaluation. Each column represents the mean and the bars are standard deviation. Data are representative of at least three independent experiments. **P*,0.05, ***P*,0.01 versus control without NAC treatment (Utsumi et al. 2013)

Kurake et al. (2016a, 2017) monitored H_2O_2 and NO_2^- levels in Dulbecco's modified Eagle's medium exposed to an atmospheric-pressure plasma at room temperature using ESR and other methods and found that these species were present in mM concentrations. To understand the main synthetic pathway, the roles of OH and NO were investigated. However, it was determined that the majority of the H_2O_2 and NO generated in PAM did not originate from these radicals in the aqueous phase. NO_2^- was produced in the gas phase or at the gas–liquid interface via the reaction:

$$NO + OH \rightarrow HNO_2, \tag{9.1}$$

such that NO in the gas phase was not directly dissolved. H_2O_2 was subsequently generated in the gas phase or gas–liquid interface by the reactions of oxygen, OH and HO_2, based on the equations:

$$H_2O \rightarrow OH + H\,(\text{gas}), \tag{9.2}$$

$$H + O_2 \rightarrow HO_2(\text{gas}) \tag{9.3}$$

and

$$OH + HO_2 \rightarrow H_2O_2(\text{gas}) \rightarrow H_2O_2(\text{liquid}). \tag{9.4}$$

At the gas–liquid interface in PAM, OH in the aqueous phase was mainly generated by photodissociation (based on VUV or UV radiation) or by impacts with electrons via the reaction:

$$H_2O \rightarrow OH + H. \quad (9.5)$$

This OH did not contribute to the formation of H_2O_2 but rather to the oxidation of organic matter. Based on these results, the mechanism presented in Fig. 78 was devised (Kurake et al. 2017). The concentrations of H_2O_2 and NO_2^- in PAM were measured, because these stable ROS play important roles in killing cancer cells, and to ensure that constant levels of H_2O_2 and NO_2^- were administered to the cancer cells. Figure 79 indicates that the former species had a cancer cell killing effect but not the latter. Nevertheless, the effect of H_2O_2 was synergistically enhanced by the presence of NO_2^-, such that both contributed to the destruction of cancer cells. PAM has been reported to exhibit not only the synergistic effect described here but also even stronger cancer cell killing properties (Kurake et al. 2016a).

On the basis of such results, Bauer et al. (2019) studied the dynamic processes in PAM by kinetic analysis combined with the use of specific inhibitors at set time intervals. This work established the reactions of H_2O_2 and NO_2^- in PAM using transcriptional experiments. In addition, pretreated and untreated cells were mixed and the bystander signal was monitored. They proposed that $^1O_2$ was the key active species leading to cancer cell death in such systems, via the reactions:

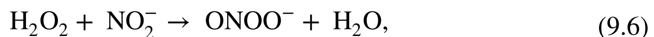

$$H_2O_2 + NO_2^- \rightarrow ONOO^- + H_2O, \quad (9.6)$$

$$ONOO^- + H^+ \rightarrow ONOOH, \quad (9.7)$$

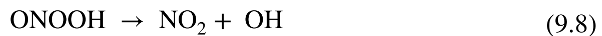

$$ONOOH \rightarrow NO_2 + OH \quad (9.8)$$

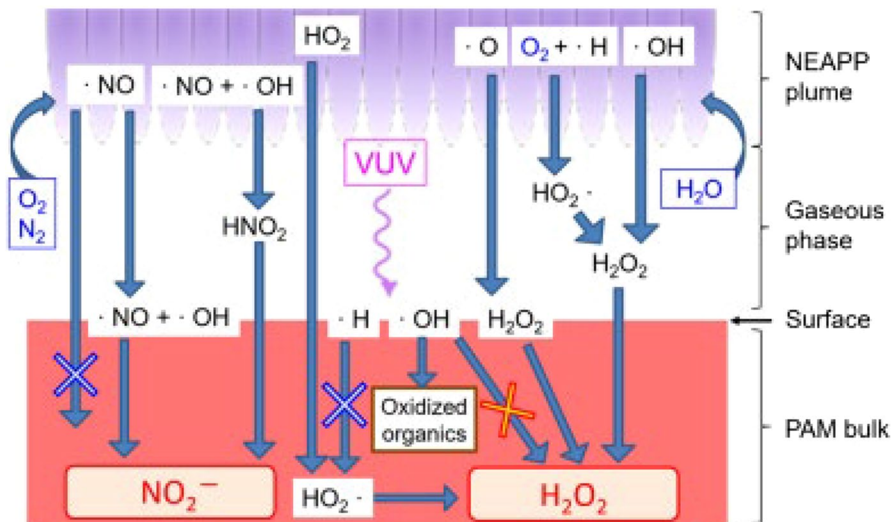

Fig. 78 Schematic representation of reaction pathways in the low temperature atmospheric pressure plume, the gas phase, the surface, and the PAM bulk. Feed (blue), precursor (black), and antitumor (red) species are shown (Kurake et al. 2017)

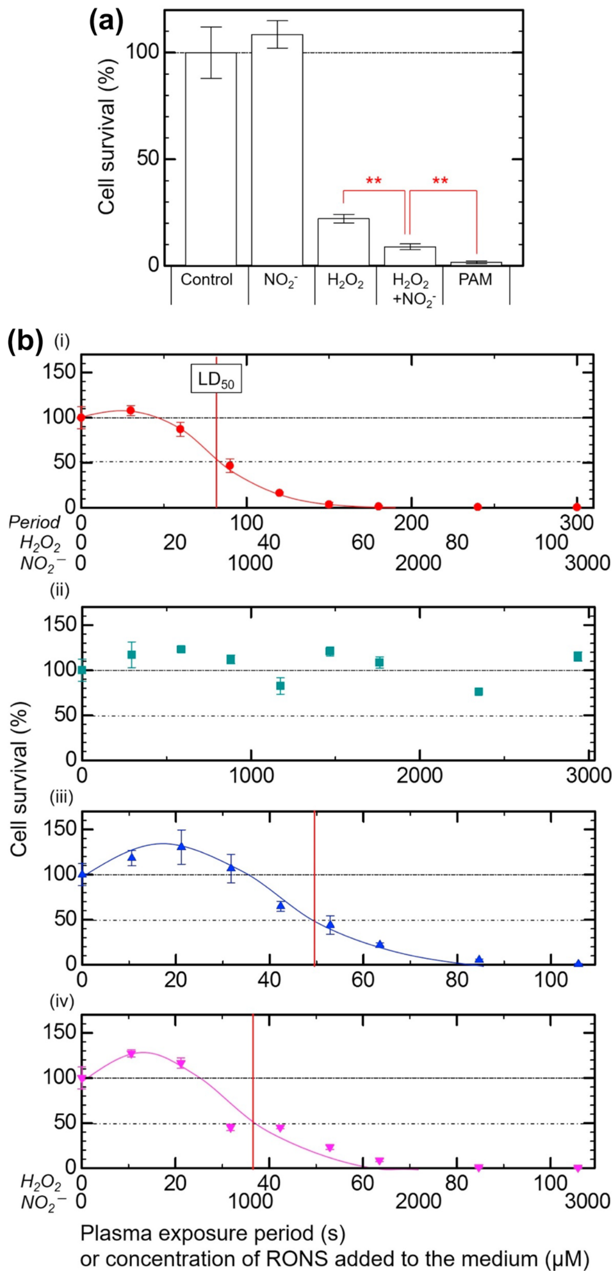

Fig. 79 U251SP cell survival measured using the MTS assay after 24 h incubation with **a** control, NO_2, H_2O_2, both H_2O_2 and NO_2 or PAM irradiated for 180 s and **b** (i) PAM, (ii) NO_2, (iii) H_2O_2 and (iv) both H_2O_2 and NO_2 plotted as a function of the plasma irradiation time. Those added H_2O_2 and NO_2 concentrations were equivalent as generated in PAM, 63 mM and1890 mM in (**a**). These samples did not contain FBS or P/S (Kurake et al. 2016a)

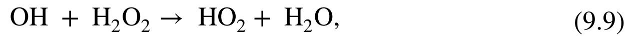

$$OH + H_2O_2 \rightarrow HO_2 + H_2O, \quad (9.9)$$

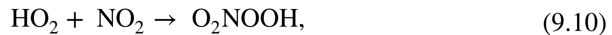

$$HO_2 + NO_2 \rightarrow O_2NOOH, \quad (9.10)$$

$$O_2NOOH \rightarrow H + O_2NOO \quad (9.11)$$

and

$$O_2NOO^- \rightarrow {}^1O_2(\text{primary singlet oxygen}) + NO_2^-. \quad (9.12)$$

In this series of reactions, $^1O_2$ causes the local inactivation of membrane-associated catalase. Subsequently, the remaining H_2O_2 and $ONOO^-$ at the site of the inactivated catalase generate secondary $^1O_2$ that may further inactivate the catalase and thus trigger autoamplification of $^1O_2$ generation. This species may also activate fetal bovine serum (FAS) receptors and enhance the activity of NOX1 and NOS so as to provide more effective $^1O_2$ generation, as shown in Fig. 80. The reactions of the secondary $^1O_2$ induce a rapid bystander effect that promotes catalase inactivation. This highly dynamic process is essentially driven by NOX1 and NOS in tumor cells and ultimately induces apoptosis by the cell-to-cell migration of singlet oxygen. These studies concluded that the specific response of tumor cells in which secondary $^1O_2$ is

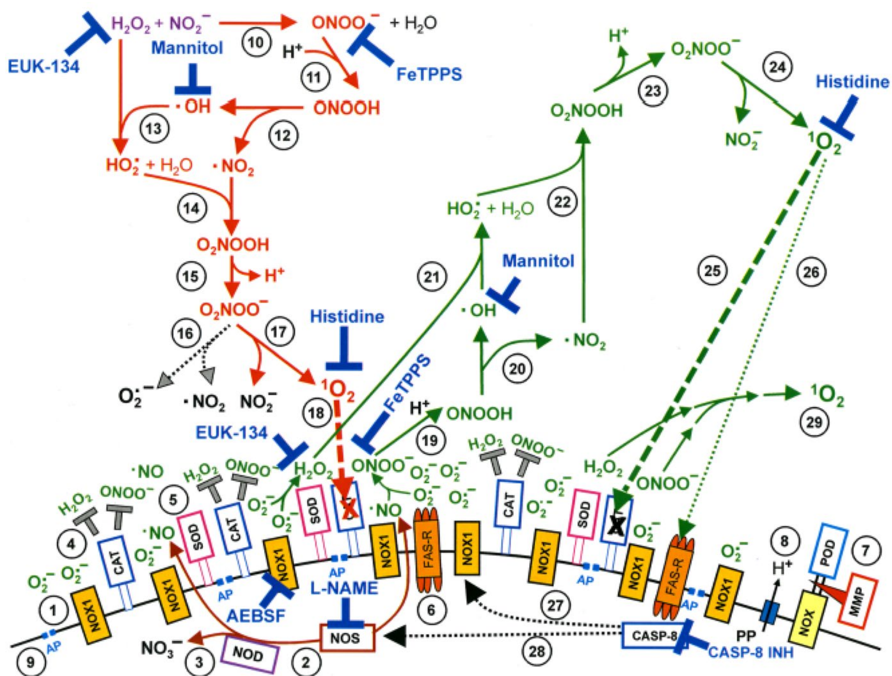

Fig. 80 Apoptosis induction PAM is mediated by the generation of primary and secondary singlet oxygen ($^1O_2$) (Bauer et al. 2019)

generated is the key driving force for tumor cell self-destruction after the $^1O_2$ mediated triggering process is initiated by PAM.

Tanaka et al. (2013, 2014, 2015, 2017) reported that PAM triggers signaling that leads to apoptosis through the activation of caspase3/7 proteins in brain tumors and ovarian cancer. In addition, the activities of RAS–MAPK and PI3K–Akt signaling pathways, which are homeostatically activated as signaling mechanisms for survival and amplification, were decreased in brain tumors. These results suggested that PAM induces apoptosis by suppressing the survival and proliferation signaling network, which is an intracellular molecular mechanism.

Comprehensive gene expression analyses by microarray and real-time polymerase chain reaction studies revealed that PAM promotes apoptosis in cultured brain tumor cells in response to oxidative stress stimulation of GADD45a, GADD45b, c-JUN and ATF3 genes, which constitute a transcription factor referred to as the AP-1 complex. These genes are involved in the GADD45 signaling pathway that leads to apoptosis in response to oxidative stress (Tanaka et al. 2019).

Adachi et al. (2014) investigated PAM-induced intracellular signaling circuits in A549 cells, a human lung adenocarcinoma epithelial cell line. Their work found that PAM induces apoptosis by a spiral cascade involving the mitochondrial–nuclear network, and that H_2O_2 and its ROSs disrupt the mitochondrial–nuclear network by decreasing mitochondrial membrane potential ($\Delta\psi$m), reducing the expression ratio of Bcl2/Bax, activating PARP-1, releasing AIF and depleting NAD^+. These changes are accompanied by endoplasmic reticulum stress. It was concluded that the accumulation of ADPR and extracellular/intracellular H_2O_2 produced in the above reactions activates TRPM2, causing Ca^{2+} influx into the extracellular space and release from intracellular stores, resulting in cell death.

Despite such prior work, the specific active species in PAM are still not well understood. In fact, approximately 30 different compounds have been identified in PAM, and the examination of the active species that are primarily responsible for the selective death of cancer cells is ongoing. It has been shown that plasma-activated Ringer's lactate solution (PAL), an intravenous infusion containing only four components, has selective anti-tumor and apoptosis-inducing effects on cell culture media containing many components that are similar to PAM (Tanaka et al. 2016). PAL is a simple, biocompatible solution that is expected to assist in elucidating the associated reaction mechanisms together with the in vivo studies (Sato et al. 2018).

Recently, two groundbreaking research studies concerning PAL have been reported. Jiang et al. (2021) found that PAL specifically kills malignant mesothelial cells, and established the details of the intracellular molecular mechanism by metabolomic analysis. In the initial mechanism, malignant mesothelial cells initiate autophagy and attempt to adopt to PAL, but an increase in NO in the lysosomes leads to an explosive increase in intracellular lipid oxidation. This effect, in turn, results in a specific iron-dependent necrotic pathway known as ferroptosis (Fig. 81). Although the reaction mechanism is expected to be different depending on the type of cell, it has already been reported that the extent of intracellular oxidation associated with PAL is lower than that obtained with PAM, and that the intracellular mechanism is also very different (Tanaka et al. 2019). The discovery that PAL

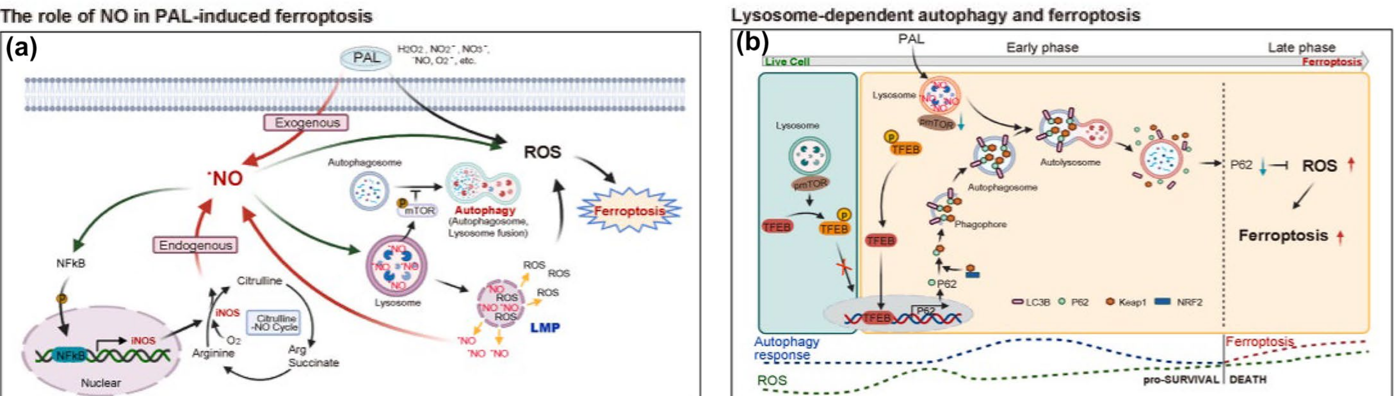

Fig. 81 **a** Role of NO in PAL-induced ferroptosis in MM cells. PAL provides MM cells with an immediate impact of exogenous NO, a component of PAL. The initial stimulation of NO activates transcription factor NF-κB in MM cells, upregulating the downstream iNOS as revealed by metabolome analysis. In return, this positive feedback loop leads to sustained accumulation of NO in lysosomes. Simultaneously, NO accumulation in lysosomes starts autophagic process, eventually resulting in lysosomal membrane permeabilization (LMP) upon certain threshold according with increase in lysosomal lipid peroxidation. The whole process eventually leads to ferroptosis. **b** Molecular switch from autophagy to ferroptosis in MM cells. In the absence of PAL stress, mTOR binds to p-TFEB, which keeps the autophagy event in a physiological level. Under PAL exposure, MM cells, by responding to exogenous reactive species, start autophagic processes, initialized by translocation of TFEB into the nucleus and the subsequent upregulation of p62 transcription. During this early event, autophagy serves as a survival mechanism and the following p62-Keap1–Nrf2 axis-mediated antioxidant response would keep the balance of ROS for a period of time. However, sustained accumulation of NO-derived oxidants mediated lipid peroxidation, and lysosomal dysfunction eventually results in ferroptosis, when autophagic process is terminated. The molecular switching of cell fate from autophagy for survival to ferroptosis occurs when autophagic proteins, such as p62, are downregulated as a consequence of accumulated lipid peroxidation in lysosomes (Jiang et al. 2021)

induces the generation of NO radicals in living cells is of significant interest as this demonstrates the radical control process in vivo.

In an additional study, Nakamura et al. (2021) examined the activation of anti-tumor immunity based on the involvement of M1-type macrophages (a type of immune cell) to assess the mechanism by which PAL suppresses the peritoneal dissemination of microscopic ovarian cancer. This process is difficult to detect with the naked eye during histological analysis of disseminated foci with a large network. Intraperitoneal lavage therapy using PAL was found to significantly prolong the survival of a mouse model for the peritoneal dissemination of ovarian cancer without showing any serious side effects.

It is the standard of care for early stage ovarian cancer in which peritoneal dissemination is not evident and shows potential for preventing recurrence. Therefore, they have named it " Intraperitoneal washing therapy" as an effective method to improve the clinical outcome of ovarian cancer. The active species responsible for the selective killing of cancer by PAL have been intensively studied and several possible candidates have been identified (Tanaka et al. 2021) but are not yet completely clear.

10 Radical-induced material processing in liquids and/or at interfaces

The synthesis of nanomaterials using the interactions between plasmas and liquids has attracted much attention. As an example, the rapid synthesis of nanographene using a plasma in alcohols has been reported (Hagino et al. 2012). In this work, the ultrafast production of highly crystalline nanographene was realized using an ethanol-based in-liquid nonequilibrium micro-hollow atmospheric-pressure plasma having an extremely high electron density. The synthesis rates for carbon materials were 0.61 mg/min when using ethanol in this process (Fig. 82), and the multilayer nanographene structures that were obtained had an interlayer spacing of 0.33 nm corresponding to that of the (002) planes in graphite. The G-, D-, D'- and 2D-band peaks in the Raman spectrum of the product also confirmed the formation of nanographene. In contrast, a rate of 1.72 mg/min was obtained using butanol but the quality of the product was degraded. The mechanism by which the gradual growth of six-membered ring structures occurred was determined by gas chromatographic analyses of a filtrate and the combination of this plasma with ethanol was found to produce 2,3-butanediol, phenylethylene, indene, naphthalene and biphenylene during the in-liquid plasma discharge. Six-membered ring structures were gradually formed via the elimination and dehydration reactions of organic radicals.

This research assessed the effects of various alcohols and hydrocarbon solutions on the synthesis rate and nanographene crystallinity. As the number of carbons in the raw material increased, the synthesis speed also increased although the quality of the graphene was decreased (Ando et al. 2018), as predicted by Hagino et al. (2012). This effect resulted from the formation of various radicals as a consequence of the interactions between the plasma and the raw liquid, resulting in decomposition and/or polymerization reactions together with the formation of nanographene

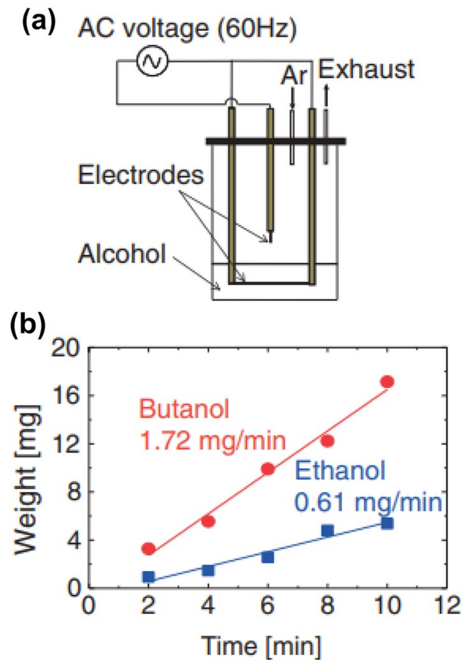

Fig. 82 **a** Schematic illustration of experimental apparatus and **b** synthesis rate of carbon materials using an in-liquid plasma with butanol or ethanol (Hagino et al. 2012)

having six-membered rings. It should be noted that carbon-based materials could not be obtained using methanol as the liquid phase. The reactions in this liquid system were based on the generation of hydroxyl groups or O and CH_2OH from the methanol, all of which promoted oxidation reactions. Eventually, these radical-induced oxidation reactions decomposed any unstable organic compounds and so did not contribute to the formation of six-membrane ring structures.

The radical species appearing in various alcohol/water mixtures when using this atmospheric-pressure plasma were monitored using an ESR spin-trapping technique, employing 3,5-dibromo-4-nitrosobenzene sulfonate as the water-soluble trapping compound. Uchiyama et al. (2018) reported the associated reaction mechanism on the basis of these data. The major radical species were formed by H abstraction from alcohol molecules as a result of the OH produced from the decomposition of H_2O and H_2O_2. In the case of the ethanol/water mixture, CH_2CH_2OH produced by H abstraction from ethanol and CH_3 radicals were detected. The latter resulted from the decomposition of unstable CH_3•CHOH radicals to form CH_3 and formaldehyde (HCHO) via C–C bond fission, as shown in Fig. 83. This generation of CH_3 was only observed in ethanol/water mixtures because of reactions between abundant OH and alcohol molecules and may have served as a precursor to the formation of six-membrane ring structures. As discussed in Sect. 4, it is vital to identify the important radicals that efficiently form these ring structures. In the case of in-liquid plasma processing, numerous radical-based reactions will be predominant, and thus controlling the formation and behavior of these organic radicals is an important aspect of plasma chemistry.

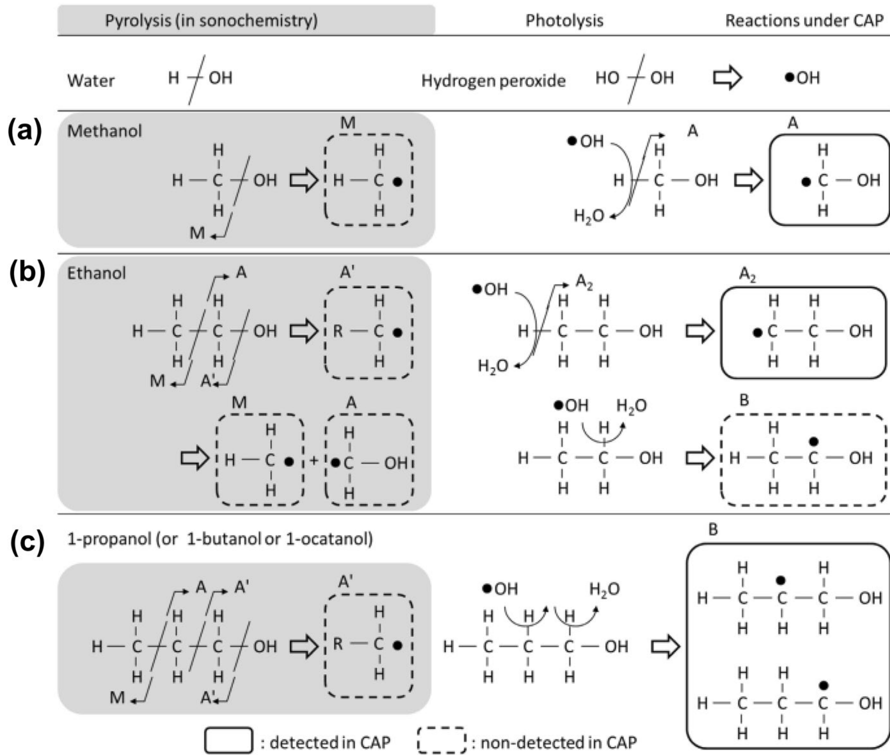

Fig. 83 The reaction schemes of **a** methanol, **b** ethanol and **c** 1-propanol were displayed in figure. Their chemical reactions suggested that hydrogen abstraction indirectly was dominant (Uchiyama et al. 2018)

Amano et al. (2018) synthesized micron-sized graphene flakes containing iron by irradiating ethanol containing iron phthalocyanine (FePc) based on the interaction between atmospheric-pressure plasma and a liquid (Fig. 84). The goal was to rapidly synthesize catalytic materials as replacements for Pt. Working at atmospheric-pressure, gas phase Ar plasmas were generated as well as liquid phase plasmas comprising bubbles and liquid solutions. It will be important in future to elucidate the radical reaction mechanism in liquids by which these graphene flakes were synthesized, especially the reactions between organic radicals and the metal.

Kurake et al. (2016b) reported that metastable crystals of oxalic acid were synthesized after 24 h irradiation of a cell culture medium with a high density Ar atmospheric-pressure plasma at a relatively short distance (Fig. 85). The original culture medium contained components, such as NaCl, D-glucose, $CaCl_2$ and $NaHCO_3$, but no oxalate or oxalic acid. The oxalate was apparently synthesized in the medium as thermodynamically unstable calcium oxalate dihydrate (COD) [CaC_2O_4•$(2+x)H_2O$ ($x \leq 0.5$); JCPDS 17–0541] crystals during the plasma irradiation. In the reaction field caused by the plasma irradiation, glucose was oxidized by RONS to produce gluconic acid. This was followed by the decomposition of the carboxyl group by high-energy electrons from the plasma to produce glycolic acid and glyoxylic acid.

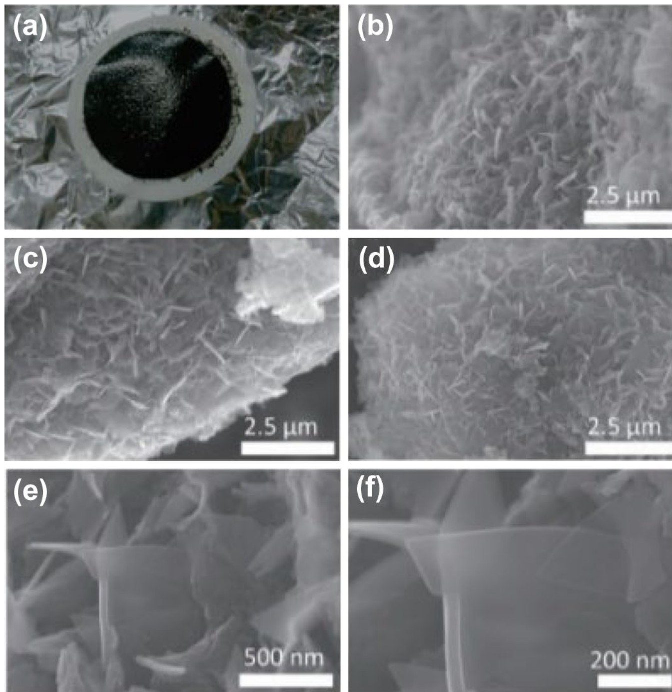

Fig. 84 **a** Image of carbon residue filtrates synthesized in ethanol with DMF-solvated FePc. SEM images: **b–d** 2.5 μm scale, e 500 nm scale, and **f** 200 nm scale (Amano et al. 2018)

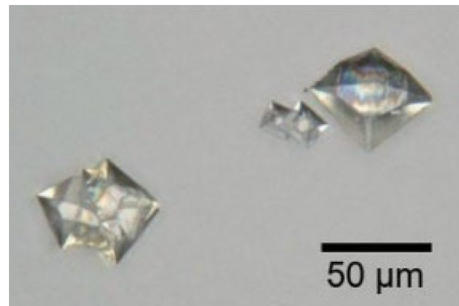

Fig. 85 Morphology of the particulates synthesized during 24-h incubation of the culture medium irradiated for 10 min with atmospheric pressure low-temperature plasma (Kurake et al. 2016b)

Finally, carboxylic acid radicals were generated and oxalic acid was synthesized. The associated reactions were

$$\mathrm{COH} + \mathrm{O} \rightarrow \mathrm{COOH}, \tag{10.1}$$

$$\mathrm{COOH} + \mathrm{e\,(high\ energy)} \rightarrow \mathrm{R} + \mathrm{COOH} \tag{10.2}$$

and

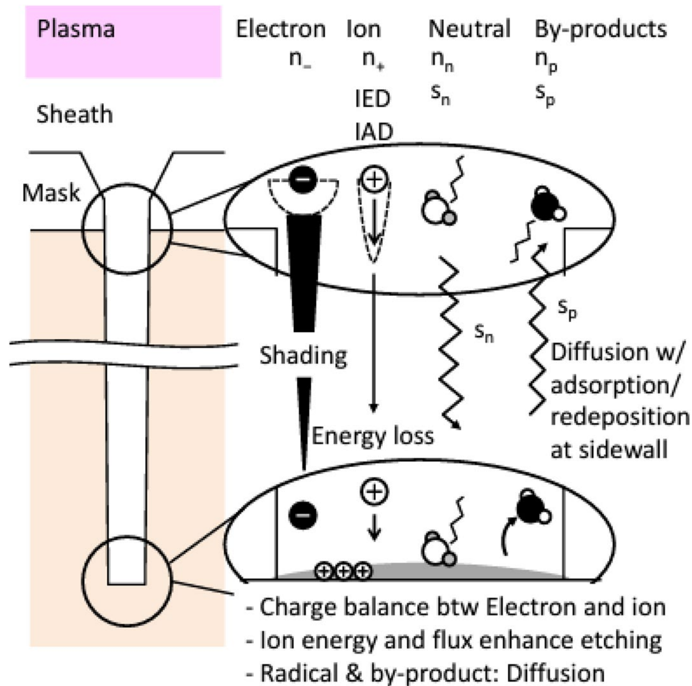

Fig. 86 Etching rates are influenced by transport of ions and neutrals inside HAR features. The reaction probability for the targeted etching reaction and the net fluxes of reactants reaching the bottom determine the etching rates and aspect ratio dependence characteristics. n is density of particles and s is surface sticking coefficient (Ishikawa et al. 2018)

$$2\text{-COOH} \rightarrow (\text{COOH})_2 \tag{10.3}$$

In this manner, octahedral crystals several tens of micrometers in size primarily comprising COD were obtained. In humans, oxalic acid is an intrinsic metabolite of glycine. The similarities between the reactions in vivo and the radical reaction field induced by plasma irradiation require further examination, but it is interesting to note that crystals were generated by the interaction of ROS with organic materials.

11 Future prospects

11.1 Digital processing with radicals

Advanced devices will require the fabrication of complex 3D structures as designs become increasingly ultra-fine, and Fig. 86 shows a typical scheme for high-aspect-ratio (HAR) etching (Ishikawa et al. 2018). The complex processing characteristics obtained using plasmas in device manufacturing include the distortion of fine

patterns due to electron shading effects, Reactive Ion Etching (RIE) lag and micro-loading. These phenomena can cause differences in etching rates depending on the pattern dimensions, the extent of plasma-induced damage and the pattern edge roughness that transfers the resolution and molecular weight distribution of resist polymers in the lithography process to the material during etching. The transport of radicals during the formation of a HAR deep pore geometric pattern can be represented by Knudsen transport. In this model, thermally excited incoming radicals randomly enter the upper inlet of the HAR geometry and are transported to the bottom of the pore via Knudsen transport. The attachment of these radicals to the sidewalls determines the flux of radicals to the bottom of the HAR, and analyses of the bulk or surface diffusion of the adhering radicals should take into account the microscopic-scale solid surface reactions of the radicals. In particular, when ions are obliquely incident on the sidewalls, cross-reactions of ions and radicals can occur such that the attachment and surface reactions at both the sidewalls and the base of the pattern are affected by the density, energy and chemical reactivity of the ions. Therefore, the reactions at the sidewalls of the HAR geometry pores are very complex. The flux of radicals transported to the bottom will be higher if the attachment of radicals at the sidewalls is reduced.

Furthermore, as the etching progresses, the reactions at both the sidewalls and bottom of the HAR geometry become more complex such that a highly precise procedure controls the etching process from the top surface to the bottom surface of the HAR in a time-resolved manner. Basic data regarding the reproducibility of radical reactions inside the HAR geometry is presently being accumulated. One etching method that deals with these issues related to complexity is atomic layer etching (ALE)/atomic layer deposition (ALD). As indicated in Fig. 87 (Kanarik et al. 2015), in such processes, conformal atomic layers are deposited in a 3D manner and are then irradiated with ions or other directional particles. Etching does not progress after the atomic etching reaction layer has been consumed, and so layer-by-layer etching (that is, digital etching) is possible. In these systems, only the bottom

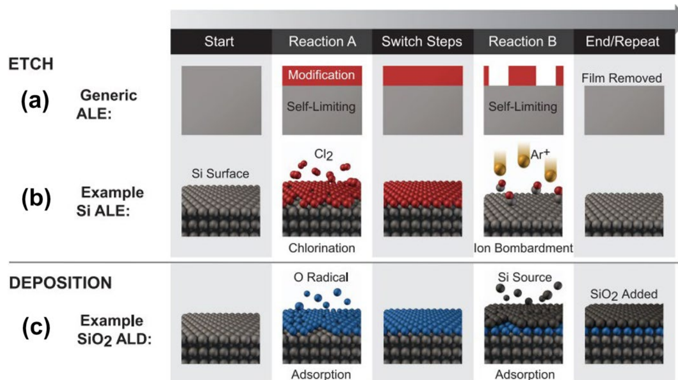

Fig. 87 Schematic of ALE **a** generic concept, **b** for the silicon case study, and **c** in comparison to ALD. ALE is similar to ALD except that removal takes place instead of adsorption in reaction B (Kanarik et al. 2015)

surface of the HAR is irradiated with fast, high-energy ions and etching is performed sequentially in a time-varying manner due to the mutual reactions between radicals and ions. Naturally, the etching time is slower but this technique solves many of the problems of conventional etching and can produce highly accurate shapes (Fig. 88) (Ishikawa et al. 2018).

11.2 Visualization of radical dynamics in nano-reaction fields

Various radicals generated from plasmas form reaction fields with gas phases, liquids and solids, and the control of these reaction fields has led to academic innovations and innovations in the fields of devices, materials, environment, medicine and agriculture. To control the radical-induced non-equilibrium physicochemical reaction fields of low-temperature plasmas, in situ observations and visualizations of the reaction fields are necessary. In the case of semiconductor manufacturing, the target size is shrinking toward 1 nm and so means of performing observations at the atomic level are needed. As an example, the interactions between radicals and materials have been observed using transmission electron microscope (TEM). Recently, 2D nanosheets have attracted attention as new materials for the fabrication of electronic and optical devices. Graphene, a typical sheet-like material, exhibits specific properties depending on the number of layers, and so controlling the number of layers is the key to exploiting the properties of this material, such as its bandgap, optical characteristics and carrier mobility. Plasma processes have been adapted for this purpose although, considering the potential damage caused by charged particles in the plasma, functionalization by layer-by-layer etching and surface modification using radical-controlled processes is necessary. To understand the radical etching of such materials, it is necessary to observe the process in situ and study the etching mechanism.

In situ TEM and electron energy loss spectroscopy (EELS) have allowed physicochemical observations of the boundary reactions between gases and liquids. The reactions between reactive neutrals species such as O(^{3}P, ^{1}D) and excited O_2 ($^1\Delta$) have been assessed using a specialized sample holder custom built for high-voltage TEM. Using this apparatus, graphene was irradiated with O generated in a remote

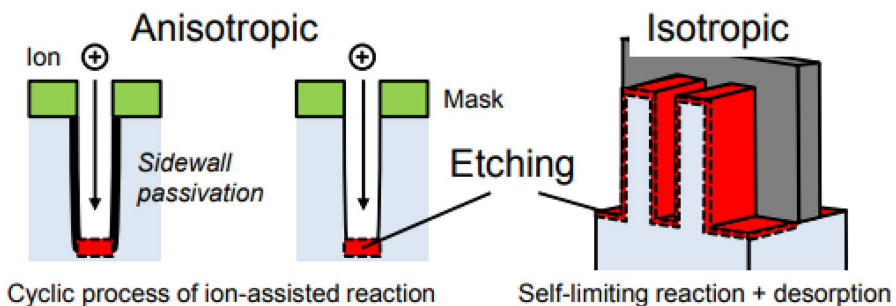

Fig. 88 ALD and ALE technologies into anisotropic and isotropic etching in the HAR hole (Ishikawa et al. 2018)

plasma excited by microwaves. Figure 89 presents a TEM image showing the structure of a thin multilayer graphene specimen. In this image, the center shows the face of the graphene, while the right-hand side shows the edge of the sample, and a portion of the thick graphene is visible in the upper left. The evident temporal changes in contrast due to oxygen radical irradiation show that the multilayer graphene was etched and hence became smaller (Sugiura et al. 2020). EELS spectra were acquired from the dotted circular region of the TEM image and a plasmon loss peak was observed in the low-loss region, and decreased in intensity with increasing irradiation time (Fig. 90a). Estimations of the change in the number of layers from the actual spectra for each oxygen radical irradiation demonstrated that the number of graphene layers decreased. In Fig. 90b, the range of $[\pi+\sigma]/[\pi]$ for each number of layers is indicated by a thick bar on the plot. The experimental data are also plotted in the same manner and it can be seen that the estimated number of layers decreased in a linear fashion from 8 to 4. Figure 90c shows the etching of the layers as a function of the irradiation time with oxygen radicals. Sugiura et al. (2020) demonstrated layer-by-layer etching of multilayer graphene using oxygen radicals at room temperature. These prior studies demonstrate the necessity of developing a system capable of observing the various reactions induced by radicals in real time at the atomic level. The present results will also contribute to the development of simulations of radical processes and the construction of a plasma processing science.

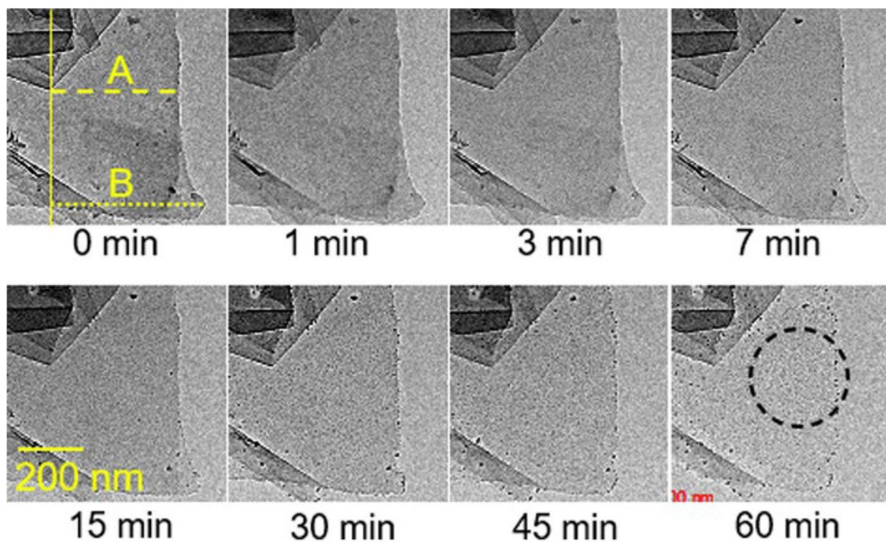

Fig. 89 Multi-layer Graphene etching process observed in situ by TEM. TEM images of multi-layer graphene etching. The total remote oxygen plasma irradiation time is shown in the bottom of each figure. The lines A and B indicate the measurement lines for calculation of etching rate. The dashed circle indicates the measurement area of EELS and electron diffraction (Sugiura et al. 2020)

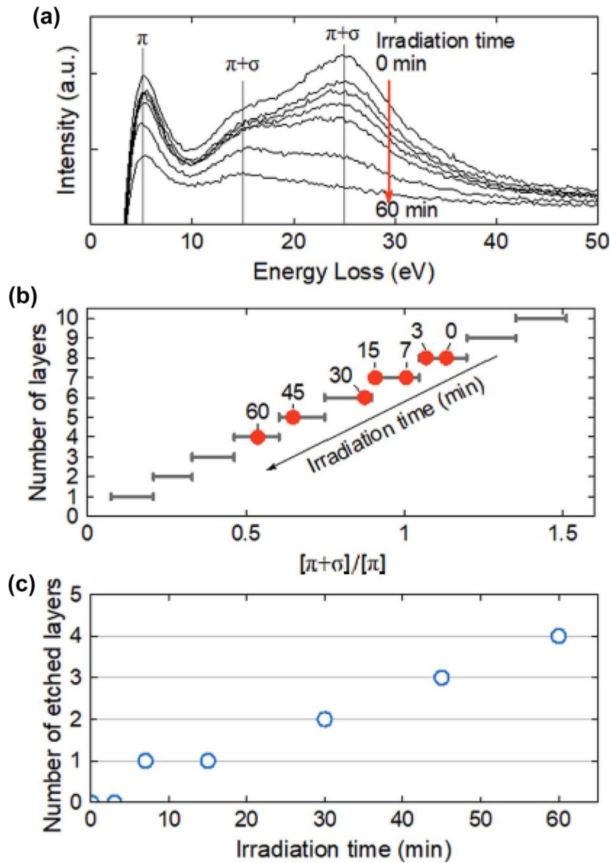

Fig. 90 Graphene etching process observed in situ by TEM and EELS analysis. **a** Plasmon peaks of EEL spectra in low-loss region after background subtraction. **b** Relationship between number of layers and [π + σ] /[π] (compiled from data obtained by Jovanovic [12]). The red dots indicate the [π + σ] /[π] measured in the present experiment for remote oxygen plasma irradiation. **c** Number of etched layers as a function of irradiation time. (Sugiura et al. 2020)

11.3 Pioneering radical-induced self-assembly reactions

The development of ULSIs requires atomic-scale control of the processing dimensions. As noted in Sect. 5.10.1, vertical graphene structures (in the form of carbon nanowalls) having widths of 2 nm and a high aspect ratio of 1000 cannot be fabricated by 3D microfabrication (top-down) techniques using plasma etching technology. That is, carbon nanowalls must grow via self-organization reactions in reaction fields caused by radicals and ions via bottom-up processes. To construct a variety of 3D microstructures in the future, it will be necessary to integrate top-down and bottom-up processes in the radical-induced reaction field.

Figure 91 shows the results obtained from the etching of an organic thin film during which a fine pattern was formed in advance and then trimmed using nitrogen and

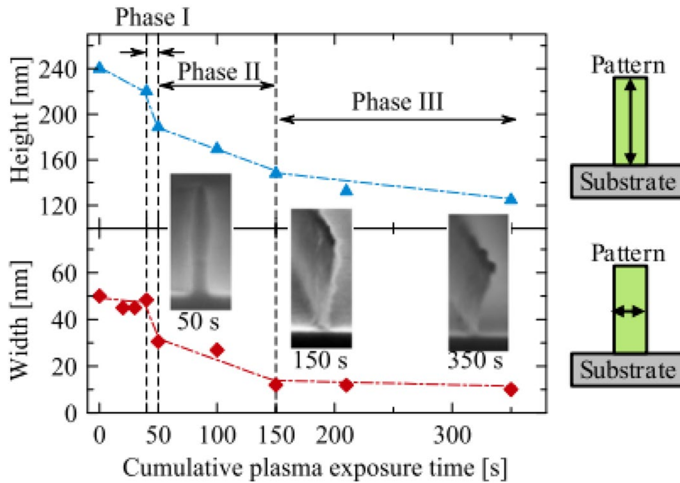

Fig. 91 Pattern profile parameters for cumulative plasma exposure times with cross-sectional or overhead SEM images of samples (Fukunaga et al. 2019)

hydrogen radicals. During this trimming, isotropic etching of the pattern sidewalls occurred and the etching was observed to stop at a distance of approximately 8 nm, indicating a self-limiting reaction. As indicated in the figure, hydrogen radicals etched the organic film, while nitrogen radicals simultaneously nitrided the surface, resulting in the formation of a CN layer. Both etching and surface modification proceeded from the sidewalls of the pattern until the organic film on the sidewalls was thinned and eventually completely transformed into a CN layer. The etching process was evidently self-limiting due to the high resistance of the CN layer to attack by hydrogen radicals (Fukunaga et al. 2019). The development of such radical-induced self-assembly reactions is becoming increasingly important.

11.4 Modeling and simulation of interactions of radicals with surfaces of materials and cells

Fabrication processes controlled at the atomic layer level will require highly precise control of radicals based on a mapped processing science, as described in Sect. 4, or the use of radical-induced self-organized reactions. These advancements will require analyses of the interactions between radicals and materials not only by experiments but also by simulations. As an example, during the atomic layer etching of polymeric materials using O, the oxidation of the polymer by these radicals must initially be self-organized. This means that the interactive reactions between the O and the polymer modify the surface such that it is saturated with O and that the underlying surface must not be volatilized. The surface of the modified layer must then be removed by a subsequent exposure to low-energy ions such that only the modified layer is removed on the atomic scale. Simulations of the interactions between O and polymer surfaces have been performed based on first principles to gain additional insights into this process.

Fukunaga et al. (2020) performed in situ analyses of a polymer surface exposed to O using X-ray photoelectron spectroscopy (XPS) together with simulations based on density functional theory (DFT) calculations. Figure 92 provides the results obtained from simulations of the reactions between a polymer surface and O. Figure 92a shows the initial and final structures of a polystyrene (PS) ribbon in association with the adsorption of seven oxygen atoms, roughly corresponding to 30% of the exposed upper C atoms. Figure 92b shows the PS surface after exposure to a dense flux of 20 oxygen atoms at room temperature, equivalent to 100% coverage of the top surface. In this case, a part of the PS structure was etched, as shown in the right-hand side of the figure, which was consistent with the results of XPS and FTIR analyses. This agreement between the simulation and experimental results is very important to the construction of radical-controlled plasma processes. Computer simulations can provide fundamental information regarding the processes occurring in plasmas and, more importantly, on the surfaces of cells. However, until now, very little such modelling has been reported, especially with regard to the study of interactions.

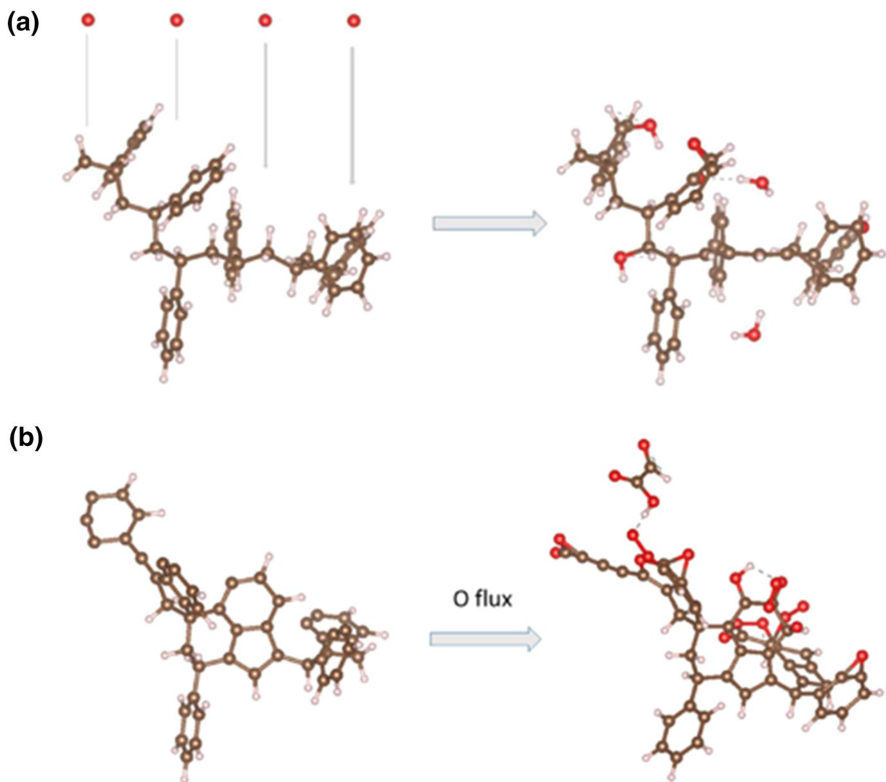

Fig. 92 **a** Polystyrene (PS) structure before and after the adsorption of seven oxygen atoms, which represents 30% of upper surface coverage, approximately, and **b** PS structure after hydrogen removal and adsorption of oxygen atoms representing 100% of upper surface coverage (Fukunaga et al. 2020)

Yusupov et al. (2013) investigated the mechanisms associated with the interactions of OH, H_2O_2, O, O_3, O_2 and H_2O with the cell walls of peptidoglycan (PG) bacteria on the atomic level by means of reactive molecular dynamics (MD) simulations. Figure 93 shows the rupture of bonds in the PG, which is composed of repeating units of disaccharides (N-acetylglucosamine and N-acetylmuramic acid (GlcNAc-MurNAc)), a stem unit (L-alanine-D-iso-glutamine-L-lysine-D-alanine (L-Ala1-D-iso-Gln2-L-L-Lys3-D-Ala4)) and a bridging unit (L-Ala1-D-iso-Gln2-L-L-Lys3-D-Ala4). A repeating unit consisting of a bridge (L-Ala1-D-iso-Gln2-L-Lys3-D-Ala4), L-alanine-D-iso-glutamine-L-lysine-D-alanine (L-Ala1-D-iso-Gln2-L-L-Lys3-D-Ala4) and a second bridge (pentaglycine (Gly1–Gly2–Gly3–Gly4–Gly5) interpeptide) connect one PG chain to the D-Ala4 group of an adjacent chain via an OH. This work established the effects of OH on the bond breaking process and showed that OH, O, O_3 and H_2O_2 resulted in significant bond cleavage and ultimately damage to the bacterial cells. These active species were also found to exhibit very different reaction mechanisms. Such quantitative information regarding the chemical reactivity of these reactive oxygen species can help to highlight the effectiveness of plasmas in decontamination and sterilization applications.

Recently, Yusupov et al. (2021) reported research regarding CD44 and hyaluronan (HA). CD44 is a major cell adhesion receptor expressed on cancer and cancer stem cells and aids in cell–cell and cell–matrix interactions, proliferation, differentiation, invasion and migration, while HA influences the biomechanical, physical and structural properties of tissues. This work used reactive MD simulations based on the density functional-tight binding method to determine the interactions of HA

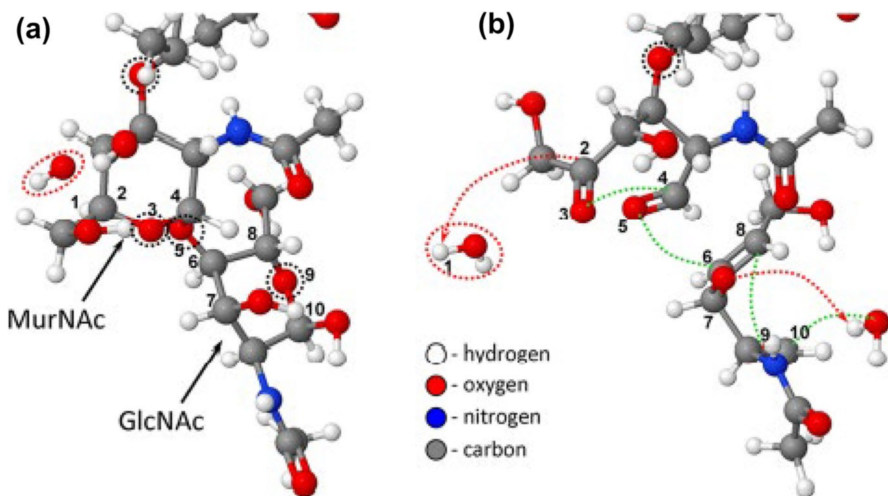

Fig. 93 Snapshots from MD simulations, presenting the consecutive breaking of three important ether C–O bonds in the disaccharide (see black dashed circles in MurNAc, GlcNAc, and between them) upon OH impact. **a** OH (see red dashed circle) first approaches H1. **b** OH abstracts the H1 atom, which is connected to C2, forming a water molecule (see red dashed circle). Subsequently, some double bonds are created, which lead to the dissociation of three ether C–sO bonds [cf. the bonds between numbered atoms from (**a**) and (**b**)]. The hydrogen abstraction reaction and the breaking of bonds are indicated by red dashed arrows and by green dashed lines, respectively (Yusupov et al. 2013)

with RONSs (O, HO, HO_2, NO and NO_2), H_2O_2 and O_3, and NO_2^- and NO_3^-. The results indicated that the associated reductions in binding energy reduced the survival of cancer cells exposed to radioactive materials but also changed the conformation of CD44 on cell surfaces. Interestingly, the accompanying decrease in binding energy affected the signal transduction pathway of cancer cells and ultimately suppressed their growth. Thus, simulations have revealed that the oxidative damage to the HA–CD44 interaction provided by RONS is a fundamental mechanism in oxidative stress-induced cancer therapy. Future studies are expected to further analyze the interactions of various radicals generated from plasma with cells based on simulations.

11.5 Pioneering pharmaceutical applications of plasmas

The previous section described the manner in which the administration of PAL kills a variety of cancers, and so could be considered a drug. Plasma-activated solutions have potential applications in the fields of medicine and agriculture and new research into plasma pharmacology is ongoing. It is anticipated that novel pharmaceuticals may be produced via the chemical reactions of plasma radicals with solids and solutions, although the licensing of such products according to regulatory requirements demands further attention. A pioneering study by Kuzuya et al. (1983) assessed the use of plasmas in a drug delivery system (DDS) based on plasma-initiated polymerization. In this work, radicals generated in a plasma were reacted with monomers on a solid surface to synthesize new organic materials. The plasma-induced radicals formed on a variety of conventional polymers were analyzed using ESR with the aid of systematic computer simulations. Diffusion-controlled matrix devices are currently among the most widely used DDSs, because the release rate can be determined by the pore size of the matrix structure. Therefore, based on differences in polymer degradation rates, controlled-release tablets have been prepared by exposing double-compressed tablets to oxygen-based plasmas.

Kuzuya et al. (1994) developed a method for synthesizing polymers using a mechanochemical reaction. In this process, the application of mechanical energy (such as vibratory grinding) to plasma-irradiated polymer powder induces the recombination of solid surface radicals before the radicals can undergo typical reactions to produce stable antimagnetic molecules. The control of such solid radicals could be applied to the synthesis of materials for drug delivery, prodrugs and new bio-applications (Yamauchi et al. 2020) via the interactions between these radicals and cells or living organisms. The potential of plasma-based processes in pharmaceutical applications has attracted much attention recently, and it is expected that a new interdisciplinary field will result from such work (Woedtke et al. 2013; Gao et al. 2021).

Porto et al. (2017) fabricated nano-capsules consisting of a polymeric hydrocarbon shell surrounding a core containing vancomycin in a single-step process, using an aerosol-assisted atmospheric-pressure plasma deposition process, as shown in Fig. 94. These capsules have uses as active vectors for various compounds, especially for drug delivery. The unique kinetics of surface radicals in aerosol-assisted atmospheric-pressure plasmas involving precursor atomization could extend the

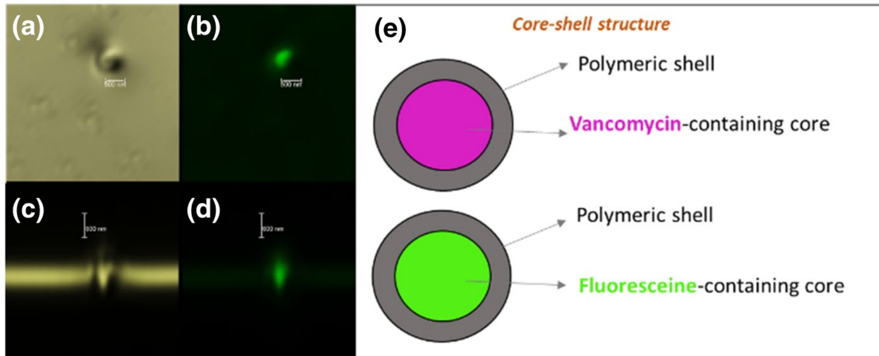

Fig. 94 Confocal microscopy images: top view reflection (**a**) and top view fluorescence (**b**), section reflection (**c**) and section fluorescence (**d**) of the nano-capsules deposited in continuous plasma mode, feeding the aerosol with fluorescein. A scheme of the hypothesized core–shell structure for vancomycin and fluorescein containing beads is shown (**e**) (Porto et al. 2017)

range of applications of plasmas (Palumbo et al. 2020). Radicals generated from plasmas sometimes interact with electrons, ions and radiation to induce non-equilibrium physicochemical reactions on the surfaces and subsurfaces of solids to achieve the etching deposition and surface modification of semiconductors and functional materials. Figure 95 shows the future trends in radical processing science. In early studies, non-equilibrium physicochemical reactions induced by radicals were examined and spatiotemporally controlled based on information engineering systems, such as AI. Eventually, various phenomena were combined to realize integrated circuits and quantum devices to further advance the field of electronics. The second generation of such research will enable new applications in medicine, pharmacy, agriculture and other fields, including cancer treatment, regenerative medicine, new therapeutic drugs, plant growth promotion and the production of functional agricultural products. This will be accomplished through the interactions of radicals with solutions composed of inorganic and organic substances and of radical-active solutions with living organisms. In the third generation, the various signal circuits in biological reactions induced and expressed by radicals will be elucidated and controlled, and complexation or fusion through self-organized reactions between inorganic, organic and biological systems will be realized. Ultimately, it is expected that the creation of artificial life will be possible based on combining living organisms with advanced super-integrated circuit devices controlled by a single molecule or atom.

11.6 Radical generation and control by nanosecond pulsed plasma

In recent years, nanosecond atmospheric pressure pulsed plasmas have attracted much attention. Interesting phenomena have been reported not only in plasma physics but also in plasma chemistry. Recently, Britun et al. (2021) studied atmospheric pressure plasmas with nanosecond pulses and showed that the vicinity of the spark-to-glow transition exhibits optimal performance for nitric oxide (NO) radical

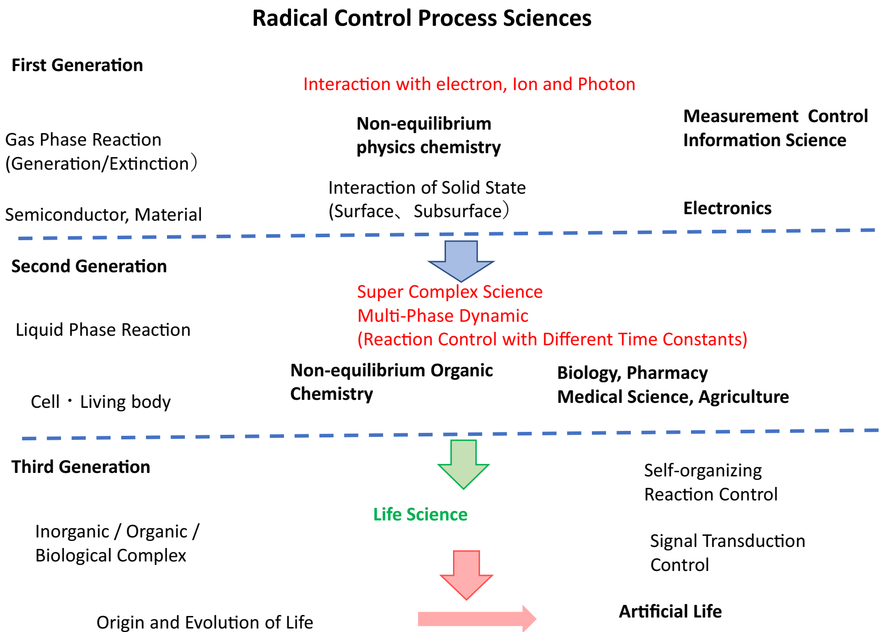

Fig. 95 Future trends in radical processing science

production. In the spark region, the NO production efficiency was found to be below 4 eV/molecule, close to the Zeldovich reaction enthalpy of NO production (about 3 eV/molecule). This result means that the energy efficiency of a single spark may exceed the modern Haber–Bosch cycle of which energy conversion for ammonia is about 5 eV/molecule (Patila et al. 2015).

Nanosecond pulsed plasmas are likely to open new avenues in the highly efficient generation and control of radicals.

11.7 Need to understand and systematize the interaction of radicals with electrons, ions, and light in microscopic regions of a surface or subsurface

In this review, radicals are defined as electrically neutral, active species with relatively short lifetimes, as described in Sect. 1, and the characteristics and role of radicals in plasma processes are specifically described. The role of radicals in plasma processes may be like that of a detonator in plasma-induced physicochemical reactions. These radicals interact with electrons, ions, and light in plasma processes, resulting in etching, deposition, and surface modification, as well as complex reactions in solutions and living organisms. For example, as reported by Coburn and Winters (1979), the reaction between a combination of XeF_2 and Ar ions on a Si surface increases the Si etching rate more dramatically than XeF_2 or Ar alone. This is because the kinetic energy of the Ar ions allows the radicals to contribute to the

physicochemical reaction as a detonator. On the other hand, when an Al surface is irradiated with a combination of F_2 and Ar ions, the reaction between these ions causes the Al etching rate to be lower than that using F_2 or Ar ions alone. This suggests that the radical species act as a detonator to inhibit etching. It has also been found that irradiating a Si surface with both XeF_2 and electrons increases the etching rate compared to that using XeF_2 alone, suggesting that the radical reaction can be promoted by excitation by electrons.

Moon et al. (2010) developed a combinatorial plasma process for obtaining a large amount of data in a single trial. They evaluated the contribution of the interaction between fluorocarbon radicals and VUV light, and between fluorocarbon radicals and ions, to the SiO_2 etching rate using fluorocarbon gas plasma. Their results showed that the use of VUV light is only a few percent more effective than ions in the etching process. In these reactions, the kinetic energy imparted by the ions to the solid surface plays a major role in the synergistic reaction with the radicals.

Although the etching reaction is accelerated in proportion to the energy of the ions, the ion penetration depth is only a few nanometers, but the plasma-induced damage layer is much thicker. Minami et al. (2011) investigated the damage caused by $Cl_2/SiCl_4/Ar$ plasma etching of GaN/InGaN single quantum well structures and found that whereas physical damage is restricted to within 2 nm from the surface, UV damage extends to depths of more than 60 nm, indicating that the synergistic effects of ions and light increase the damage. Surprisingly, it has also been reported that irradiation of Sb-doped Ge with Ar or CF_4 plasma broadens the depth distribution of defects associated with electron trapping by Sb, reaching depths of up to 3 μm (Kusumandari et al. 2013). The depth effects caused by interaction of radicals with electrons, ions and light in such plasma processes, as well as the microscopic effects of the interaction of plasma with solids, are of great importance not only from a scientific point of view but also in the manufacture of semiconductor devices.

On the other hand, the interaction of radicals with electrons, ions and light during plasma irradiation of liquids and living organisms is even more complex, and represents an entirely new scientific field. In these radical reactions, as described in Sect. 4, the most important concept is to identify the radicals that are effective in semiconductor and biological reactions from among the diverse range of radicals, and to categorize them using their substantial effects as indicators. For example, in semiconductor plasma processes, substantial effects are represented by Eqs. (2.10) and (2.11) as the loss probability of radical. In the field of plasma medicine, Cheng et al. (2020) focused on RONS, which are known to have an effect on living organisms, and defined the equivalent total oxidation potential (ETOP) as the plasma dose, to provide insights into the effect of plasma on living organisms.

In liquid and biological reactions caused by plasma irradiation, the effects can extend over ranges of several millimeters. On the other hand, radicals are generally not transported over long distances, as they instantly form new reactants or react with biological materials and are deactivated. The basic equation describing the behavior of radicals [Eq. (2.1)] involves a balance between creation and annihilation. Basically radical reactions do not extend to a few micrometres in liquid. In biological applications of plasma, a distinction needs to be made between radicals and RONS: the latter include radicals, such as O^-, OH, HO_2, CO_3^-, eroxyl RO_2,

alkoxyl RO, CO_2^-, $^1O_2$, NO and NO_2, while others are H_2O_2, O_3, ROOH, $ONOO^-$, ONOOH, HNO_2, N_2O_3, ROONO and so on as non-radical species (Graves 2012). In liquids and living organisms, OH and other radicals generated from plasma recombine to form H_2O_2 as non-radicals and disappear instantly, as shown in Eq. (9.4). However, H_2O_2 also affects the organism, for example by inducing oxidative stress. In other words, even if the radicals are deactivated, their effect continues through a chain reaction of RONS, and the reactive species generated may affect biological reactions at a distance. In addition, radicals such as NO are produced by enzymes in vivo and affect biological reactions. It is, therefore, very interesting to note that in vivo, quite unlike the mutual reaction between radicals and solids in semiconductors, a mechanism occurs in which the annihilation of radicals and the generation of RONS occurs continuously and causes long-range effects in organisms. It is hoped that these radical generation and deactivation schemes will be used in the future as a basis for a unified scientific understanding of semiconductor plasma processes and plasma bioprocesses.

12 Summary

Apart from dark matter and dark energy, the existence of which has yet to be identified, 99.9% of the universe is in a plasma state, and it is proposed that plasma processing will continue to be a technological driving force on Earth. Radicals play the most important role in plasma processing, and because radicals are electrically neutral, it has thus far been very difficult to gain insight into their behavior. However, with the ongoing accumulation of data concerning the gas phase and solid surface reactions of radicals based on spectroscopy, modeling of the reactions of various radical species in complex plasma processes has progressed. Even so, the reactions of radicals generated from plasmas with inorganic and organic solutions have produced many unexplained phenomena, and the study of these processes has developed into a new academic field. In particular, the behavior of short-lived radicals generated in solution as a consequence of the reactions of plasma-induced radicals has attracted attention in the field of electrochemistry. Elucidating the electrochemical effects of these radicals is expected to lead to the development of new material processes, systems for the reduction of CO_2, novel conversion and cleaning technologies, and new research into radical electrochemistry. During the redox reactions that occur in living organisms, radicals are constantly generated and annihilated, and studies of the reactions between gas and liquid phase plasma radicals, ions, radiation and cells comprise the field of plasma biotechnology that is expected to impact medical and agricultural research. The effects of plasma-induced radicals generated external to cells or organisms on the radical reactions that maintain life is also an unexplored avenue of study. It is evident that the control of radical behavior could lead to breakthroughs in the areas of plasmas, materials and devices, environmental remediation, and the pharmaceutical and biological sciences. Ultimately, such research is expected to produce new scientific theories, while the ongoing development of radical-controlled plasma processes will contribute to future technological progress.

Acknowledgements The author thanks Professor Hiromasa Tanaka (Center for Low-temperature Plasma Sciences, Nagoya University) for his assistance. This work was supported in part by a Grant-in-Aid for Specially Promoted Research (no. 19H05462) from the Ministry of Education, Culture, Sports, Science and Technology of Japan.

Declarations

Conflicts of interest We confirm that there are no known conflicts of interest associated with this publication and there has been no significant financial support for this work that could have influenced its outcome.

Open Access This article is licensed under a Creative Commons Attribution 4.0 International License, which permits use, sharing, adaptation, distribution and reproduction in any medium or format, as long as you give appropriate credit to the original author(s) and the source, provide a link to the Creative Commons licence, and indicate if changes were made. The images or other third party material in this article are included in the article's Creative Commons licence, unless indicated otherwise in a credit line to the material. If material is not included in the article's Creative Commons licence and your intended use is not permitted by statutory regulation or exceeds the permitted use, you will need to obtain permission directly from the copyright holder. To view a copy of this licence, visit http://creativecommons.org/licenses/by/4.0/.

References

H. Abe, M. Yoneda, N. Fujiwara, Developments of plasma etching technology for fabricating semiconductor devices. Jpn. J. Appl. Phys. **47**, 1435–1455 (2008)

Y. Abe, A. Fukushima, K. Takeda, H. Kondo, K. Ishikawa, M. Sekine, M. Hori, Critical flux ratio of hydrogen radical to film precursor in microcrystalline silicon deposition for solar cells. Appl. Phys. Lett. **101**, 172109 (2012)

Y. Abe, A. Fukushima, K. Takeda, H. Kondo, K. Ishikawa, M. Sekine, M. Hori, Surface loss probability of H radicals on silicon thin films in SiH_4/H_2 plasma. J. Appl. Phys **113**(1), 013303 (2013)

Y. Abe, K. Ishikawa, K. Takeda, T. Tsutsumi, A. Fukushima, H. Kondo, M. Sekine, M. Hori, Absolute density of precursor SiH_3 radicals and H atoms in H_2-diluted SiH_4 gas plasma for deposition of microcrystalline silicon films. Appl. Phys. Lett. **110**, 043902 (2017)

Y. Abe, Studies on fabrication of silicon thin films using plasma enhanced chemical vapor deposition and behaviors of radicals. Dissertation, 1–172 (2013)

T. Adachi, H. Tanaka, S. Nonomura, H. Hara, S. Kondo, M. Hori, Plasma-activated medium induces A549 cell injury via a spiral apoptotic cascade involving the mitochondrial-nuclear network. Free Radic. Biol. Med. **79**, 28–44 (2014)

T.H. Ahn, K. Nakamura, H. Sugai, Negative ion measurements and etching in a pulsed-power inductively coupled plasma in chlorine. Plasma Sources Sci. Technol. **5**, 139–144 (1996)

T. Amano, H. Kondo, K. Ishikawa, T. Tsutsumi, K. Takeda, M. Hiramatsu, M. Sekine, M. Hori, Rapid growth of micron-sized graphene flakes using in-liquid plasma employing iron phthalocyanine-added ethanol. Appl. Phys. Express **11**, 015102 (2018)

A. Ando, K. Ishikawa, H. Kondo, T. Tsutsumi, K. Takeda, T. Ohta, M. Ito, M. Hiramatsu, M. Sekine, M. Hori, Nanographene synthesis employing in-liquid plasmas with alcohols or hydrocarbons. Jpn. J. Appl. Phys. **57**, 026201 (2018)

G. Bauer, D. Sersenova, D.B. Graves, Z. Machala, Dynamics of singlet oxygen-triggered, RONS-based apoptosis induction after treatment of tumor cells with cold atmospheric plasma or plasma-activated medium. Sci. Rep. **9**, 13931 (2019)

R.W. Boswell, D. Henry, Pulsed high rate plasma etching with variable Si/SiO_2 selectivity and variable Si etch profiles. Appl. Phys. Lett. **47**, 1095–1097 (1985)

N. Britun, V. Gamaleev, M. Hori, Evidence of near-the-limit energy cost NO formation in atmospheric spark discharge. Plasma Sources Sci. Technol. **30**, 08LT02 (2021)

P.J. Bruggeman, M.J. Kushner, B.R. Locke, J.G.E. Gardeniers, W.G. Graham, D.B. Graves, R.C.H.M. Hofman-Caris, D. Maric, J.P. Reid, E. Ceriani et al., Plasma–liquid interactions: a review and roadmap. Plasma Sources Sci. Technol. **25**, 053002 (2016)

P.J. Chantry, A simple formula for diffusion calculations involving wall reflection and low density. J. Appl. Phys. **62**, 1141–1148 (1987)
H. Cheng, J. Xu, X. Li, D. Liu, X. Lu, On the dose of plasma medicine: Equivalent total oxidation potential (ETOP). Phys. Plasmas **27**, 063514 (2020)
Y. Chinzei, H. Shindo, Y. Horiike, Highly selective SiO_2/Si etching and related kinetics in time-modulated helicon wave plasma. Jpn. J. Appl. Phys. **35**, 3585–3589 (1996)
R.C. Chittick, J.H. Alexander, H.F. Sterling, The preparation and properties of amorphous silicon. J. Electrochem. Soc. Solid State Sci. **116**, 77–81 (1969)
H.J. Cho, H. Kondo, K. Ishikawa, M. Sekine, M. Hiramatsu, M. Hori, Density control of carbon nanowalls grown by CH_4/H_2 plasma and their electrical properties. Carbon **68**, 380–388 (2014)
J.W. Coburn, H. Winters, Ion-and electron-assisted gas-surface chemistry-An important effect in plasma etching. J. Appl. Phys. **50**, 3189–3196 (1979)
Y. Fukunaga, T. Tsutsumi, H. Kondo, K. Ishikawa, M. Sekine, M. Hori, Narrow free-standing features fabricated by top-down self-limited trimming of organic materials using precisely temperature-controlled plasma etching system. Jpn. J. Appl. Phys. **58**, 020906 (2019)
Y. Fukunaga, R.C. Longo, P.L.G. Ventzek, B. Lane, A. Ranjan, G.S. Hwang, G. Hartmann, T. Tsutsumi, K. Ishikawa, H. Kondo et al., Interaction of oxygen with polystyrene and polyethylene polymer films: A mechanistic study. J. Appl. Phys. **127**, 023303 (2020)
L. Gao, X. Shi, X. Wu, Applications and challenges of low temperature plasma in pharmaceutical field. J. Pharm. Anal. **11**, 28–36 (2021)
S.M. George, Atomic layer deposition: An overview. Chem. Rev. **110**, 111–131 (2010)
T. Goto, Radical measurements in plasma processing. Adv. at. Mol. Opt. Phys. **44**, 99–125 (2001)
M. Goto, K. Azuma, T. Okamoto, Y. Nakata, Surface wave plasma oxidation at low temperature under rare gas dilution. Jpn. J. Appl. Phys. **42**, 7033–7038 (2003)
D.B. Graves, The emerging role of reactive oxygen and nitrogen species in redox biology and some implications for plasma applications to medicine and biology. J. Phys. D: Appl. Phys. **45**, 26300 (2012)
T. Hagino, H. Kondo, K. Ishikawa, H. Kano, M. Sekine, M. Hori, Ultrahigh-speed synthesis of nanographene using alcohol in-liquid plasma. Appl. Phys. Express **5**, 035101 (2012)
H. Hashizume, T. Ohta, J. Fengdong, K. Takeda, K. Ishikawa, M. Hori, M. Ito, Inactivation effects of neutral reactive-oxygen species on Penicillium digitatum spores using non-equilibrium atmospheric-pressure oxygen radical source. Appl. Phys. Lett. **103**, 153708 (2013)
H. Hashizume, T. Ohta, K. Takeda, K. Ishikawa, M. Hori, M. Ito, Quantitative clarification of inactivation mechanism of Penicillium digitatum spores treated with neutral oxygen radicals. Jpn. J. Appl. Phys. **54**, 01AG05 (2015)
H. Hayashi, S. Morishita, T. Tatsumi, Y. Hikosaka, S. Noda, H. Nakagawa, S. Kobayashi, M. Inoue, Mechanism of C_4F_8 dissociation in parallel-plate-type plasma. J. Vac. Sci. Technol. A **17**(5), 2557–2571 (1999)
M. Hiramatsu, M. Hori, Fabrication of carbon nanowalls using novel plasma processing. Jpn. J. Appl. Phys. **45**, 5522–5527 (2006)
M. Hiramatsu, K. Shiji, H. Amano, M. Hori, Fabrication of vertically aligned carbon nanowalls using capacitively coupled plasma-enhanced chemical vapor deposition assisted by hydrogen radical injection. Appl. Phys. Lett. **84**, 4708–4710 (2004)
M. Hori, H. Kondo, M. Hiramatsu, Radical-controlled plasma processing for nanofabrication. J. Phys. D Appl. Phys. **44**, 174027 (2011)
M. Hori, T. Goto, Measurement techniques of radicals, their gas phase and surface reactions in reactive plasma processing. Appl. Surf. Sci. **192**, 135–160 (2002)
M. Hori, T. Goto, Progress of radical measurements in plasmas for semiconductor processing. Plasma Sources Sci. Technol. **15**, S74–S83 (2006)
M. Hori, T. Goto, Insight into sticking of radicals on surfaces for smart plasma nano-processing. Appl. Surf. Sci. **253**, 6657–6671 (2007)
Y. Horiike, M. Shibagaki, A new chemical dry etching. Jpn. J. Appl. Phys. **15**, 13–18 (1976)
S.-N. Hsiao, T. -T. -Nga Nguyen, T. Tsutsumi, K. Ishikawa, M. Sekine, M. Hori, On the etching mechanism of highly hydrogenated SiN films by CF_4/D_2 plasma: Comparison with CF_4/H_2. Coatings **11(12)**, 1535 (2021)
S.-N. Hsiao, K. Ishikawa, T. Hayashi, J. Ni, T. Tsutsumi, M. Sekine, M. Hori, Selective etching of SiN against SiO_2 and poly-Si films in hydrofluoroethane chemistry with a mixture of CH_2FCHF_2, O_2, and Ar. Appl. Surf. Sci. **541**, 148439 (2021)

Y. Ikehara, H. Sakakita, N. Shimizu, S. Ikehara, H. Nakanishi, Formation of membrane-like structures in clotted blood by mild plasma treatment during hemostasis. J. Photopolym. Sci. Technol. **26**, 555–557 (2013)

S. Ikehara, H. Sakakita, K. Ishikawa, Y. Akimoto, T. Yamaguchi, M. Yamagishi, J. Kim, M. Ueda, J. Ikeda, H. Nakanishi et al., Plasma blood coagulation without involving the activation of platelets and coagulation factors. Plasma Process. Polym. **12**, 1348–1353 (2015)

M. Inayoshi, M. Ito, M. Hori, T. Goto, M. Hiramatsu, Surface reaction of CF_2 radicals for fluorocarbon film formation in SiO_2 /Si selective etching process. J. Vac. Sci. Technol. A **16**, 233–238 (1998)

H. Inui, K. Takeda, H. Kondo, K. Ishikawa, M. Sekine, H. Kano, N. Yoshida, M. Hori, Measurement of hydrogen radical density and its impact on reduction of copper oxide in atmospheric-pressure remote plasma using H_2 and Ar mixture gases. Appl. Phys. Express **3**, 126101 (2010)

S. Iseki, T. Ohta, A. Aomatsu, M. Ito, H. Kano, Y. Higashijima, M. Hori, Rapid inactivation of Penicillium digitatum spores using high-density nonequilibrium atmospheric pressure plasma. Appl. Phys. Lett. **96**, 153704 (2010)

S. Iseki, T. Ohta, A. Aomatsu, M. Ito, H. Kano, Y. Higashijima, M. Hori, Inactivation of penicillium digitatum spores by a high-density ground-state atomic oxygen-radical source employing an atmospheric-pressure plasma. Appl. Phys. Express **4**, 11621 (2011)

T. Ishijima, M. Ikeda, H. Sugai, Control of electron temperature by inert gas selection in inductive RF discharge. Transworld Research Network **37/661(2),** Fort P.O., Trivandrum-695 023, Kerala, India, 1–15 (2008)

K. Ishikawa, H. Mizuno, H. Tanaka, K. Tamiya, H. Hashizume, T. Ohta, M. Ito, S. Iseki, K. Takeda, H. Kondo, M. Sekine, M. Hori, Real-time in situ electron spin resonance measurements on fungal spores of Penicillium digitatum during exposure of oxygen plasmas. Appl. Phys. Lett. **101**, 013704 (2012)

K. Ishikawa, K. Karahashi, T. Ishijima, S.Il. Cho, S. Elliott, D. Hausmann, D. Mocuta, A.Wilson, K. Kinoshita, Progress in nanoscale dry processes for fabrication of high-aspect-ratio features: How can we control critical dimension uniformity at the bottom. Jpn. J. Appl. Phys. **57**, 06JA01 (2018)

N. Itabashi, K. Kato, N. Nishiwaki, T. Goto, C. Yamada, E. Hirota, Measurement of the SiH_3 radical density in silane plasma using infrared diode laser absorption spectroscopy. Jpn. J. Appl. Phys. **27**, L1565–L1567 (1988)

N. Itabashi, N. Nishiwaki, M. Magane, T. Goto, A. Matsuda, C. Yamada, E. Hirota, SiH_3 radical density in pulsed silane plasma. Jpn. J. Appl. Phys. **29**, 585–590 (1990)

S. Ito, K. Nakamura, H. Sugai, Radical control by wall heating of a fluorocarbon etching reactor. Jpn. J. Appl. Phys. **33**, L1261–L1264 (1994)

H. Itoh, M. Nagamine, H. Satake, A. Toriumi, A study of atomically-flat SiO_2/Si interface formation mechanism, based on the radical oxidation kinetics. Microelectron. Eng. **48**, 71–74 (1999)

M. Iwasaki, M. Ito, T. Uehara, M. Nakamura, M. Hori, Ion attachment mass spectrometry of nonequilibrium atmospheric-pressure pulsed remote plasma for etching. J. Appl. Phys. **100**, 093304 (2006)

M. Iwasaki, H. Inui, Y. Matsudaira, H. Kano, N. Yoshida, M. Ito, M. Hori, Nonequilibrium atmospheric pressure plasma with ultrahigh electron density and high performance for glass surface cleaning. Appl. Phys. Lett. **92**, 081503 (2008)

L. Jiang, H. Zheng, Q. Lyu, S. Hayashi, K. Sato, Y. Sekido, K. Nakamura, H. Tanaka, K. Ishikawa, H. Kajiyama et al., Lysosomal nitric oxide determines transition from autophagy to ferroptosis after exposure to plasma-activated Ringer's lactate. Redox. Biol. **43**, 101989 (2021)

R.W. Johnson, A. Hultqist, S.F. Bent, A brief review of atomic layer deposition: from fundamentals to applications. Mater. Today **17**, 236–246 (2014)

K.J. Kanarik, T. Lill, E.A. Hudson, S. Sriraman, S. Tan, J. Marks, V. Vahedi, R.A. Gottscho, Overview of atomic layer etching in the semiconductor industry. J. Vac. Sci. Technol. **A33**, 020802 (2015)

S. Kanazawa, M. Kogoma, T. Morikawa, S. Okazaki, Stable glow plasma at atmospheric pressure. J. Phys. D: Appl. Phys. **21**, 838–840 (1988)

H. Kawasaki, H. Ohkura, T. Fukuzawa, M. Shiratani, Y. Watanabe, Y. Yamamoto, S. Suganuma, M. Hori, T. Goto, Roles of SiH_3 and SiH_2 radicals in particle growth in rf silane plasma. Jpn. J. Appl. Phys. **36**, 4985–4988 (1997)

U. Kogelschatz, Dielectric-barrier discharges: Their history, discharge physics, and industrial applications. Plasma Chem. Plasma Process. **23**, 1–46 (2003)

S. Kondo, M. Hori, K. Yamakawa, S. Den, H. Kano, M. Hiramatsu, Highly reliable growth process of carbon nanowalls using radical injection plasma-enhanced chemical vapor deposition. J. of Vac. Sci. Technol. **B26**, 1294–1300 (2008)

S. Kondo, S. Kawai, W. Takeuchi, K. Yamakawa, S. Den, H. Kano, M. Hiramatsu, M. Hori, Initial growth process of carbon nanowalls synthesized by radical injection plasma-enhanced chemical vapor deposition. J. Appl. Phys. **106**, 094302 (2009)

Y. Kondo, K. Ishikawa, T. Hayashi, Y. Miyawaki, K. Takeda, H. Kondo, M. Sekine, M. Hori, Silicon nitride etching performance of CH_2F_2 plasma diluted with argon or krypton. Jpn. J. Appl. Phys. **54**, 040303 (2015a)

Y. Kondo, Y. Miyawaki, K. Ishikawa, T. Hayashi, K. Takeda, H. Kondo, M. Sekine, M. Hori, Hydrofluorocarbon ion density of argon- or krypton-diluted CH_2F_2 plasmas: generation of CH_2F^+ and CHF_2^+ by dissociative ionization in charge exchange collisions. J. Phys. D: Appl. Phys. **48**, 045202 (2015b)

A. Kono, N. Koike, K. Okuda, T. Goto, Laser-induced -fluorescence detection of SiH_2 radicals in a radiofrequency silane plasma. Jpn. J. Appl. Phys. **32**, L543–L546 (1993)

A. Kono, N. Koike, H. Nomura, T. Goto, Lase-induced-fluorescence study of the SiH_2 density on RF SiH_4 plasmas with Xe, Ar, He and H_2 dilution gases. Jpn. J. Appl. Phys. **34**, 307–311 (1995)

A. Kono, T. Sugiyama, T. Goto, H. Furuhashi, Y. Uchida, Production of high-density non-equilibrium plasma in the atmosphere using microgap discharge excited by microwave. Jpn. J. Appl. Phys. **40**(3B), L238–L241 (2001)

N. Kurake, H. Tanaka, K. Ishikawa, T. Kondo, M. Sekine, K. Nakamura, H. Kajiyama, F. Kikkawa, M. Mizuno, M. Hori, Cell survival of glioblastoma grown in medium containing hydrogen peroxide and/or nitrite, or in plasma-activated medium. Arch. Biochem. Biophys. **605**, 102–108 (2016a)

N. Kurake, H. Tanaka, K. Ishikawa, K. Nakamura, H. Kajiyama, F. Kikkawa, M. Mizuno, Y. Yamanishi, M. Hori, Synthesis of calcium oxalate crystals in culture medium irradiated with non-equilibrium atmospheric-pressure plasma. Appl. Phys. Express **9**, 096201 (2016b)

N. Kurake, H. Tanaka, K. Ishikawa, K. Takeda, H. Hashizume, K. Nakamura, H. Kajiyama, T. Kondo, F. Kikkawa, M. Mizuno et al., Effects of OH and NO radicals in the aqueous phase on H_2O_2 and NO_2^- generated in plasma-activated medium. J. Phys. D: Appl. Phys. **50**, 155202 (2017)

N. Kusumandari, W. Taoka, M. Takeuchi, M. Fukudome, O. Sakashita, S. Nakatsuka, Zaima, Broad defect depth distribution in germanium substrates induced by CF_4 plasma. Appl. Phys. Lett. **103**, 033511 (2013)

M. Kuzuya, U. Niwa, Y. Yamauchi, S. Kondo, Mechanochemical reactions of plasma induced surface radicals. J. Photopolym. Sci. Technol. **7**, 315–318 (1994)

M. Kuzuya, K. Kamiya, T. Kawaguchi, T. Okuda, Concerning a trigger of plasma-initiated polymerization of methyl methacrylate and characterization of the resulting polymers. J. Photopolym. Sci. Technol. Part B: Polymer Letters **21**, 509–514 (1983)

M.A. Lieberman, S. Ashida, Global models of pulse-power-modulated high-density, low-pressure discharges. Plasma Sources Sci. Technol. **5**, 145–158 (1996)

X. Lu, G.V. Naidis, M. Laroussi, S. Reuter, D.B. Graves, K. Ostrikov, Reactive species in non-equilibrium atmospheric-pressure plasmas: Generation, transport, and biological effects. Phys. Rep. **630**, 1–84 (2016)

A. Madan, S.R. Ovshinsky, E. Benn, Electrical and optical properties of amorphous Si:F: H alloys. Phil. Mag. **B40**, 259–277 (1979)

A. Matsuda, Thin-film silicon - growth process and solar cell application. Jpn. J. Appl. Phys. **43**, 7909–7920 (2004)

A. Matsuda, Microcrystalline silicon: Growth and device application. J. Non-Cryst. Solids **338–340**, 1–12 (2004)

A. Matsuda, K. Nomoto, Y. Takeuchi, A. Suzuki, A. Yuuki, J. Perrin, Temperature dependence of the sticking and loss probabilities of silyl radicals on hydrogenated amorphous silicon. Surf. Sci. **227**, 50–56 (1990)

M. Minami, S. Tomiya, K. Ishikawa, R. Matsumoto, S. Chen, M. Fukasawa, F. Uesawa, M. Sekine, M. Hori, T. Tstsumi, Analysis of GaN damage induced by $Cl_2/SiCl_4/Ar$ Plasma. Jpn. J. Appl. Phys. **50**, 08JE03 (2011)

K. Miyamoto, S. Ikehara, H. Takei, Y. Akimoto, H. Sakakita, K. Ishikawa, M. Ueda, J. Ikeda, M. Yamagishi, J. Kim et al., Red blood cell coagulation induced by low-temperature plasma treatment. Arch. Biochem. Biophys. **605**, 95–101 (2016)

K. Miyata, M. Hori, T. Goto, Infrared diode laser absorption spectroscopy measurements of CF_x (X=1–3) radical densities in electron cyclotron resonance plasmas employing C_4F_8, C_2F_6, CF_4, and CHF_3 gases. J. Vac. Sci. Technol. A **14**, 2343–2350 (1996)

K. Mizuno, K. Yonetamari, Y. Shirakawa, T. Akiyama, R. Ono, Anti-tumor immune response induced by nanosecond pulsed streamer discharge in mice. J. Phys. D: Appl. Phys. **50**, 12LT01 (2017)

C.S. Moon, K. Takeda, M. Sekine, Y. Setsuhara, M. Shiratani, M. Hori, Etching characteristics of organic low-k films interpreted by internal parameters employing a combinatorial plasma process in an inductively coupled H_2/N_2 plasma. J. Appl. Phys. **107**, 113310 (2010)

G.E. Moore, Cramming more components onto integrated circuits. Electronics **38**, 114–117 (1965)

H. Nagai, M. Hiramatsu, M. Hori, T. Goto, Etching organic low dielectric film in ultrahigh frequency plasma using N_2/H_2 and N_2/NH_3 gases. J. Appl. Phys. **94**, 1362–1367 (2003)

M. Nagai, T. Hayashi, M. Hori, H. Okamoto, Low-k SiOCH film etching process and its diagnostics employing $Ar/C_5F_{10}O/N_2$ plasma. Jpn. J. Appl. Phys. **45**, 7100–7104 (2006)

K. Nakamura, N. Yoshikawa, Y. Mizuno, M. Ito, H. Tanaka, M. Mizuno, S. Toyokuni, M. Hori, F. Kikkawa, H. Kajiyama, Preclinical verification of the efficacy and safety of aqueous plasma for ovarian cancer therapy. Cancers **13**, 1141 (2021)

H. Nomura, A. Kono, T. Goto, Effect of dilution gases on the SiH_3 radical density in an RF SiH_4 plasma. Jpn. J. Appl. Phys. **33**, 4165–4169 (1994)

G.S. Oehrlein, D. Metzler, C. Lia, Atomic layer etching at the tipping point: An overview. ECS J. Solid State Sci. Technol. **4**(6), N5041–N5053 (2015)

S. Okazaki, M. Kogoma, M. Uehara, Y. Kimura, Appearance of stable glow discharge in air, argon, oxygen and nitrogen at atmospheric pressure using a 50 Hz source. J. Phys. d: Appl. Phys. **26**, 889–892 (1989)

F. Palumbo, C. Lo Porto, F. Fracassi, P. Favia, Recent advancements in the use of aerosol assisted atmospheric pressure plasma deposition. Coatings **10**, 440 (2020)

B.S. Patila, Q. Wanga, V. Hessela, J. Langb, Plasma N_2-fixation: 1900–2014. Catalysis Today 256 Part 1, 49–66 (2015)

J. Perrin, Plasma and surface reactions during a-Si: H film growth. J. Non-Cryst. Solids **137–138**, 639–644 (1991)

J.J. Perrin, M. Shiratani, P. Kae-Nune, H. Videlot, J. Jolly, J. Guillon, Slough reaction probabilities and kinetics during a-Si:H and a-C:H evaporation from H_2, SiH_3, Si_2H_5, CH_3 and C_2H_4 discharges. J. Vac. **16**(1), 278–289 (1998)

C. Lo Porto, F. Palumbo, G. Palazzoa, P. Favia, Direct plasma synthesis of nano-capsules loaded with antibiotics. Polym. Chem. **8**, 1746–1749 (2017)

R.L. Puurunen, A short history of atomic layer deposition: Tuomo Suntola's atomic layer epitaxy. Chem. Vap. Deposition **20**, 332–344 (2014)

M. Sakakibara, M. Hiramatsu, T. Goto, Measurement of Si atom density in radio-frequency silane plasma using ultraviolet absorption spectroscopy. J. Appl. Phys. **69**, 3467–3471 (1991)

Y. Sato, S. Yamada, S. Takeda, N. Hattori, K. Nakamura, H. Tanaka, M. Mizuno, M. Hori, Y. Kodera, Effect of plasma-activated lactated ringer's solution on pancreatic cancer cells in vitro and in vivo. Ann. Surg. Oncol. **25**, 299–307 (2018)

M. Sekine, K. Horioka, T. Arikado, H. Okano, Highly selective etching of polycrystalline silicon on silicon dioxide at low wafer temperature, employing magnetron plasma. J. Appl. Phys. **73**, 1505–1508 (1993)

K. Sekine, Y. Saito, M. Hirayama, T. Ohmi, Highly reliable ultrathin silicon oxide film formation at low temperature by oxygen radical generated in high-density krypton plasma. IEEE Trans. Electron Devices **48**, 1550–1555 (2001)

T. Shibano, N. Fujiwara, M. Hirayama, H. Nagata, K. Demizu, Etching yields of SiO_2 by low energy CF_x^+ and F^+ ions. Appl. Phys. Lett. **93**, 2336–2338 (2008)

M. Shiratani, H. Kawasaki, T. Fukuzawa, Y. Watanabe, Y. Yamamoto, S. Suganuma, M. Hori, T. Goto, A study on the time evolution of SiH_3 surface loss probability on hydrogenated amorphous silicon films in SiH_4 rf discharge using infrared diode-laser absorption spectroscopy. J. Phys. D: Appl. Phys. **31**, 776–780 (1998)

W.E. Spear, P.G. LeComber, Substitutional doping of amorphous silicon. Solid State Commun. **17**, 1193–1196 (1975)

H. Sugai, K. Nakamura, Y. Hikosaka, M. Nakamura, Diagnostics and control of radicals in an inductively coupled etching reactor. J. Vac. Sci. Technol. A **13**, 887–893 (1995)

H. Sugai, T. H. Ahn, I. Ghanashev, M. Goto, M. Nagatsu, K. Nakamura, K. Suzuki, H. Toyoda, Diagnosis for advanced plasma control of materials process. Plasma Phys. Control. Fusion **39**, A445–A458 (1997)

H. Sugiura, H. Kondo, K. Higuchi, S. Arai, R. Hamaji, T. Tsutsumi, K. Ishikawa, M. Hori, Reaction science of layer-by-layer thinning of graphene with oxygen neutrals at room temperature. Carbon **170**, 93–99 (2020)

H. Sugiura, L. Jia, H. Kondo, K. Ishikawa, T. Tsutsumi, T. Hayashi, K. Takeda, M. Sekine, M. Hori, Effects of gas residence time of CH_4/H_2 on sp^2 fraction of amorphous carbon films and dissociated methyl density during radical-injection plasma-enhanced chemical vapor deposition. Jpn. J. Appl. Phys. **57**, 06JE03 (2018)

K. Takahashi, M. Hori, T. Goto, Control of fluorocarbon radicals by on-off modulated electron cyclotron resonance plasma. Jpn. J. Appl. Phys. **32**, L1088–L1091 (1993)

K. Takahashi, M. Hori, T. Goto, CF_x (x=1-3) radicals controlled by on-off modulated electron cyclotron resonance plasma and their effects on polymer film deposition. Jpn. J. Appl. Phys. **33**, 4181–4185 (1994)

K. Takahashi, M. Hori, M. Inayoshi, T. Goto, Evaluation of CF_2 radical as a precursor for fluorocarbon film formation in highly selective SiO_2 etching process using radical injection technique. Jpn. J. Appl. Phys. **35**, 3635–3641 (1996a)

K. Takahashi, M. Hori, T. Goto, Fluorocarbon radicals and surface reactions in fluorocarbon high density etching plasma. I. O_2 addition to electron cyclotron resonance plasma employing CHF_3. J. Vac. Sci. Technol. **A 14(4)**, 2004–2010 (1996b)

S. Takahashi, R. Kawauchi, S. Takashima, S. Den, T. Katagiri, H. Kano, T. Ohta, M. Ito, T. Suzuki, K. Takeda, M. Hori, An autonomously controllable plasma etching system based on radical monitoring. Jpn. J. Appl. Phys. **51**, 076502 (2012)

S. Takashima, M. Hori, T. Goto, A. Kono, M. Ito, K. Yoneda, Vacuum ultraviolet absorption spectroscopy employing a microdiacharge hollow-cathode lamp for absolute density measurements of hydrogen atoms in reactive plasmas. Appl. Phys. Lett. **75**, 3929–3931 (1999)

S. Takashima, M. Hori, T. Goto, K. Yoneda, Behavior of hydrogen atoms in ultrahigh-frequency silane plasma. J. Appl. Phys. **89**(9), 4727–4731 (2001)

K. Takeda, S. Takashima, M. Ito and M. Hori, Absolute density and temperature of $O(^1D_2)$ in highly Ar or Kr diluted O_2 plasma. Appl. Phys. Lett. **93**, 021501 (2008)

K. Takeda, Y. Kubota, A. Serdyuchenko, S. Takashima, M. Ito, Y. Matsumi, M. Hori, Diagnostics of surface wave excited Kr/O_2 plasma for low-temperature plasma oxidation processes. J. Appl. Phys. **102**, 013302 (2007)

K. Takeda, K. Ishikawa, H. Tanaka, M. Sekine, M. Hori, Spatial distributions of O, N, NO, OH and vacuum ultraviolet light along gas flow direction in an AC-excited atmospheric pressure Ar plasma jet generated in open air. J. Phys. D: Appl. Phys. **50**, 195202 (2017)

K. Takeda, H. Yamada, K. Ishikawa, H. Sakakita, J. Kim, M. Ueda, J. Ikeda, Y. Akimoto, Y. Kataoka, N. Yokoyama, Y. Ikehara et al., Systematic diagnostics of the electrical, optical, and physicochemical characteristics of low-temperature atmospheric-pressure helium plasma sources. J. Phys. D: Appl. Phys. **52**, 165202 (2019)

H. Tanaka, Z. Chuanjie, Y. Hayakawa, M. Hirayama, A. Teramoto, S. Sugawa, T. Ohmi, High-quality silicon oxide film formed by diffusion region plasma enhanced chemical vapor deposition and oxygen radical treatment using microwave-excited high-density plasma. Jpn. J. Appl. Phys. **42**, 1911–1915 (2003)

H. Tanaka, M. Mizuno, K. Ishikawa, K. Nakamura, H. Kajiyama, H. Kano, F. Kikkawa, M. Hori, Plasma activated medium selectively kills glioblastoma brain tumor cells by down-regulating a survival signaling molecule, AKT Kinase. Plasma Med. **1**, 265–277 (2013)

H. Tanaka, M. Mizuno, K. Ishikawa, K. Nakamura, F. Utsumi, H. Kajiyama, H. Kano, S. Maruyama, F. Kikkawa, M. Hori, Cell survival and proliferation signaling pathways are downregulated by plasma activated medium in glioblastoma brain tumor cells. Plasma Med. **2**, 207–220 (2014)

H. Tanaka, K. Ishikawa, M. Mizuno, S. Toyokuni, H. Kajiyama, F. Kikkawa, H.-R. Metelmann, M. Hori, State of the art in medical applications using non-thermal atmospheric pressure plasma. Rev. Mod. Plasma Phys. **1**(3), 1–89 (2017)

H. Tanaka, M. Mizuno, S. Toyokuni, S. Maruyama, Y. Kodera, H. Terasaki, T. Adachi, M. Kato, F. Kikkawa, M. Hori, Cancer therapy using non-thermal atmospheric pressure plasma with ultra-high electron density. Phys. Plasmas **22**, 122004 (2015)

H. Tanaka, K. Nakamura, M. Mizuno, K. Ishikawa, K. Takeda, H. Kajiyama, F. Utsumi, F. Kikkawa, M. Hori, Non-Thermal atmospheric pressure plasma activated lactate in Ringer's solution for anti-tumor effects. Sci. Rep. **6**, 36282 (2016)

H. Tanaka, M. Mizuno, Y. Katsumata, K. Ishikawa, H. Kondo, H. Hashizume, Y. Okazaki, S. Toyokuni, K. Nakamura, N. Yoshikawa et al., Oxidative stress-dependent and -independent death of glioblastoma cells induced by non-thermal plasma-exposed solutions. Sci. Rep. **9**, 13657 (2019)

H. Tanaka, Y. Hosoi, K. Ishikawa, J. Yoshitake, T. Shibata, K. Uchida, H. Hashizume, M. Mizuno, Y. Okazaki, S. Toyokuni, K. Nakamura, H. Kajiyama, F. Kikkawa, M. Hori, Low temperature plasma irradiation products of sodium lactate solution that induce cell death on U251SP glioblastoma cells were identified. Sci. Rep. **11**, 18488 (2021)

T. Tatsumi, H. Hayashi, S. Morishita, S. Noda, M. Okigawa, N. Itabashi, Y. Hikosaka, M. Inoue, Mechanism of radical control in capacitive RF plasma for ULSI processing. Jpn. J. Appl. Phys. **37**, 2394–2399 (1997)

K.J. Taylor, G.R. Tynan, Control of dissociation by varying oxygen pressure in noble gas admixtures for plasma processing. J. Vac. Sci. Technol. A **23**, 643–650 (2005)

T. Tsutsumi, Y. Fukunaga, K. Ishikawa, K. Takeda, H. Kondo, T. Ohta, M. Ito, M. Sekine, M. Hori, Feedback control system of wafer temperature for advanced plasma processing and its application to organic film etching. IEEE Trans. Semicond. Manuf. **28**, 515–520 (2015b)

T. Tsutsumi, T. Ohta, K. Ishikawa, K. Takeda, H. Kondo, M. Sekine, M. Hori, M. Ito, Rapid measurement of substrate temperatures by frequency-domain low-coherence interferometry. Appl. Phys. Lett. **103**, 182102 (2013)

T. Tsutsumi, T. Ohta, K. Ishikawa, K. Takeda, H. Kondo, M. Sekine, M. Hori, M. Ito, Robust characteristics of semiconductor-substrate temperature measurement by autocorrelation-type frequency-domain low-coherence interferometry. Jpn. J. Appl. Phys. **54**, 01AB03 (2015a)

H. Uchiyama, K. Ishikawa, Q.-L. Zhao, G. Andocs, N. Nojima, K. Takeda, M.C. Krishna, T. Ishijima, Y. Matusya, M. Hori et al., Free radical generation by non-equilibrium atmospheric pressure plasma in alcohol–water mixtures: an EPR-spin trapping study. J. Phys. D: Appl. Phys. **51**, 095202 (2018)

T. Ueno, A. Morioka, S. Chikamura, Y. Iwasaki, Low-temperature and low-activation-energy process for the gate oxidation of Si substrates. Jpn. J. Appl. Phys. **39**, L327–L329 (2000)

F. Utsumi, H. Kajiyama, K. Nakamura, H. Tanaka, M. Mizuno, K. Ishikawa, H. Kondo, H. Kano, M. Hori, F. Kikkawa, Effect of indirect nonequilibrium atmospheric pressure plasma on antiproliferative activity against chronic chemo-resistant ovarian cancer cells in vitro and in vivo. PLoS ONE **8**, e81576 (2013)

Th. von Woedtke, B. Haertel, K.-D. Weltmann, U. Lindequist, Plasma pharmacy-physical plasma in pharmaceutical applications. Pharmazie **68**, 492–498 (2013)

Y. Watanabe, M. Shiratani, Y. Kubo, I. Ogawa, Effects of low-frequency modulation on rf discharge chemical vapor deposition. Appl. Phys. Lett. **53**, 1263–1265 (1988)

K. Yamakawa, M. Hori, T. Goto, S. Den, T. Katagiri, H. Kano, Ultrahigh-speed etching of SiO_2 with ultrahigh selectivity over Si in microwave-excited non equilibrium atmospheric pressure plasma. Appl. Phys. Lett. **85**, 549–551 (2004)

K. Yamakawa, M. Hori, T. Goto, S. Den, T. Katagiri, H. Kano, Etching process of silicon dioxide with nonequilibrium atmospheric pressure plasma. J. Appl. Phys. **98**, 013301 (2005a)

K. Yamakawa, M. Hori, T. Goto, S. Den, T. Katagiri, H. Kano, Ultrahigh-speed etching of organic films using microwave-excited nonequilibrium atmospheric-pressure plasma. J. Appl. Phys. **98**, 043311 (2005b)

Y. Yamamoto, H. Nomura, T. Tanaka, M. Hiramatsu, M. Hori, T. Goto, Measurement of absolute densities of Si, SiH and SiH_3 in electron cyclotron resonance SiH_4/H_2 plasma. Jpn. J. Appl. Phys. **33**, 4320–4324 (1994)

H. Yamamoto, H. Kuroda, M. Ito, T. Ohta, K. Takeda, K. Ishikawa, H. Kondo, M. Sekine, M. Hori, Feature profiles on plasma etch of organic films by a temporal control of radical densities and real-time monitoring of substrate temperature. Jpn. J. Appl. Phys. **51**, 016202 (2012)

M. Yamato, Y. Tamura, H. Tanaka, K. Ishikawa, Y. Ikehara, M. Hori, Y. Kataoka, Brain cell proliferation in adult rats after irradiation with nonequilibrium atmospheric pressure plasma. Appl. Phys. Express. **14**, 067002 (2021)

Y. Yamauchi, N. Doi, S. Kondo, Y. Sasai, M. Kuzuya, Synthesis and characterization of polymer-linked prodrug of antibacterial agent for the targeted delivery to the colon by cold plasma technique. J. Photopolym. Sci. Technol. **33**, 343–348 (2020)

D. Yan, H. Cui, W. Zhu, N. Nourmohammadi, J. Milberg, L.G. Zhang, J.H. Sherman, M. Keider, The specific vulnerabilities of cancer cells to the cold atmospheric plasma-stimulated solutions. Sci. Rep. **7**(4479), 1–12 (2017)

F. Ye, H. Kaneko, Y. Nagasaka, R. Ijima, K. Nakamura, M. Nagaya, K. Takayama, H. Kajiyama, T. Senga, H. Tanaka et al., Plasma-activated medium suppresses choroidal neovascularization in mice: A new therapeutic concept for age-related macular degeneration. Sci. Rep. **5**, 7705 (2015)

M. Yusupov, A. Bogaerts, S. Huygh, R. Snoeckx, A.C.T. van Duin, E.C. Neyts, Plasma-induced destruction of bacterial cell wall components: A reactive molecular dynamics simulation. J. Phys. Chem. C **117**, 5993–5998 (2013)

M. Yusupov, A. Privat-Maldonado, R.M. Cordeiro, H. Verswyvel, P. Shaw, J. Razzokov, E. Smits, A. Bogaerts, Oxidative damage to hyaluronan–CD44 interactions as an underlying mechanism of action of oxidative stress-inducing cancer therapy. Redox. Biol. **43**, 101968 (2021)

Publisher's Note Springer Nature remains neutral with regard to jurisdictional claims in published maps and institutional affiliations.

Authors and Affiliations

Masaru Hori[1]

✉ Masaru Hori
hori@nuee.nagoya-u.ac.jp

[1] Nagoya University, Furo-cho, Chikusa-ku, Nagoya 464-8603, Japan